THE DEVELOPMENT OF A SILICON BASED NEURONAL INTERFACE

Andrew Humphrey Mayne

A thesis submitted in partial fulfilment of the requirements
for the degree of Doctor of Philosophy
in the Faculty of Applied Sciences
of De Montfort University.

July 2002

Department of Chemistry
De Montfort University
Leicester

INDEX

TABLES

FIGURES

GRAPHS

Abstract

Current methods for directly measuring neural activity involve the use of patch clamps or optical recording. The first method is bi-directional, but does not have the ability to make reliable one-to-one connections to single neurones over an extended period, due to its intrusive nature. The second method only enables recording, and requires imaging technology if an automatic system is to be used. Furthermore, this method requires the storage of large volumes of data and the development of software to interpret the firing patterns. Like patch clamping, the fluorescent dyes used for optical imaging are not suitable for long-term measurements, as the lifespan of treated cells is measured in hours.

Following on from preliminary studies in this area, the aim of this project was to investigate the application of silicon and porous silicon for the development of a new generation of devices that could be biologically interfaced. To achieve this aim a series of silicon-based substrates were produced to provide optimal conditions for both cell growth and adherence by modifying the surface topography. Methods for the deposition and modification of indium tin oxide (ITO), gold, silicon and porous silicon were developed to enable the production of several devices. Toxicology studies were done using MTT (3-(4,5-dimethylthiazol-2-yl)-2,5 diphenyltetrazolium bromide; thiazolyl blue) and NRU (Neutral Red Uptake) assays, which both demonstrated the low toxicity of the component materials used in construction of the device. The final device was constructed from a glass substrate onto which ITO was deposited and etched to form contact strips, followed by the deposition of a silicon layer, which was either made porous or left as a translucent 1μm layer. These devices enabled the culturing of a neuronal cell line over the top of electrodes to facilitate transmission of an electrical signal from the cell to a data collection device. The growth of B50 rat hippocampal neurones was assessed on the different substrates investigated using scanning electron microscopy, which enabled visualisation of the cells forming contacts with the porous silicon surface. Positioning and contact to these substrates was tested via confocal microscopy at Daresbury Laboratories. Mechanical stimulation of cells, demonstrating calcium signal transmission, transduction and propagation using fluorescent dyes and time based photodiode detection, was also carried out at Daresbury. Finally, via potassium-mediated (60 mMol) stimulation of the neuronal cells cultured on the device, the propagation of action potentials was recorded using the MEA recording facility in the Department of Neuroscience, University of Nottingham, and visualised using the *spikeworks* (Plexon Inc,) software package.

Thus this project has provided an important early step in the production of a bioinert device which can be further developed to form a three-dimensional structure enabling measurement of cell signals in several planes.

ACKNOWLEDGMENTS

I would like to thank Professor Sue Bayliss for her determined support throughout my studies, Professors Stuart Laurie and Brian Swanwick for their support, and Jefferson Guillon for understanding GLP and making sure I did.

For both practical and moral support Dr. Mark Tobin at Daresbury for guiding me to and trusting me with his SYCLOPS, Ian Fletcher for the training and insight while using the SEM. To Chris Warrington and Dave "Disney" Bazeley for their practical solutions to impractical problems and Dr. Mike Needham for his blind support! All in the Hoof Group for the use of their equipment. Drs Andre Sapelkin and Vyacheslav Chesnokov for doing their powerful computing things.

On a financial note I would like to express my gratitude to both the British Council (Spain) and EPSRC for monies, enabling me to attend conferences and meetings.

I would also like to thank numerous members of staff both within and without the department, including Professors Roger Latham, Nick Phillips, Hans Bjelkhagen, Andrew Hugill, Dr Martin Turner, The Drs Dewhurst.....and the list goes on....

I would like to thank the postgraduate body in the Hawthorn Building and SERCentre for all pulling together and being friends.

I would like to thank my parents for all their support and inspiration, and the late Dr. M. Mayne for her encouragement. My siblings, Luke, Ruth (my twin - no we are not identical) and Madeline, thank you for your encouragement.

I would like to thank Professor A.R. Green and Professor J.M. Elliot for hiring a student named Annis Mechan who became Mrs Mayne.

And finally to my wife for just being her.

PUBLICATIONS

PAPERS

MAYNE, A.H., BAYLISS, S.C., BARR, P., TOBIN, M. & BUCKBERRY, L.D. (2000) Biologically interfaced porous silicon devices. *Physica Status Solidi A-Applied Research.* **182**(1): 505-513

BAYLISS, S.C., BUCKBERRY, L.D. & MAYNE, A. (2000) Interaction of biomaterials with porous silicon. *Frontiers of Nano-optoelectronic Systems*. 199-207

ORAL PRESENTATIONS

Biologically interfaced devices *(Invited speaker)*
Porous Semiconductors Science and Technologies (PSST 2000)
12 - 17th March 2000
Madrid

I*n vitro* investigations into nanostructured silicon as a biomaterial
EPSRC Networks: Silicon and Neurobiology, Second Meeting
24-25th November 1999
Stirling

POSTERS

Development of a porous silicon based multi-electrode array for stimulating and recording neuronal signals
Daresbury Users Meeting 2001
CLRC, Daresbury Laboratory, Warrington

ABBREVIATIONS

Ω	ohms
$(C_2H_5)_4NOH$	tetraethyl ammonium hydroxide
$(CH_3)_4NOH$	tetramethyl ammonium hydroxide
μF	microFarrad
λ_p	plasma reflection wavelength
ΔV	applied potential
A	area
A_{Base}	area of passivation layer
AC	alternating current
Ag	silver
Ag/AgCl	silver/silver chloride
AGE	amine gallate etch
Al	aluminium
$Al(OH)_3$	aluminium hydroxide
Al_2O_3	aluminium oxide
Ar	argon
A-T	adenine-thymine
A_{tip}	tip area
Au	gold
A-U	adenine-uracil
BDNF	brain-derived neurotrophic factor
BID	biologically interfaced device
Ca^+	calcium ion
C_d	glass wall capacitance
Cdks	cyclin dependent kinases
cDNA	complementary deoxyribonucleic acid
CdO	cadmium oxide
C_e	electrode capacitance
CH_3COOH	acetic acid
CHO	Chinese hamster ovary cells
Cl^-	chloride ions

CMOS	complementary metal-oxide semiconductor
CNTF	ciliary neurotrophic factor
CO_2	carbon dioxide
Cr	chromium
CrO_3	green rouge
C_{tip}	tip capacitance
Cu	copper
d	thickness of passivation layer
DC	direct current
ddH_2O	double distilled water
DMEM	Dulbecco's modified Eagle medium
DMSO	dimethyl sulphoxide
DMU	De Montfort University
DNA	deoxyribonucleic acid
DRAM	dynamic random access memory
DSP	digital signal processing
dt	change in time
dV	change in voltage
ECM	extra cellular matrix
EDP	ethylene diamine pyrocatechol
EDW	ethylene diamine pyrocatechol-water
E_g	bandgap energy
ELISA	enzyme-linked immunosorbent assay
EPSP	excitatory postsynaptic potential
EtOH	ethanol
eV	electron volts
F	Faraday constant
f	Frequency
FBS	fetal bovine serum
FET	field-effect transistor
FTIR	Fourier transform infrared spectroscopy
G-C	guanine-cytosine
GHz	gigahertz

h	height
H; H_2	hydrogen
H^+	proton
H_2O	water
H_2O_2	hydrogen peroxide
H_2SiF_6	fluorosilicic acid
H_2SO_4	sulphuric acid
HCl	hydrochloric acid
HeCd	helium – cadmium (laser)
HF	hydrofluoric acid
HNO_2	nitrous acid
HNO_3	nitric acid
HPLC	high performance liquid chromatography
hr(s)	hour(s)
HSA	human serum albumin
I	iodine
i	induced current
i_0	exchange current density
I_i	incident current
In_2O_3	indium oxide
I_{on}	current on
IR	infrared
ITO	indium tin oxide
j	current density
k	dielectric constant; ε
K^+	potassium ions
KCl	potassium chloride
KHz	kilohertz
KI	potassium iodide
$KMnO_4$	potassium permanganate
KOAc	potassium acetate
KOH	potassium hydroxide
l	length

L	length
LPCVD	low pressure chemical vapour deposition
MΩ	megaohms
mbar	millibar
MEA	microelectrode array
MEMs	microelectrode machines
mHz	megahertz
min	minutes
MOS	metal-oxide semiconductor
MPU	microprocessor unit
MTT	3-(4,5-dimethylthiazol-2-yl)-2,5 diphenyltetrazolium bromide; thiazolyl blue
mV	millivolts
N_2O_4	nitrogen tetroxide
Na^+	sodium ions
Na_2CrO_4	sodium chromate
$NaNO_2$	sodium nitride
NaOH	sodium hydroxide
NGF	nerve growth factor
$NH_2(CH_2)2NH_2$	ethylene diamine
NH_4F	ammonium flurate
NH_4OH	ammonium hydroxide
NO^+	nitronium ion
NO_2	nitric oxide
NRU	neutral red uptake
OCP	open-circuit potential
OD	optical density
OH	hydroxide
OH^-	hydroxyl group
pA	
PBS	phosphate buffered saline
PNA	peptide nucleic acid
PP	passivation potential
ppm	parts per million

PS	porous silicon
PTFE	polytetrafluoroethylene
PZT	piezoelectric
Q_i	charge
r	Radius
R	gas constant
RAM	random access memory
r.f.	radio frequency
R_e	electrode resistance
rms	route mean squared
RNA	ribonucleic acid
RO	reverse osmosis
R_{tip}	tip resistance
S/D	shallow drain
S/N	signal to noise ratio
SDR	silicon dissolution reaction
SEM	scanning electron microscope
Si	silicon
$Si(OH)_4$	silicon hydroxide
Si_3N_4	silicon nitride
SIA	Semiconductor Industry Association
SiF_2	silicon fluoride
SiF_4	silicon tetrafluoride
SiO_2	silicon dioxide
Sn	tin
SnO	tin oxide
SnO_2	tin dioxide
SYCLOPS	synchrotron radiation for confocal optical scanning microscope
T	temperature
Ta_2O_5	tantalum oxide
TFT	thin film transistor
TGA	targa (tagged graphic array)
ti	time

TiO_2	titanium oxide
TLV	threshold limit value
TMAH	tetra methyl ammonium hydroxide
T_{ox}	oxide thickness
uv	ultraviolet
V_a	applied potential
V_{con}	ohmic metal-semiconductor contact potential
V_{dd}	minimum ligic gate voltage
V_e	electrode voltage
V_h	Helmholtz potential
V_m	resting membrane potential
V_{ref}	reference voltage
V_{scr}	space-charge potential
a	angle
e_0	dielectric permittivity of free space
e_r	relative dielectric permittivity of passivation layer
r	resistivity

CHAPTER 1

GENERAL INTRODUCTION

1 GENERAL INTRODUCTION

In order to design, develop and construct a device to enable the embedding of semiconductor devices onto a microelectrode array (MEA) a thorough understanding of several areas of the physical sciences, from semiconductors through to cell biology was required. Chapter 1 examines the background in these areas and how they related the device under development.

1.1 SEMICONDUCTORS

1.1.1 History of semiconductors

The first semiconducting materials were studied at the beginning of the nineteenth century and, until the mid 1950s, germanium was considered to be the most important of these materials (Smith, 1979). However, devices constructed from germanium exhibit current leakage, and germanium dioxide has poor dielectric properties and is chemically unstable. In contrast, silicon devices exhibit much lower current leakage, and thermally grown silicon dioxide has excellent insulating and structural properties. In addition, ease of processing and relatively low cost, compared to other semiconductor materials, have contributed to the success of silicon in integrated circuit technology, making it the most widely used material in semiconductor device fabrication.

The development of silicon based semiconductor technology has led to faster and smaller processors together with a growing expectation of increased processing power. However, in 1965, Gordon Moore, then research director of Fairchild Semiconductor and subsequent co-founder of Intel, suggested that there was an empirical relationship between the number of transistors that could be placed onto an integrated circuit and the production lead-time. This observation has become known as Moore's Law, which states,

> "*the pace of microchip technological change is such that the amount of data storage that a microchip can hold doubles every year*" (Moore, 1965).

Following this rule, semiconductor-based technology will eventually reach the physical constraints of the materials used. The National Technology Roadmap for Semiconductors was first published by the Semiconductor Industry Association (SIA) in 1992 (being updated in 1994, 1997 and 1999), and is widely quoted throughout the industry. The characteristics which are regarded by the SIA as being most important for the future development of semiconductors are displayed in Table 1.1 (Semiconductor Industry Association 1999).

In 1999, the gate length and oxide thickness, together with the supply voltage of MOS transistors were all projected to drastically reduce in size in future years. Furthermore, the maximum power has been projected not to increase significantly, while the total number of transistors on each chip (the product of the transistor's density and the chip size) will rise enormously (SIA, 1999). In June 2001, Intel reported the design and production of transistors that are only 0.02 μm in size. Such devices are significantly smaller than transistors currently in use, where the distance across the transistor gate is only 0.18 μm. The recently produced Pentium 4® processors comprise approximately 42 million transistors and run at 2.1 gigahertz (GHz), which indicates that future microprocessors may contain up to one billion transistors running at 20 GHz. Graph 1 describes the relationships between feature size and the number of transistors per chip against time.

1.1.2 Approaching the density limit

As any electronic device requires electron flow in order to function, then the size of the electron and electron density in a given system are constraining factors. With low current densities, a defined binary result becomes less certain. Silicon dioxide has been used as the primary gate-dielectric material in field-effect devices since 1957, when the usefulness of the Si/SiO_2 material system was first demonstrated. At first single devices and then integrated devices were made, and the thickness of SiO_2 films decreased with each generation (Atalla, 1959; Frosch & Derick, 1957, Kilby, 1976). In the gate for the new Intel transistor it is silicon dioxide which prevents the upper metal layer from short-circuiting the lower silicon layer when current is passed through it, and is, theoretically, only three atoms thick. Semiconductors with transistor gates of 0.02 μm

		YEAR					
	Size	**1999**	**2002**	**2005**	**2008**	**2011**	**2014**
Technology generation	µm	0.18	0.13	0.1	0.07	0.05	0.035
Dense lines: DRAM half pitch	µm	0.18	0.13	0.1	0.07	0.05	0.035
Isolated lines: MPU gate length	µm	0.14	0.85 - 0.9	0.065	0.045	0.03 - 0.032	0.02 -0.022
Equivalent gate oxide thickness	nm	1.9 - 2.5	1.5 - 1.9	1 - 1.5	0.8 - 1.2	0.6 - 0.8	0.5-0.6
Nominal S/D extension junction depth	nm	42 - 70	25 - 43	20 - 33	16 - 26	11 - 19	8 - 13
Supply voltage, desktop	V	1.5 - 1.8	1.2 - 1.5	0.9 - 1.2	0.6 - 0.9	0.5 - 0.6	0.3 - 0.6
Maximum power, high performance	W	90	130	160	170	174	183
Maximum power, portables	W	1.4	2	2.4	2	2.2	2.4
Substrate diameter	mm	200	300	300	300	300	450
MPU logic transistors density	cm	6.6 M	18 M	44 M	109 M	269 M	664 M
MPU chip size	mm	340	356	408	468	536	615

Table 1.1 **Important characteristics of the SIA International Technology Roadmap for Semiconductors (Semiconductor Industry Association 1999).**

DRAM: dynamic random access memory; *MPU*: microprocessor unit; *S/D*: shallow drain

width should last for one more processor generation, typically 3 – 4 years of production, and Moore's Law should hold true into the next decade. Subsequently, the dimensions become so small that a new material will be required, and current projections highlight that the effective physical SiO_2 thickness could be compromised due to polysilicon depletion and quantum effects in such thin layers. The SIA suggests that for low-performance applications the ratio of minimum logic gate voltage (V_{dd}) to the thickness of the oxide (T_{ox}) is selected to maintain $V_{dd}/T_{ox} \leq 8$ mV/cm due to oxide reliability concerns, where V_{dd}/T_{ox} denotes the electric field in the oxide (SIA, 1999). For high-performance applications, high k materials have been proposed. "high k" refers to a material with a dielectric constant significantly higher than that of SiO_2, these fall into three categories and include but are not limited to those with $4 < k < 10$ such as SiN_x, those with $10 < k < 100$ such as Ta_2O_5, Al_2O_3, and TiO_2, and those with $k > 100$ such as PZT compounds. Those with k values between 10 and 100 have been used in transistors, such as TFTs. A thick layer is used to prevent the top-to-bottom metal shortage that would significantly diminish the yield.

The high k dielectric material is usually used in combination with a high quality dielectric interface layer to lower the interface density of states. For example, in the a-Si:H TFT case, the N-rich SiN_x is exclusively used as the interface layer. The resultant gate leakage current is much smaller than for the oxide dielectric with the equivalent oxide thickness, allowing smaller T_{ox} and providing a route for higher current on (I_{on}) for the high k case. The $V_{dd}/T_{ox} \leq 8$ mV/cm requirement may not hold for the high k materials. From a reliability point of view, T_{ox} may be scaled further for these materials. Current research is directed towards these high k gate dielectrics (Weldon *et al.,* 2002), and, although results are promising, there are no operational devices as yet. It can be seen from the above considerations that the way forward for the next generation is not so clear or straightforward, and other theories and alternate technologies proposed include quantum computing, optical signal transduction and organic semiconductors.

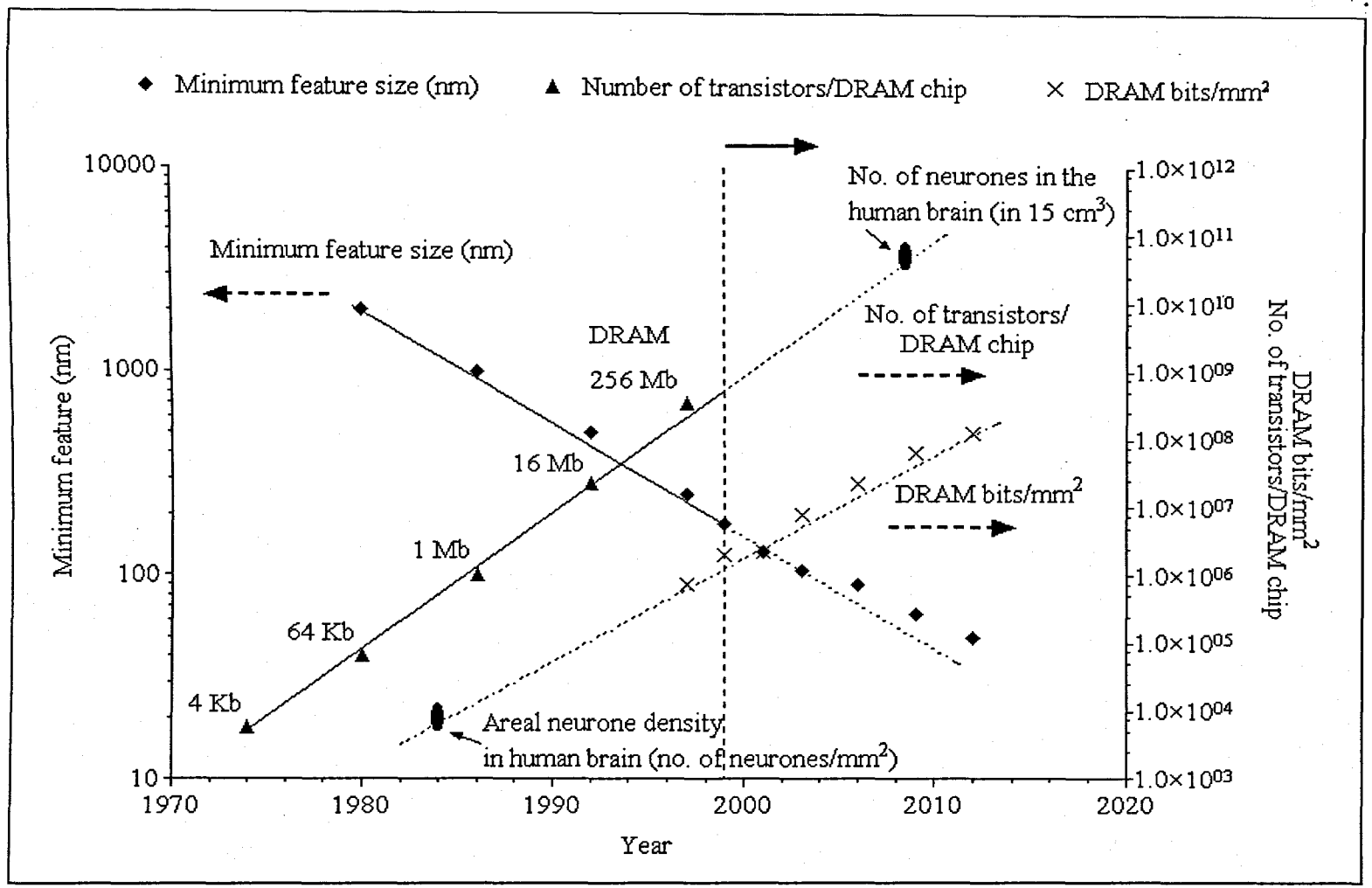

Figure 1.1 **Roadmap for feature size, relative density of DRAM and transistor quantity per chip. (Semiconductor Industry Association 1999. http://notes.sematech.org/1999_SIARoadmap/Home.htm)**
DRAM: dynamic random access memory.

1.2 THE "BIOCHIP"

One proposed progression of microelectronic development is the integration of established electronic technologies with biological systems. This would enable the computational power of a biological system to utilise the signal transduction capabilities of silicon-based semiconductors. Devices have already been developed which rely upon the interpretation of signals generated by the coupling of organic and inorganic systems. Thus developments in both modification and immobilisation of DNA and proteins, such as enzymes and antibodies, have led to the production of "biochips". Terminologies that have been used in the literature to describe this technology include, but are not limited to:- "biochip", "DNA chip", "DNA microarray" and "gene array". For example, *Affymetrix, Inc.* have developed the *GeneChip*®, which describes a number of high density, oligonucleotide-based DNA arrays. However, "gene chip" has also been used as a generic term referring to microarray technology. A more correct description would be that of "genome chip" or "genomic chip", indicating that this technology is intended to monitor the whole genome on a single chip. "Genome chip" would also include the increasingly important and feasible protein chip technology (Joshi, 2001).

An array is an ordered arrangement of samples. A DNA array provides a medium for matching known and unknown DNA samples based on base-pairing rules (A-T and G-C for DNA; A-U and G-C for RNA). The underlying principle of the DNA microarray is hybridisation, which provides a mechanism for identifying the unknown sequences. The sample spot sizes in a microarray are typically less than 200 μm in diameter. DNA microarrays, or DNA chips, are fabricated on glass, or occasionally nylon, substrates for which probes (tethered nucleic acids with known sequence) are used to determine complementary binding, allowing extensive parallel gene expression and gene discovery studies. An experiment with a single DNA chip can provide information on thousands of genes simultaneously; the "target" being the free nucleic acid sample whose identity/abundance is being detected.

There are two major applications for DNA microarray technology:

(1) Identification of sequence (gene / gene mutation);

(2) Determination of expression level (abundance) of genes.

Furthermore, there are two specific types of DNA microarray technology, involving arrayed DNA sequences of known identity:

Format I:

Probe cDNA (500~5,000 bases long) is immobilised to a solid surface, such as glass, using robotic spotting and exposed to a set of targets either separately or in a mixture. This method, which is commonly termed a DNA microarray, was originally developed at Stanford University (Ekins, 1999).

Format II:

An array of oligonucleotide (20~80-mer oligos) or peptide nucleic acid (PNA) probes is synthesised either *in situ* (on-chip) or by conventional synthesis followed by on-chip immobilisation. The array is exposed to labelled sample DNA, hybridised, and the identity/abundance of complementary sequences determined. This methodology was developed by Affymetrix, Inc., which manufactures photolithographically fabricated products under the GeneChip® trademark. Oligonucleotide based chips are now being manufactured using alternative *in situ* synthesis or depositing technologies (Lockhart *et al.*, 1996).

1.3 CELL-INTERFACED ELECTRONICS

Both of the technologies described above rely on the immobilisation of constituents of the cell, not the whole cell. Although these products have been termed "biochips" they do not conform to the standard properties of a "chip". In order to be classed as a true "chip" technology, there should be bi-directional communication between the components of the chip; in this case, cell and substrate (Buitenweg *et al.*, 2000). The development of a device to enable the interfacing of living cells with silicon technology would facilitate *in vitro* pharmacokinetic studies of drug mechanics.

The development of cell-interfaced electronics is reliant upon:

(1) Biocompatibility: the ability to culture living cells on semiconductor materials. The semiconductor must be biocompatible and the biological system must not degrade the semiconductor.

(2) Bi-directional communication: between cell and semiconductor.

(3) Sophisticated signal separation techniques.

Each of these prerequisites is now discussed:

1.3.1 Biocompatibility

Materials have physical, chemical, and electrical surface characteristics that influence interactions with other materials, and cells themselves will respond to materials placed in their environment (Kamalesh *et al.* 2000; Khouw *et al.* 2000; Kidd *et al.* 2002). The cellular response by a host to an internalised structure can be classed as either:-

Bio-incompatible: whereby the defence mechanism in the host causes a self/non-self immunological response resulting in damage to the foreign material that may, in turn, compromise the host.

Bioinert: whereby the defence mechanism in the host fails to recognise the material as a material at all, consequently there is no cellular response.

Biocompatible: whereby the defence mechanism in the host identifies the material as self and interacts as if it had originated from the host. This is the optimal situation for a bi-directional communication device.

Electronic devices that employ bulk silicon have been available for *in vitro* bio-sensing applications for some time, however they are encased in silicone to overcome short-term problems with bio-incompatibility.

1.3.2 Bi-directional communication

There are two fundamental types of electronic devices constructed from semiconductor materials - the transistor and the laser-diode. While transistors are silicon based, laser-

diodes are gallium arsenide based. From an electronics perspective, it would be both practical and economical to construct transistors and laser-diodes from the same material. However, the good electrical characteristics of silicon contrast with its poor light emitting properties. This is due to silicon having an indirect band gap of 1.12 eV (emission from bulk crystalline silicon being in the near-infrared) and its inefficiency is due to non-radiative processes prevailing over radiative recombination of charge carriers. The development of semiconductor optoelectronics has thus been dominated by the III-V compound semiconductors (such as gallium arsenide), many of which have a direct band gap.

For the purposes of developing biologically interfaced devices, the search for suitable materials of this type is of some urgency, as gallium arsenide is toxic to biological systems. The search for an efficient, luminescent semiconductor that could fulfil the combined roles of waveguide, laser diode, transistor and detector moved closer to success when nanoporous silicon was found to demonstrate these properties (Canham 1990)

1.3.3 Sophisticated signal separation techniques

Technology has evolved from single sharp electrodes that permit clean observation of single unit activity to arrays containing many electrodes. However, electrodes which do not isolate a single cell generally record action potentials from more than one neurone, thus requiring the use of spike shape sorting to separate the several activities for further analysis. Computational techniques available for shape sorting have been reviewed by Lewicki (1998), although all methods involve mapping some measure of individual spike shape to a point in multi dimensional property space (Gray & Singer, 1989). The clustering of points in this space is then used to identify and differentiate among the several different spike trains present in the recording. Closely spaced arrays of electrodes have been used, these are termed either –stereotrodes, triodes, tetrodes (Gray *et al.*, 1995; McNaughton *et al.*, 1983).

The action potential from a given neurone is recorded by more than one electrode. The signal seen by each such electrode differs due to its relative position in three-

dimensional space with respect to the neurone. Measured values obtained from different electrodes with known relative position can enhance the accuracy of the results obtained as waveform sorting can be more effective.

The effects of signal to noise ratio in electrophysiological recordings also become critical if the signal to noise ratio is favourable, then recorded events should produce clusters, these should be well isolated with deviation, thus separation process will incur fewer errors due to recording anomalies. If however the spike waveform does not rise significantly above the background noise, and particularly if this background noise has similar spectral content to the desired spikes, the clusters in the property space will overlap. It is then impossible to define clean boundaries, and hence there are inevitably errors of inclusion or exclusion in the assignment of an individual action potential to a particular neurone. Such poor sorting can render subsequent analysis at best inaccurate, and at worst invalid. Errors can be especially serious for cross-correlation and related analyses (Gerstein, 2000).

1.4 ETCHING CHEMISTRY

Silicon has been an ideal candidate for the electronics industry in part due to its ability to undergo etching. This is achieved either *en masse* or as a selective process. Wet etching is either isotropic or anisotropic. Isotropic etching results in the same etch rate in all directions i.e. the lateral etch rate is about the same as the vertical etch rate and is independent of the orientation of any applied mask edge. In anisotropic etching the rate depends upon orientation to crystalline planes and thus the lateral etch rate can be much larger or smaller than the vertical etch rate, depending upon the orientation of the mask edge to crystalline axes. The mask edge and the details of the mask pattern determine the final etched shape. This method is used for making complex shapes though only "standard" shapes are routinely used.

In order for etching to occur the following events must take place: transport of reactants to the surface, followed by a surface reaction and subsequent transport of the products of that reaction from the surface. In order to achieve this there must be an oxidizer (i.e. H_2O_2, HNO_3), an acid or base in which to dissolve the oxidized surface (i.e. H_2SO_4,

NH_4OH) must be present, and a dilute media to transport the reactants and products (i.e. H_2O, CH_3COOH).

Etching is inherently an electron/hole transfer surface reaction and is therefore an electrochemical process, requiring the oxidation of one or more species and simultaneous reduction of others (Redox reaction).

1.4.1 HNA etching of silicon

HNA etching of silicon derives its name from the ingredients of the etching solution, **H**ydrofluoric acid, **N**itric acid and **A**cetic acid. This method produces nearly isotropic etching of silicon and the overall reaction is:

$$Si + HNO_3 + 6HF \rightarrow H_2SiF_6 + HNO_2 + H_2O + H_2 \qquad \text{(Equation 1)}$$

Etching occurs via a redox reaction followed by dissolution of the oxide by the HF that acts as a complexing agent. Points on the silicon surface randomly become oxidation or reduction sites and act as localised electrochemical cells, sustaining corrosion currents of ~100 A/cm^2 (relatively large). Each of these points becomes both an anode and cathode site over the cycle of the etching process. If the time spent on each is the same, the etching will be uniform; otherwise selective etching will occur.

Silicon is promoted to a higher oxidation state at an anodic site which supplies positive charge in the form of holes, (h^+).

$$SiO + 2h^+ \rightarrow Si^{2+} \qquad \text{(Equation 2)}$$

NO_2 from the nitric acid is simultaneously reduced at a cathode site which produces free holes:

$$2NO_2 \rightarrow 2NO^{2-} + 2h^+ \qquad \text{(Equation 3)}$$

The Si^{2+} combines with OH^- to form SiO_2:

$$Si^{2+} + 2OH^- \rightarrow Si(OH)_2 \rightarrow SiO_2 + H_2O \qquad \text{(Equation 4)}$$

The SiO_2 is then dissolved by HF to form a water soluble complex of H_2SiF_6:

$$SiO_2 + 6HF \rightarrow H_2SiF_6 + 2H_2O \qquad \text{(Equation 5)}$$

The behaviour of nitric acid is more complex. Initially it is dissociated in water, and this is termed deprotonation:-

$$HNO_3 \leftrightarrow NO_3^- + H^+ \quad \text{(Equation 6)}$$

followed by the autocatalytic cycle for production of holes and HNO_2:

$$HNO_2 + HNO_3 \rightarrow N_2O_4 + H_2O \quad \text{(Equation 7)}$$

$$N_2O_4 \leftrightarrow 2NO_2 \leftrightarrow 2NO_2^- + 2h^+ \quad \text{(Equation 8)}$$

$$2NO_2^- + 2H^+ \leftrightarrow 2HNO_2 \quad \text{(Equation 9)}$$

In this scenario NO_2 is the oxidiser as its reduction supplies holes for the oxidation of the silicon. HNO_2 is regenerated by the reaction (autocatalytic) and the oxidising potential of the etch is governed by the quantity of undissociated HNO_3.

1.4.2 Role of acetic acid (CH_3COOH)

Acetic acid can be substituted for water as the dilutent although it has a lower dielectric constant than water, 6.15 for CH_3COOH versus 81 for H_2O. The result of this is less dissociation of the HNO_3 which yields a higher oxidation power for the etch. Acetic acid also enhances the wetting properties of the etch solution for hydrophobic wafers, as it is less polar than water. The above processes are summarised in Figure 1.2. Figure 1.3 describes the interaction of the differing components of the etch and their effect on the mechanism for driving the reaction.

1.4.3 Anisotropic etching of silicon

The differing hybridised (sp^3) orbital orientation on different crystal planes causes significant differences in etch rate. Etch rates are typically: (100) > (110) > (111).
The (111) crystallographic planes are considered the "stop" planes for anisotropic etching. There are 8 planes along the $\pm x \pm y \pm z$ directions. At intersections of these planes with each other and (100) etch pits, the usual anisotropic etched structures for (100) Si wafers are produced: V-grooves, pyramidal pits, pyramidal cavities (Figures 1.4 and 1.5).

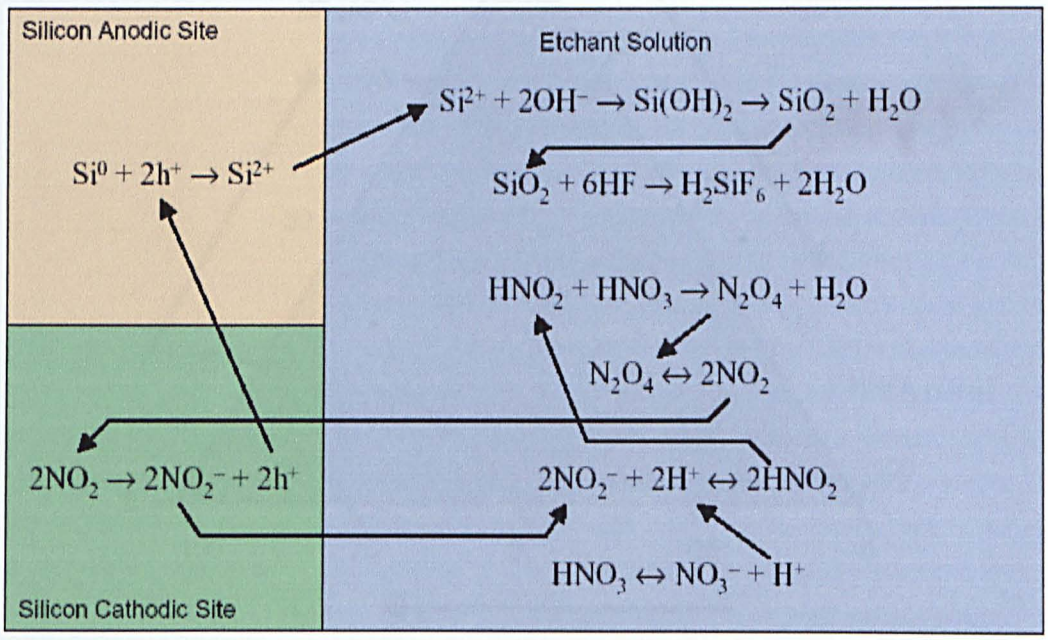

Figure 1.2 **Summary of the HNA etching of silicon as described in the text section 1.4.1.**

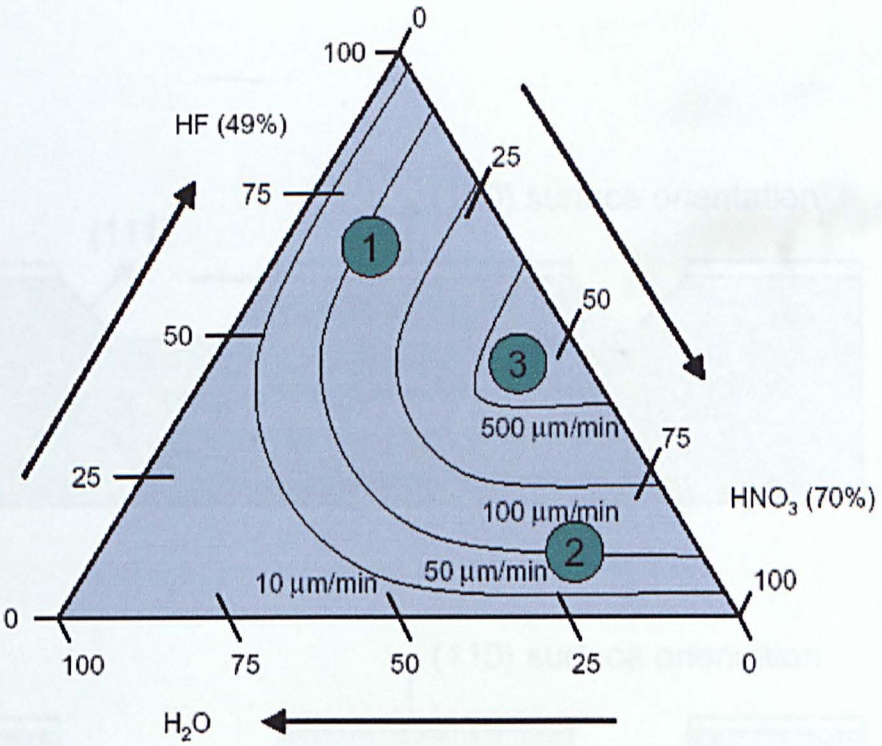

Figure 1.3 Iso-concentration lines indicating the effect of etch rate relative to percentage composition of either HF (49%): HNO_3(70%): H_2O.

In Region 1 there are high HF concentrations and contours are parallel to the lines of constant HNO_3; thus the etch rate is controlled by HNO_3 which leaves little residual oxide and is limited by oxidation process.

For Region 2 there are high HNO_3 concentrations, contours are parallel to the lines of constant HF; therefore the etch rate is controlled by HF which leaves a residual 30-50 Å of SiO_2. This process is self-passivating limited by oxide dissolution and is the area where polishing occurs.

Region 3 is initially not very sensitive to the amount of H_2O, etch rate falling of sharply for 1:1 HF:HNO_3 ratios.

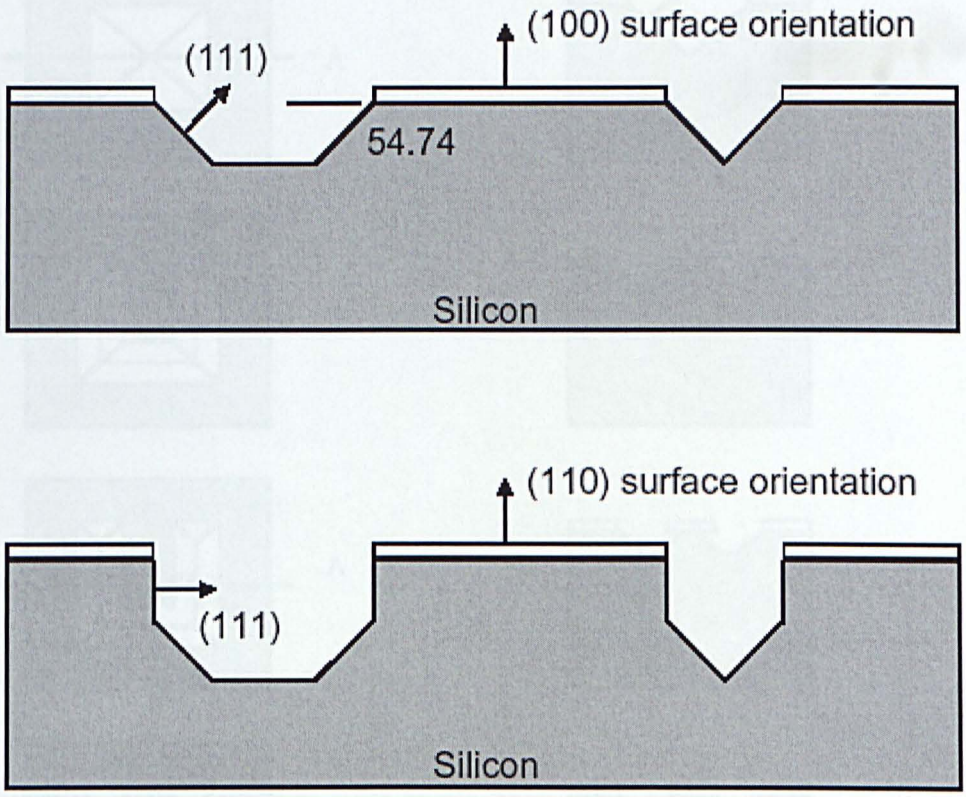

Figure 1.4 **Side view of anisotropic etched structures in silicon wafers producing V-grooves, pyramidal pits, pyramidal cavities (100, 110 and 111 denote orientation of lattice)**

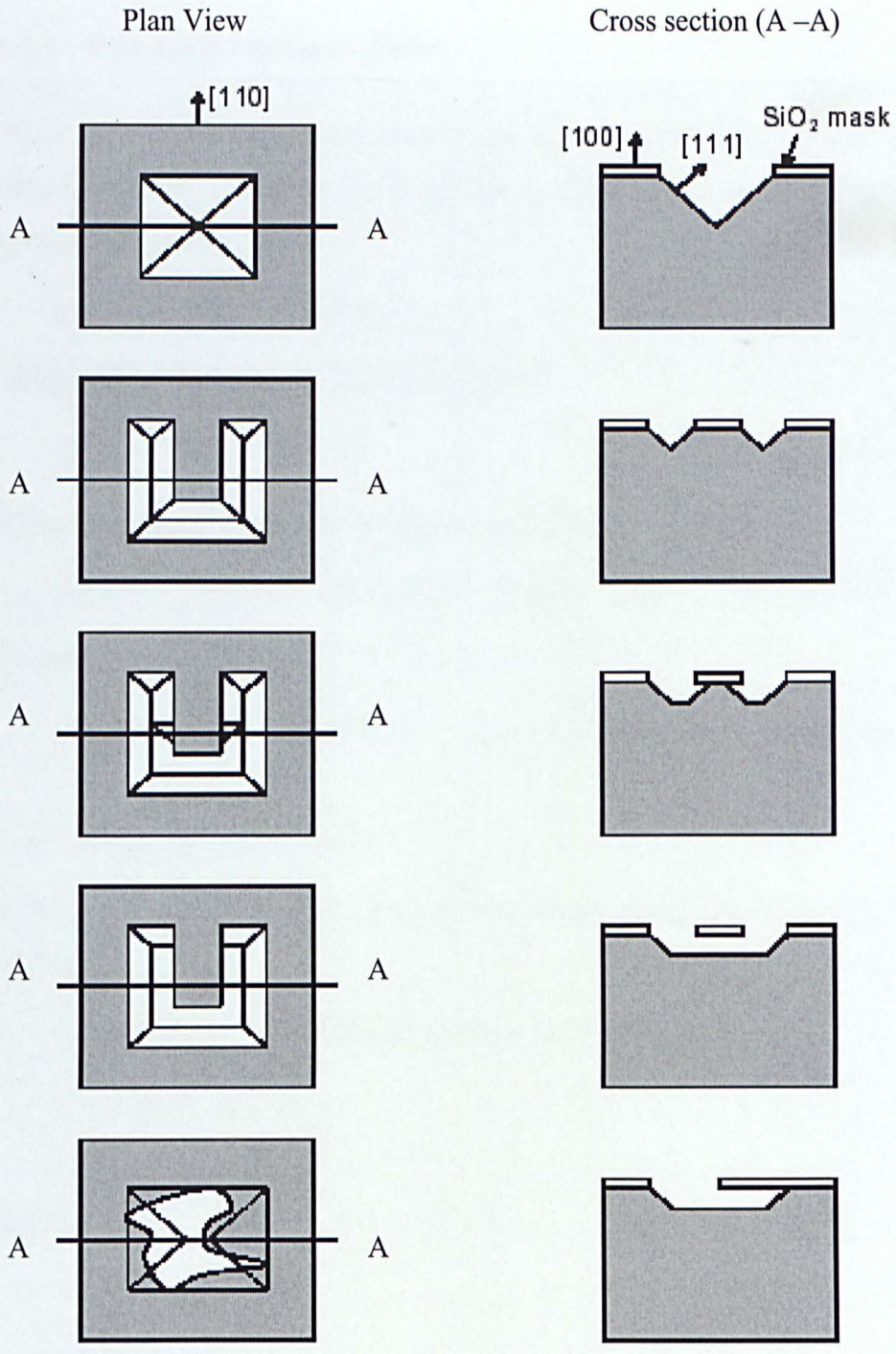

Figure 1.5 **The influence of selective masking by SiO_2 on crystallographic planes during HF etching.**

1.4.4 Hydroxide etching of silicon

There are several hydroxides used in the etching of silicon: KOH, NaOH, CeOH, RbOH, NH_4OH, TMAH:$(CH_3)_4NOH$. The resultant is the oxidation of silicon by the hydroxyls to form a silicate:

$$Si + 2OH^- + 4h^+ \rightarrow Si(OH)_2^{++} \quad \text{(Equation 10)}$$

At the same time there is a reduction of water:

$$4H_2O \rightarrow 4OH^- + 2H_2 + 4h^+ \quad \text{(Equation 11)}$$

Silicate further reacts with hydroxyls to form a water soluble complex:

$$Si(OH)_2^{++} + 4OH^- \rightarrow SiO_2(OH)_2^{2-} + 2H_2O \quad \text{(Equation 12)}$$

The overall redox reaction is:

$$Si + 2OH^- + 4H_2O \rightarrow Si(OH)_2^{++} + 2H_2 + 4OH^- \quad \text{(Equation 13)}$$

1.4.5 KOH etching of silicon

KOH is one of the most used of the hydroxide etches. The etch rates achieved are typically:

~1 mm/min for (100) Si planes however it stops at p^{++} layers

~14 Å/hr for Si_3N_4

~20 Å/min for SiO_2

Anisotropy: (111):(110):(100) ~ 1:600:400

1.4.6 EDP etching of silicon

Ethylene Diamine Pyrocatechol (EDP) is also referred to as Ethylene Diamine - Pyrocatechol – Water (EPW). EDP etching is readily masked by SiO_2, Si_3N_4, Au, Cr, Ag, and Cu. However it is unsuitable for aluminium as it aggressively etches this metal.

Anisotropy: (111):(100) ~ 1:35

The main drawback of EDP is that it is very corrosive and highly carcinogenic. Typical etch rates for (100) silicon:

70°C 14 mm/hr

80°C 20 mm/hr

90°C 30 mm/hr = 0.5 mm/min

97°C 36 mm/hr

The action of EDP is outlined below. Initially the ionisation of ethylene diamine:

$$NH_2(CH_2)2NH_2 + H_2O \rightarrow NH_2(CH_2)2NH_3^+ + OH^- \qquad \text{(Equation 14)}$$

Is followed by the oxidation of Si and reduction of water:

$$Si + 2OH^- + 4H_2O \rightarrow Si(OH)_6^{2-} + 2H_2 \qquad \text{(Equation 15)}$$

Then chelation of hydrous silica occurs:

$$Si(OH)_6^{2-} + 3C_6H_4(OH)_2 \rightarrow Si(C_6H_4O_2)_3^{2-} + 6H_2O \qquad \text{(Equation 16)}$$

The disadvantages with this mechanism are that the chemicals are highly volatile which requires a reflux condenser to keep volatile ingredients from evaporating. It is incompatible with MOS or CMOS and must be used in an isolated fume-collecting bench by itself as it will rust any metal on contact leaving brown stains on surfaces which are difficult to remove. However EDP does a have faster etch rate on convex corners than other anisotropic etches and is generally used for undercutting cantilevers as it tends to leave a smoother finish, since the faster etching of convex corners produces a polishing action. EDP etching can result in deposits of polymerised $Si(OH)_4$ on etched surfaces and deposits of $Al(OH)_3$ on Al pads. These deposits can be removed by Moser's post EDP protocol (Banks, 2002).

1.4.7 Amine gallate etch

Amine gallate etch (AGE) is safer than EDP although it requires a temperature of 118°C and has a typical etch rate of ~1.7 mm/min.

Anisotropy: (111):(100): 1:50 to 1:100

1.4.8 TMAH etch

Tetra Methyl Ammonium Hydroxide (TMAH) etch is MOS/CMOS compatible, as there are no alkali metals present and it is used in non-chlorine-based positive photoresist. It does not significantly etch SiO_2 or Al and is thus considered bond wire safe.

Anisotropy: (111):(100) ~ 1:10 to 1:35

Hydroxide etches are generally safe and predictable although they normally contain an alkali metal which renders them incompatible with MOS or CMOS processing techniques. Ammonia dissolved into water produces ammonium hydroxide (NH_4OH) which is free of alkali metal. A requirement of this etch is that it is heated to 90°C volatilising ammonia, so ballasting the ammonium hydroxide with Tetramethyl Ammonium Hydroxide, ($(CH_3)_4NOH$) and Tetraethyl Ammonium Hydroxide, ($(C_2H_5)_4NOH$), which are less volatile, suppresses evaporation.

1.4.9 Hydrazine and water etch

Hydrazine and water etch produces anisotropic etching of silicon, however Hydrazine is a very powerful reducing agent used for rocket fuel. The threshold limit value (TLV) = 1 ppm by skin contact.

Etch rate ~2 mm/min at 100°C

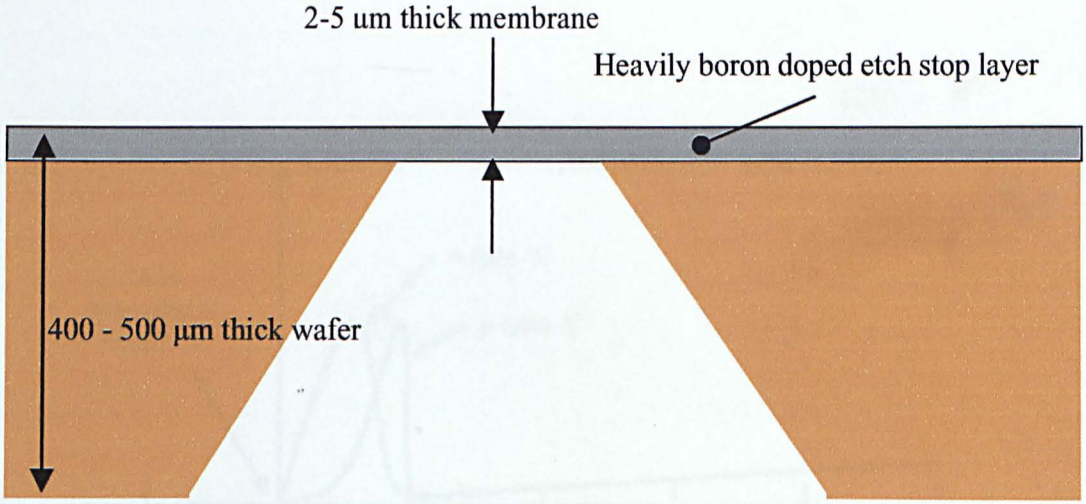

Figure 1.6 The use of doped silicon as a stop layer for selective etching.

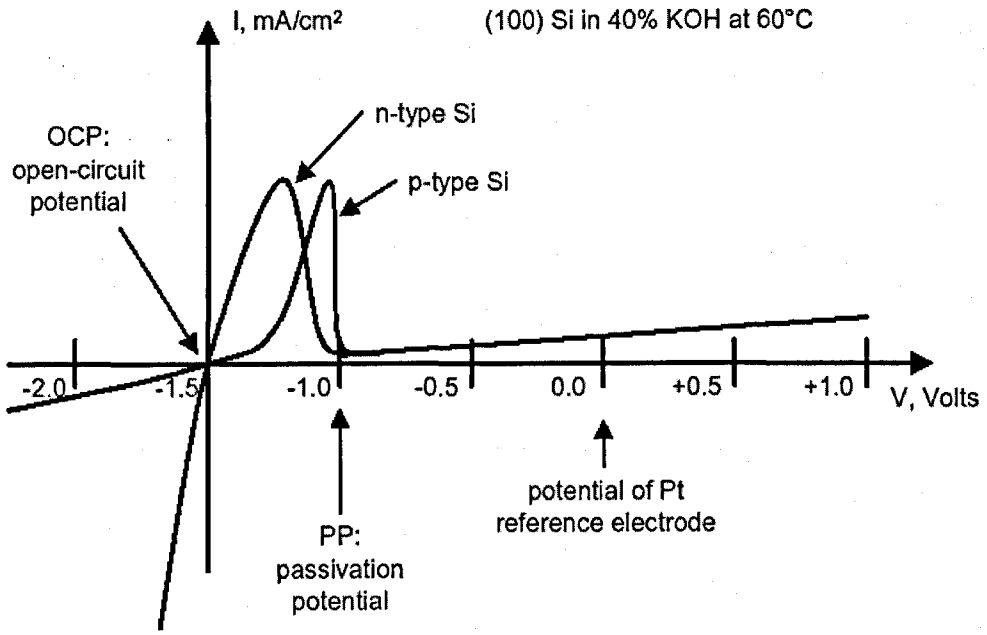

Figure 1.7 Relationship between wafer bias and its effect on etch rate.

Increasing the wafer bias above the OCP will increase the etch rate by supplying holes which will oxidize the Si. Increasing the wafer bias further will reach the passivation potential (PP) where SiO_2 forms. This passivates the surface and terminates the etch. The HF / H_2O solution does not exhibit a PP, since the SiO_2 is dissolved by the HF.

1.4.10 Anisotropic etch stop layers

Controlling the absolute depth of an etch is often difficult, particularly if the etch is going most of the way through a wafer. Etch stop layers can be used to drastically slow the etch rate, providing a stopping point of high absolute accuracy. Boron doping is most commonly used for silicon etching (Figure 1.6). Requirements for specific etches:

HNA etch actually speeds up for heavier doping

KOH etch rate reduces by 20′ for boron doping > 1020 cm^{-3}

NaOH etch rate reduces by 10′ for boron doping > 3 ′ 1020 cm^{-3}

EDP etch rate reduces by 50′ for boron doping > 7 ′ 1019 cm^{-3}

TMAH etch rate reduces by 10′ for boron doping > 1020 cm^{-3}

1.4.11 Electrochemical etch

HF normally etches SiO_2 and terminates on silicon. If a bias is maintained across the electrodes, holes are injected by the external circuit which will oxidise the Si and form hydroxides which the HF can then dissolve. The relationship between etch rate and applied bias is described in Figure 1.7. As discussed below, this produces a polishing etch that can be effectively masked by LPCVD films of Si_3N_4.

If etching is performed in very concentrated HF (48% HF, 98% EtOH), then the Si does not fully oxidize when etched, and results in porous silicon which is brownish in colour as reported by Uhlir (1956).

It was decided that the use of KOH for the etching of silicon surfaces, with either electrochemical or stain etch techniques utilised where the porous silicon surfaces was required, would minimise the deposition of toxic substances on the silicon and also enable the possible integration of CMOS components onto any device produced.

1.5 POROUS SILICON

In 1990, L.T. Canham reported that strong room temperature visible photoluminescence of porous silicon (PS), was dependent upon nanostructure (pore) size, where pores were formed by electrochemical etching of crystalline silicon (Canham, 1990). Since then, interest has surged (see review by Cullis, *et al.*, 1997), and PS (and material created from its subsequent epitaxy, oxidation and/or selective etching) has been used for the creation of semiconductor-on-insulator structures, metal-insulator-semiconductor condensers of large capacity, chemical sensors (e.g. gas, water and explosives) and biological sensors (Bogue, 1997; Carts-Powell, 1998; Chin *et al.*, 2001; Gaburro *et al.*, 2001; Mikulec *et al.*, 2002; Parce *et al.*, 1998; Sailor *et al.*, 2001; Thust *et al.*, 1996; Zurer 1997). Applications envisaged, although currently limited by manufacturing technology, include optoelectronic devices such as electroluminescent displays and photodetectors (Buriak *et al.*, 1998).

Production of PS was reported as early as 1956 by Uhlir, who described the porous layer as a "matty black, brown or red deposit" (Uhlir, 1956). Subsequently, in the early 1980s, the use of PS for producing thick silicon dioxide layers, which are necessary for the fabrication of silicon-on-insulator structures, was investigated (Imai, 1981; Konaka *et al.* 1982). Visible luminescence at liquid helium temperature was reported by Pickering (1984) whereby, in an optical study of the structure of PS films, the emission was attributed to an amorphous silicon phase (Pickering, 1984). Furthermore, since Canham (1990) proposed that photoluminescence was linked to quantum confinement, thousands of studies have been performed concerning the fundamental and technological properties of PS (Basmaji & Guimaraes, 1995; John & Singh, 1995; Jung *et al.*, 1993; Kanemitsu & Uto, 1994; Kanemitsu *et al.*, 1995).

Following investigation into the electrical properties of thermally oxidised porous silicon (Hurley *et al.*, 1991) the first solid state electroluminescent devices based on PS were developed, these consisted of a porous layer on a crystalline substrate (Koshida & Koyama, 1992; Kozlowski & Lang, 1992; Namavar *et al.*, 1992). A semi-transparent gold, or transparent conducting oxide electrode was deposited on top of the porous layer

(Qin *et al.*, 1994). These devices were reported to have very low quantum efficiencies ($< 10^{-6}$) and required high operating voltages. Different designs (Chen *et al.*, 1993; Steiner *et al.*, 1993) and better contact materials (Futagi *et al.*, 1992; Koshida *et al.*, 1993; Li *et al.*, 1994) have led to an improvement of both electrical and luminescent properties (Hirschman *et al.*, 1996: Collins *et al.*, 1997). Fauchet (1997; 1998) presented a light-emitting device with a quantum efficiency of 0.1%, integrated into a microelectronic circuit. Porous silicon layers connected via a liquid electrolyte, instead of a solid electrode, have also been shown to exhibit efficient visible luminescence (Billat, 1996; Bressers *et al.*, 1992; Bsiesy *et al.*, 1993, 1994; Canham, 1992; Halimaoui *et al.*, 1991; Meulenkamp *et al.*, 1994, 1995; Peter & Wielgosz, 1996; Uosaki *et al.*, 1996). Bressers *et al.* (1992) suggested that the electrolytic solution penetrates the pores, thus forming an intimate contact to the whole porous structure, the external lateral surface size of which ranges from 200 to 600m^2/cm^2.

There are two main mechanisms for the production of PS - electrochemical and stain etching.

1.5.1 Electrochemical etching of silicon

Electrochemical etching is the preferred method for fabrication of PS, particularly for luminescent material, due to the greater control over the range of porosities attained and thickness achieved. This control also results in greater reproducibility of material properties (Cullis *et al.*, 1997). Electrochemical etching requires the presence of an electrolyte, commonly hydrofluoric acid, and an applied current. Variables include:

(1) electrolyte composition, such as the inclusion or absence of wetting agents (e.g. ethanol)

(2) electrolyte temperature

(3) current density

(4) applied potential

(5) the physical constraints involved in the design of the polytetrafluoroethylene (PTFE) electrochemical cell (Cullis *et al.*, 1997).

Light can also be employed to assist in the formation of PS, a process called

photoelectrochemical etching (Starovoitov & Bayliss, 1998; 2000). This technique is widely used for the preparation of luminescent PS, or porous oxidised silicon layers.

The PTFE electrochemical cell follows a basic construction, with the possible major modification being the introduction of a lens or opaque area when using p-type silicon. The p-type silicon requires an initiation step – the introduction of light from a suitable light source can provide enough initiation energy. A schematic representation of the cell and its potential distribution are described below (Figure 1.8).

In order to understand PS formation, the mechanism of anodic surface dissolution needs to be elucidated and, although a detailed mechanism is still unclear, probable mechanisms are as follows:

In 1990, Lehmann and Föll postulated that highly regular arrays of macropores could be obtained in the n-Si/HF system with extremely large aspect ratios. The formation of these pores was explained using the "space charge region" model. This assumes that back-side photogenerated current is focused on pore tips due to bending of the space charge region around the tip (Lehmann & Föll, 1990). Empirical results support this model for the formation of macropores in n-type Si, especially for the regular pore arrays, and it is possible to produce pore structures as described by Lehmann (1993). A variation on Lehmann's theory is the "current burst model". This postulates that the chemical and electrochemical reactions for pore-formation follow the same mechanism for all pore types. It is proposed that pore growth in silicon can be described in the general terms of a phase separation of the silicon surface into two areas: (i) the pore tips, where the majority of current flows, and (ii) the pore walls and the remaining silicon surface where little or no current flows. This second region area is regarded as passivated against dissolution. Phase separation is considered the result of optimisation of localised events mediated by stochastic processes. Thus silicon dissolution is considered to consist of a series of charge (Qi) and time (ti) consuming processes called "current bursts". Each local current burst carries a mean current that has a specific optimum value for each system. As the current burst dissolves only a small area of the silicon only a small area is available for oxidation. The summation of these points in a

given area is specific for each type of silicon, thus in specific etch solutions the area of silicon dissolved is controlled by the current applied over the exposed area. This is termed the current density 'j', the effect is described by Lehmann and Gruning (1997).

Micro-, meso- and macropore formation, are explained by local fluctuations in the current density (j) which leads to phase separation of the silicon surface into two areas: pore tips and pore walls together with the remaining silicon surface where no current is flowing. For this to occur several points must be addressed: (i) each current burst has to overcome any existing H-passivation of the surface (nucleation phase); (ii) direct dissolution of silicon occurs; (iii) silicon may be oxidized; (iv) the silicon oxide has to be dissolved; (v) at the clean surface a (relatively slow) H-passivation starts. There is only charge transfer in (ii) and (iii). The current can be increased to its optimum value by maximizing the consumed charge, and/or minimizing the time needed. Since the pore nucleation is much easier on unpassivated surfaces, H-passivation is a process which can increase current burst (iB), by reducing the time between the beginning of H-passivation and pore nucleation, and also a mechanism which leads to a preferential pore nucleation in areas where current bursts have just stopped. This correlation in time between two subsequent current bursts is the driving force for the phase separation, i.e. the clustering of current bursts in some areas and thus meso and macro-pore formation.

The H-passivation can explain the strong crystal orientation dependence of pore formation. Since the number of dangling bonds on the (100)-surface is much higher than on the (111)-surface, the H-passivation is fastest and most effective on (111)-surfaces. Thus current bursts occur preferably on (100)-surfaces providing pore growth in (100)-directions and (111)-surfaces as preferred pore walls. The processes (ii) to (iv) are strongly influenced by changing the oxygen concentration in the electrolyte and the processes (i), (ii) and (v) by the concentration of hydrogen. This dependence on the electrolyte composition permits control of the local current density 'j' as well as the driving force for the phase separation. The current burst model provides another theory for the mechanism of pore formation in the silicon HF system.

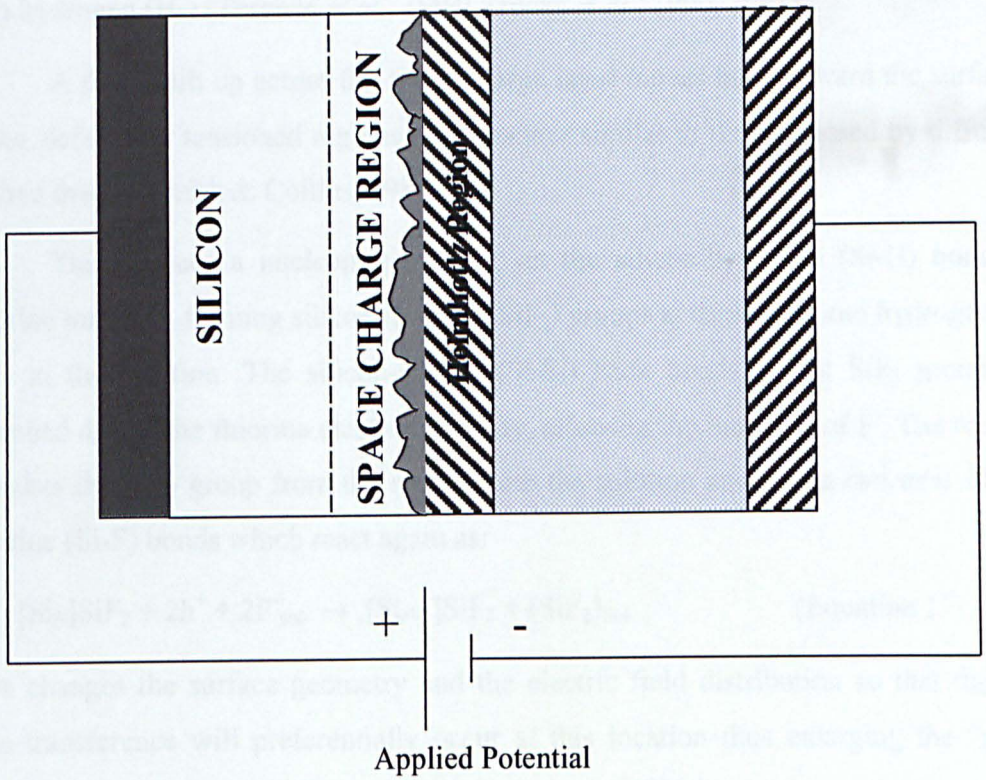

Figure 1.8 Representation of the silicon/solution anodisation circuit showing the potential drops at the various interfaces.

V_a is the applied potential, V_{ref} is the solution potential (along with the reference electrode), V_{con} is the ohmic metal-semiconductor contact potential, V_h, is the Helmholtz potential, and V_{scr}, is the space-charge potential. The direction and magnitude of all potentials drops are strictly arbitrary, although they must all sum to zero (after Smith, 1992)

(1) At the onset of the anodic current, the entire surface of the silicon is covered with hydrogen (H_2) (Teschke *et al.*, 1994; Trucks *et al.*, 1990, 1991).

(2) A field built up across the space charge layer moves holes toward the surface at kinks, defects, or tensioned regions, in a manner similar to that proposed by diffusion-limited theory (Smith & Collins, 1989).

(3) This induces a nucleophilic attack on the silicon-hydrogen (Si-H) bonds by fluorine ions (F^-), forming silicon fluoride (SiF_2) groups at these sites and hydrogen ions (H^+) in the solution. The silicon-silicon (Si-Si) back bonds of the SiF_2 groups are stretched due to the fluorine electronegativity, allowing the insertion of F^-. The reaction detaches the SiF_2 group from the surface into the solution and forms two new silicon-fluorine (Si-F) bonds which react again as:

$$[Si_N]SiF_2 + 2h^+ + 2F^-_{sol.} \rightarrow [Si_{N-1}]SiF_2 + (SiF_2)_{Sol} \qquad \text{(Equation 17)}$$

This changes the surface geometry and the electric field distribution so that the next hole transference will preferentially occur at this location thus enlarging the "pore". Equation 17 describes the silicon dissolution reaction (SDR).

(4) The intermediary product $(SiF_2)_{Sol.}$ reacts rapidly with hydrofluoride (HF), forming H_2 and silicon fluoride (SiF_4) (Memming, 1966; Theunissen, 1972):

$$(SiF_2)_{Sol.} + 2(HF)_{Sol.} \rightarrow (H_2)_{Sol.} + (SiF_4)_{Sol.} \qquad \text{(Equation 18)}$$

Strong visible electroluminescence has been observed under cathodic polarisation of n-type PS in contact with an electrolyte containing strong oxidising agents, such as peroxodisulphate and hydrogen peroxide (Bressers *et al.*, 1992; Canham, 1992). In these cases the wavelength of the cathodic emission from n-type electrodes was found to be a function of the applied potential. Strong visible luminescence has also been observed during the anodic oxidation of PS electrodes in electrolyte solutions of differing compositions (Billat, 1996; Halimaoui *et al.*, 1991; Uosaki *et al.*, 1996). However, as the oxidation of silicon is irreversible, this anodic emission is transient.

Lehmann & Gosele (1991) suggested a surface bound oxidation mechanism whereby the hole capture and subsequent electron injection produce a divalent silicon state (Equation 19). The authors further proposed that the surface is in a state of flux between

hydride and fluoride coverage at each electron/hole exchange, silicon hydride bonds passivate the silicon surface unless a hole is available. Lehmann supported his theory by citing the continued hydrogen evolution following suspension of applied potential in the formation of porous silicon. Peter *et al.* (1989), using in situ FTIR, reported the existence of a hydrogenated, amorphous silicon surface deposition during silicon anodisation in NH_4F/HF electrolytes. Raman spectroscopy also supports the hypothesis (Gupta *et al.*, 1991; Kato *et al.*,1988; Sugiyama *et al.*, 1990; Venkateswara Rao *et al.*, 1991) confirming the presence of Si-H surface bonds during formation of porous silicon.

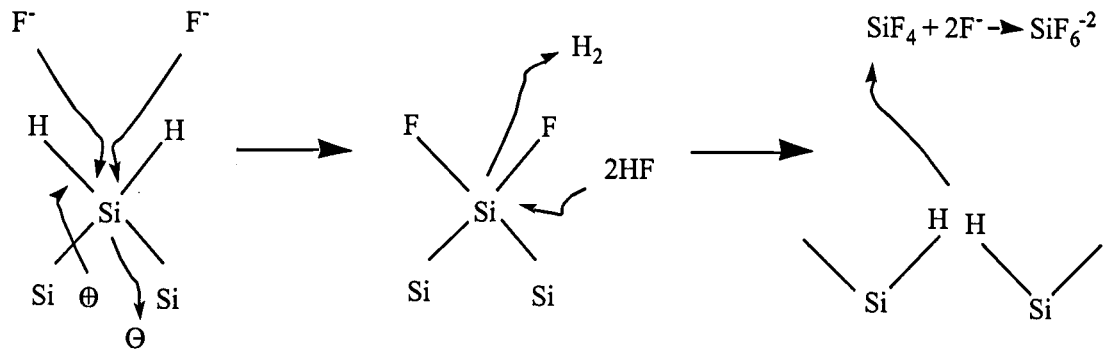

(Equation 19)

The surface of PS inevitably harbours impurities resulting from both exposure to air and the electrochemical etching process. These impurities not only affect the optical and electrical properties of the material itself, but could also potentially affect any biological systems (living cells) with which the surface is interfaced. Some common impurities found in PS are hydrogen, fluorine, and oxygen:

(1) Infrared absorption experiments have demonstrated the presence of $Si\text{-}H_x$ groups (where x=1,2,3,4), up to several months after fabrication (Sugiyama *et al.*, 1990).

(2) Fluorine has been detected using Raman spectroscopy (Gupta *et al.*, 1991) and, although the form it occurs in is unclear, $Si\text{-}F_x$ groups (where x=1,2,3,4) are the most likely structures involved. Like hydrogen, the fluorine content decreases with time and it may be replaced by Si-OH following hydrolysis by atmospheric water. Sunada *et al.*

(1990) suggested that fluorine termination of surface bound hydrogen increases the atmospheric stability of silicon surfaces treated with HF.

(3) Oxygen is normally adsorbed to levels as high as 1% within minutes of air-drying and, over a period of a few days, Si-O-Si, O-Si-H and O_3-Si-H groups are formed. The presence of such oxides on the silicon surface is thought to be crucial in the biocompatibility of the material. PS continues to react slowly with the ambient atmosphere and, consequently, its chemical properties change with time. Oxidation levels depend on a combination of elapsed time and ambient conditions. Oxygen content remains low if the PS is stored under ultra high vacuum and in the dark, whereas PS stored under atmospheric conditions can have an oxygen content as high as 50% (Naftel *et al.*, 2000).

Turner (1962) proposed the existence of a freely dissolved divalent state of silicon, $SiF_{2(aq)}$, which subsequently undergoes an auto-disproportionation reaction, depositing silicon on the pore walls:

$$2SiF_{2(aq)} + 2F^- \rightarrow Si + SiF_6^{-2}. \qquad \text{(Equation 20)}$$

Eddowes (1990) extended reaction (above) is a kinetic study of the anodic dissolution of silicon and proposed the energy dependent reaction pathway (Figure 1.9).

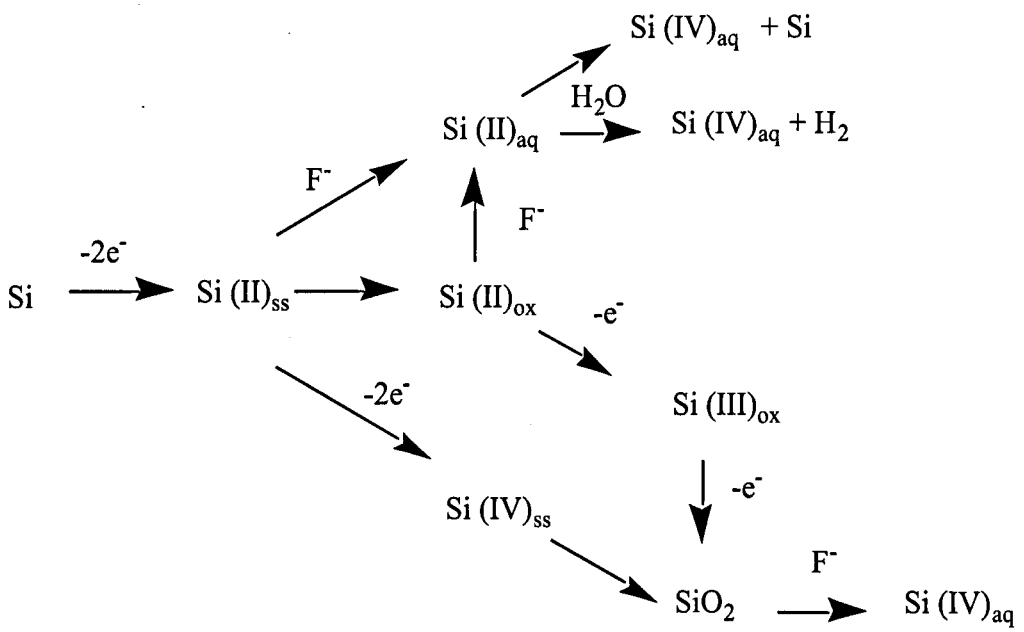

Figure 1.9 Energy based dissolution

Subscripts ss, ox, and aq refer to surface bound; surface oxide, and aqueous states, respectively, and each electron loss indicates measurable electrochemical current (as opposed to homogeneous solution oxidations which are not measurable). The disprorportionation reaction produces what Eddowes termed a "rough" or "pitted" surface (Eddowes, 1990).

1.5.2 Stain etching

An alternative method for the production of a PS layer is the use of a chemical or stain etch technique. However, stain etched PS is significantly less homogeneous than electrochemically etched PS, in addition to suffering from poor reproducibility (Cullis *et al.*, 1997). Common stain etching solutions also consist of hydrofluoric acid, with a small quantity of nitric acid (HNO_3) or other oxidising additives, such as sodium nitride ($NaNO_2$), sodium chromate (Na_2CrO_4), potassium permanganate ($KMnO_4$) or green rouge ($Cr\ O_3$) (Kelly *et al.*, 1994; Steckl *et al.*, 1993; Turner, 1962). These oxidising agents result in formation of metal ions in solution, and lead to contamination of the PS being formed, however the removal of the oxidising agents significantly increases the time required for the formation of the porous layer. In addition, Kelly *et al.* (1994) suggested that there is an incubation period whereby the nitronium ion (NO^+), the basic active oxidation agent, is accumulated above and on the surface of the sample. The required incubation period also results in increased processing time and reduced sensitivity in the control of PS formation, and thus reproducibility is compromised.

1.5.3 Porous silicon: a multi-functional semiconductor material

Due to its high surface area, structural anisotropy and optoelectronic properties, PS can be used for light and chemical detectors and wave guides. It also has luminescent properties that have been explained by a quantum confinement-based model for carriers in the structure. Any species described by quantum-mechanics has some wave-like properties, as described by its wave-function. Trapping carriers in a small space means that only particular types of wave-function are enabled. Each must satisfy the Schrödinger wave equation while under the effect of the trap. These wave-functions have both a characteristic length and specific energy. Greater confinement means that the minimum energy that an object can have is larger, and that the gaps between values of permitted energy are also larger. PS can be classified as microporous (pore size of greater than 50 nm), mesoporous (pore size of 5 – 50 nm) or nanoporous (pore size of less than 5 nm) and includes regions containing Si nanocrystals and amorphous regions that vary in size within these ranges. Raman spectroscopy has indicated (Cho *et al.*, 2000; Elhouichet & Oueslati, 2001), that the presence of the nanocrystals relaxes the

selection rules relating to the interaction of optical phonons with incident photons, so broadening the associated Raman peak and giving rise to the photoluminescent properties observed with porous but not bulk silicon.

Altogether these diverse mechanical and optoelectronic properties could be harnessed for many biological applications, such as *in vitro* and *in vivo* biosensors and drug delivery systems, and intelligent implants.

1.5.4 Porous silicon: a non-toxic biocompatible material

PS has been shown to adsorb both human serum albumin (HSA) and fibrinogen (Zangooie *et al.*, 1998). Hydration of the porous surface significantly decreases the adsorption of HSA onto the surface, but increases the amount deeper within the porous film. However, hydration failed to affect the adsorption of fibrinogen, a protein essential in blood clotting processes. Porous silicon has been shown to be reactive towards hydroxyapatite formation (Buriak *et al.*, 1998), and this was the first indication of the potential of PS as a biomaterial.

As described previously, the etched surface of PS inevitably harbours impurities from both the atmospheric air and the manufacturing process. In addition to the characterisation of the biocompatibility of the PS, the possibility of toxic effects must also be considered, since the health and viability of the cells would dictate the life of any interfaced device.

It has recently been demonstrated (Navarro *et al.*, 1996) that cells grown on a plate containing silicon substrates grow to confluence (a complete continuous sheet) both on the silicon itself and on the surrounding plastic well. It is thus possible to culture cells on a PS substrate, and the cells have been demonstrated to be viable in terms of structure and metabolism (Wallman *et al.*, 2001), indicating that PS wafers are not fatally toxic to the cells and present an acceptable surface for growth. The lack of cytotoxicity of PS offers a distinct advantage over gallium- and indium- arsenide, as both of these substrates have been shown to be toxic. The ability to culture mammalian cells directly onto PS, coupled with its apparent lack of toxicity, offers exciting

possibilities for the future of biologically interfaced sensing. This could involve the development of biologically interfaced neural networks or electronic sensing, with signal information being directly transduced from a living system to a PS device. None of the predicted applications described above will be possible unless the technology is developed to allow the passage of information (in the form of a signal) across the interface between the silicon and a living cell. This is the next great challenge for workers in this area.

1.6 NEURONAL RECORDING

1.6.1 Neuronal structure and function

Nerve cells, neurones, are highly specialised cells that consist of a cell body, axons, and dendrites all enclosed by a thin, fragile, phospholipid bilayer membrane. Neurones exist in various types, each with different structure and function. These specificities arise due to many factors, such as the relative position of the cell within the brain and levels of stress due to physical stimuli, such as pressure, or chemical stimuli, such as hydrogen ion concentration or specific localised hormone levels (Leonard, 2000). However, they share the same ability to process and transmit information rapidly and efficiently over long distances with very low energy requirements. Neurones have some unique features; a typical neurone has a number of processes (projecting parts) extending from the cell body, one of which can be in excess of a metre in length in the case of spinal axons. There is always one and only one of these per neurone. At the distal end, the axon may branch profusely into many fine terminals, these terminals, whether a few or many, connect to other neurones that may be some distance away. All the other fibres that extend from the neurone cell body are termed "dendrites". They are usually short, but there may be many of them and they may be branched, so numerous and so thickly branched that in some nerve cells the ensemble of dendrites resembles a tree. The axon has two essential functions: it conducts electrical signals in one direction, and it transports chemical substances in both directions. The major function of the dendrites is to present an extended surface area for input from other nerve cells. Dendritic branching provides the maximal membrane surface area for a given volume of cell cytoplasm. The junction between the terminal of a neurone's axon and the dendrite of another neurone

is termed a "synapse". The generalised neurone, therefore, is a biological cell whose morphology is designed to receive many inputs, and produce a single output, and have that single output rapidly distributed to one or more other neurones (Alberts 1994)..

In addition to morphology, another major difference between neurones and other cells is that the neuronal cell membrane is specialised to process and transmit information in the form of electrical signals. The basis for this is a set of unique electrical properties that are found in all nerve cells in all organisms with neural tissue. As stated above, neurones are surrounded by a lipoprotein membrane and there is an electrical potential difference between the interior and exterior of the cell due to unequilibrated ion distributions, which are maintained by ion-specific enzymatic transport processes. The membrane insulates the conducting interior from fluids surrounding the cell. Ionic pumps in the membrane transport ions from lower to higher electrochemical potential, maintaining electrochemical gradients across the cell membrane. Owing to ionic concentration gradients and differential membrane permeability, primarily to K^+, Na^+ and Cl^-, neurones sustain a d.c. potential (resting potential) across the membrane. This resting membrane potential (m) varies for different systems, with typical values of –50 mV for sea slug, –70 mV for the squid giant axon, and –90 mV for primate neurones. In neurones, the membrane potential is modulated by ionic currents through several different types of ion-specific channels across the cell membrane (Table 1.2). These channels can selectively permit different ions to cross the membrane (down their electrochemical gradients). Depending on their timing, location, and ion specificity, ionic movements alter the membrane potential with corresponding rates, amplitudes, and direction.

Name		Ion	Type	Speed	Relative potential	Threshold
Fast sodium	I_{Na}	Na^+	activating/inactivating	very fast	45 mV	-50 mV
Persistent sodium	I_{Nap}	Na^+	activating/inactivating (slow)	fast	45 mV	-65 mV
Delayed rectifier	I_K	K^+	activating	fast	-100 mV	-40 mV
A-current	I_A	K^+	activating/inactivating	fast	-100 mV	-60 mV
Ca^{2+}-dependent K^+	I_{AHP}	K^+	activating (Ca^{2+}-dependent)	moderate/slow	-100 mV	-
Slow potassium	I_M	K^+	activating	slow	-100 mV	-35 mV
Slow potassium	I_{K2}	K^+	activating/inactivating	slow	-100 mV	-40 mV
Transient Ca^{2+}	I_T	Ca^{2+}	activating/inactivating	slow	150 mV	-60 mV
High threshold Ca^{2+}	I_L	Ca^{2+}	activating	fast	150 mV	-10 mV
Sag current	I_h	Ca^{2+} and Na^+	inactivating	slow	0 - 40 mV	-
Leak	I_{leak}	Cl^-, K^+, Na^+	passive	-	-60 mV	-

Table 1.2 **List of channel types and their respective actions and dependencies.**

I: current.

The electrical properties of a neurone can be described as follows:

(1) Any area of a nerve axon membrane has two possible states: a resting state and an active state.

(2) The resting state is characterised by:

(i) low permeability to sodium ions

(ii) higher relative permeability to potassium ions.

(The resting state membrane potential difference is therefore due primarily to the unequilibrated potassium ion distribution.)

(3) When the resting state potential difference across the axon membrane is reduced by a small fraction, the membrane abruptly shifts into the active state.

(4) The active state lasts about a millisecond and is characterized by a sudden higher permeability to sodium ions than to potassium ions. The active state membrane potential difference is therefore due primarily to the unequilibrated distribution of sodium ions.

(5) The sudden higher permeability to sodium ions is transient. It ends within a millisecond, and once again the membrane is more permeable to potassium ions than to sodium ions.

(6) The result of all of the above is a transient change in the membrane potential difference of about 80 or 90 mV, a pulse that lasts about 1 millisecond before the membrane returns to its resting state. This pulse is called the "action potential"

(7) An electrical pulse initiated in the axon membrane near the cell body acts to excite the adjacent region by reducing its membrane potential, thus causing the adjacent region to switch into an active state. The result is the effective propagation of the electrical pulse away from the cell body and down the length of the axon.

There are exceptions to the above scheme, however it does describe the behaviour of most neurones in most nervous systems.

The action potential is a fast and relatively large voltage change, and by actively regenerating itself can travel much farther than passive electrical signals. By propagating along adjacent areas of active membrane, the signal can quickly travel the length of an axon and initiate synaptic transmission to the next neurone.

Thus, at the synapse, the following events occur:

(1) The propagated action potential, arriving at the presynaptic terminal of the initiating neurone, causes the terminal to release packets of transmitter molecules by calcium dependent endocytosis.

(2) These transmitter molecules diffuse across the space separating the terminal from the postsynaptic neurone, termed the synaptic cleft.

(3) The transmitter molecules interact with receptors in the membrane of the postsynaptic neurone and trigger ionic events (via ionic channel activation) ionotropic receptors and/or change the cell biochemistry (metabalotropic receptors) thus resulting in the potential difference across its membrane to either increase or decrease.

(4) All the inputs from all the presynaptic terminals to the postsynaptic neurone are summed, so that at any instant in time there is an electrical effect at the place where the axon leaves the cell body of the postsynaptic neurone (the "initial segment of the axon").

(5) The result of this electrical effect from the multiple inputs is to alter the membrane potential difference at the initial segment of the axon. If the change is a reduction in the membrane potential difference beyond a certain point, the "threshold", the axon membrane at that point undergoes a transient change in ion permeability, an action potential is produced, and from that point the action potential is automatically propagated down the length of the axon to the axon terminals, this time the axon terminals of the postsynaptic neurone.

Vertebrate neurones differ from non-vertebrate neurones as they have developed a myelinated axon. The axon is wrapped by many layers of insulating liquid-crystalline lipids, this layering is interrupted periodically along its length these interruptions are

termed nodes of Ranvier, the end result of which is to increase the velocity of propagation of the axon potential to as much as 100 meters per second. In an axon without this myelination, the propagation velocity depends primarily on the cross-sectional diameter of the axon (Alberts 1994).

The relationship between the above mechanisms for signal transduction depends upon either a passive or active signal. These two broad categories of electrical events are brought about by ionic movements. An example of a passive electrical signal is the post-synaptic potential. Channels on the post-synaptic neurone open in response to the chemical diffusing across the synapse and cause the membrane potential near that synapse to increase or decrease. This voltage change moves passively along the membrane, affecting closer areas of membrane more than distant. If enough small post-synaptic potentials combine in an area of voltage-sensitive channels, then an active, or regenerative, electrical impulse will occur. An active electrical impulse will move along the membrane whenever a changing membrane potential in one area of membrane induces a similar change in membrane potential in an adjacent area.

1.6.2 History of recording from cells

Methods that enabled study of the electrical activity of single nerve cells were not developed until 1936 (Dale *et al.*, 1936). Prior to that, the electrical activity of nerve cells could only be examined in large groups of thousands or millions of nerve fibres forming a nerve bundle Joseph Erlanger and Herbert S. Gasser used a cathode ray oscilloscope to detect rapid changes in the electrical activity of bundles of nerve fibres in the 1920s and received the Nobel Prize in Physiology and Medicine for this work in 1944. The electrical activity of the various nerve fibres provided a quantifiable electrical change that could be detected by the available instrumentation. Modern electrophysiology came with the work of Alan Hodgkin and Andrew Huxley, for which they received the Nobel Prize in Physiology and Medicine in 1963 (Hodgkin & Huxley, 1952). It was not until the 1960s that it first became possible to record currents through single ionic channels in artificial bilayer preparations (Hladky & Haydon, 1970). Gilbert Ling, a post-graduate student at the University of Chicago developed a method for measuring the internal electrical potentials of vertebrate muscle cells, using glass

micropipettes with tip diameters of less than 1 μm (Ling, 1975). These pipettes were filled with a potassium-chloride solution and inserted into squid giant nerve fibres. These two techniques - the use of giant squid axons and glass microelectrodes - guided current research, and have lead to an understanding of the electrical behaviour of neurones.

In the 1970s, Erwin Neher and Bert Sakmann developed the "patch-clamp recording technique" (Neher & Sakmann, 1976), for which they were awarded the Nobel Prize in Physiology and Medicine in 1991. This technique uses a glass microelectrode to measure the electrical activity of a single ion channel. The extracellular 'patch pipette', with its round-tipped glass micropipette, forms a seal with the cell membrane resulting in a giga ohm resistance access to the cell interior. This is in contrast to an intracellular microelectrode, which comprises a glass micropipette with a sharper tip which actually pierces the cell membrane. Although both techniques are routinely used in electrophysiology laboratories, intracellular microelectrodes are highly invasive, and thus compromise the longevity of the cell.

1.6.3 Recording devices

A wide variety of electrodes have been developed to record bioelectric events. Microelectrodes, a subclass of these electrodes are small, localised probes typically used to study neuronal signalling (Ogden, 1994). Robinson (1968) provided the ground work for the properties of the electrical components in a biological – electronic interface. This, together with an understanding of the cellular components of the system enables the system to be considered as a whole.

The electrical properties of a microelectrode determine its reliability as a recording transducer, thus design, materials and fabrication must be optimised to reduce distortion, electrical noise, and instability. There are two ways to record the transmembrane voltages associated with neuronal activity. The intracellular method uses two electrodes: one inside the cell (intra-cellular electrode), and the other outside (reference electrode). This method records transmembrane signals, i.e. post-synaptic potentials and the action potentials (impulses). The other, extracellular method, places

two electrodes outside the cell, one very close to the cell and one further away. Although the signals recorded in this way do not strictly measure the transmembrane currents generated by the neurone, any regenerative or other large currents generated nearby the electrodes may cause voltage differences between the two electrodes. Extracellular recording is therefore effective for recording action potentials, but is less likely to detect post-synaptic potentials or other small potential changes.

Most electrodes are either metallic or glass micropipettes (Brown & Flaming, 1977):

(1) Metallic

Metallic micropipettes are small, localized probes which are fabricated from the exposed tip of a sharp, insulated, conducting wire (Figure 1.10) (Ogden, 1994). In these probes the signal is transferred from the tip through the wire while a dielectric material provides the insulation between the wire and the surrounding environment. An electronic equivalence circuit for the above arrangement is described in Figure 1.11.

(2) Glass

Glass micropipettes are of sub-micrometer dimensions, being fabricated by pulling heated glass capillaries (Kandel *et al.*, 1991) (Figure 1.12). These pulled micro-capillaries are filled with an electrolyte (typically KCl or potassium acetate) and an Ag/AgCl electrode is placed in the electrolyte. The glass wall provides ionic insulation and ensures virtually no leak current.

The underlying principles between the metal and micropipette electrodes are broadly similar and in essence, all recording electrodes consist of a metal-electrolyte interface. Unlike the simple ohmic metal-metal contact, a metal-electrolyte contact is a rather complex system (Bard & Faulkner, 1980). Various chemical reactions may take place when a metal is introduced into an electrolyte. These reactions may involve dissolution of the metal in the case of partially soluble metals, or electron exchange between the metal and the solution as in the case of noble metals. The result of these chemical reactions is the formation of an equilibrium charge gradient at the interface (usually referred to as the electric double layer) which is accompanied by a build-up of an electric potential across the interface. The details of the space charge layer are predicted

by Helmholtz's theoretical models which can then be used to analyse the electrical properties of an electrode. The capacitive nature of the electric double layer, a metal-electrolyte interface results in an electrolytic capacitor (e.g. for platinum C_e =20μF/cm^2 at 1 kHz). The interface also has a resistive component. A metallic electrode and an electrolyte maintain equilibrium potential and a balance between influx and efflux currents of electrons (or ions). By applying an external potential, the equilibrium current is unbalanced, and the induced current can then be expressed (Robinson, 1968) by:

$$i = i_0 e^{F\Delta V/2RT} - i_0 e^{-F\Delta V/2RT} \qquad \text{(Equation 21)}$$

with i_0 being the exchange current density (values may range from pA/cm^2 up to 10 A/cm^2), ΔV is the applied potential, F the Faraday constant, R is the gas constant, and T is the temperature.

For small voltages, Equation (21) can be expressed as:

$$i = i_0 F/RT\Delta V \qquad \text{(Equation 22)}$$

At room temperature the electrode resistance (typically denoted as the charge transfer resistance) can be expressed as $R_e = \Delta V/i = 0.06/i_0$. For platinum, i_0 =4.5 x10^{-6} A/cm^2, which corresponds to R_e =1.3x10^{12}Ω/cm^2. Thus for very small electrodes the above expression indicates significant resistances, which affect performance of metallic electrodes.

In practical terms, the space charge layer at the metal-electrolyte interface can be modelled as a voltage source (V_e) in series with a capacitor (C_e) and a resistor (R_e) in parallel (Figure 1.12). This model is valid however only for low frequencies: at high frequencies the impedance can be modelled by an equivalent circuit of a resistor and capacitor in series (Robinson, 1968). With many materials, the values of the simplified components have been determined (Geddes, 1972; Robinson, 1968). However these elements cannot be treated as fixed value capacitive or resistive components as the values of these elements vary with frequency (Gesteland *et al.*, 1959; Kovacs, 1994; Robinson, 1968) and also with material, electrolyte, and temperature. This dependence reflects changes in the double-layer properties with these parameters (Geddes, 1972). Figures 1.10 – 1.14 shows an electrode illustrating the major electrical components: a

metallic tip and an insulated shank. The metallic tip can be represented (when placed in an electrolytic solution) by a resistor (R_e), a capacitor (C_e), and a potential source (V_e). The insulation of the electrode shank separates the metallic conductor of the electrode from the conducting electrolytic solution and therefore can be simply represented (when placed in electrolytic solution) as a capacitor (C_d). The shank and electrolyte resistances are determined by the geometric surface area of the tip (Robinson 1968; Kovacs 1994). The equivalent electric circuit of such a probe in recording conditions (with a reference electrode) is shown in Figure 1.11 and follows directly from the model in Figure 1.13, the resistance of the electrode shank, and the intra- and extracellular liquid resistances are considered negligible in comparison with other elements in the circuit.

The equivalent electrical circuit for the micropipette electrodes is shown in Figure 1.14. The metal-electrolyte resistance and capacitance (R_e and C_e) are negligible owing to the large surface area of the contact between the electrolyte and the wire. The two major components that determine the electrode impedance are the electrode resistance (tip) and the glass wall capacitance (Figure 1.11). The first is the resistance of the electrolyte through the narrow tip opening, and is determined by the tip diameter. The capacitance is determined by the glass wall thickness. Comparisons of Figures 1.11 and 1.14 suggest that the geometric differences between the two electrodes produce significant electrical differences. In metallic microelectrodes the metal-electrolyte interface is located at the recording tip and therefore accounts for almost all the impedance of the electrode.

The electrical properties of a micropipette are dominated by the resistance of the glass tip. Typically, glass micropipettes have DC resistances in the order of 10–200 MΩ, while metallic electrodes may have AC resistances in the order of 1–10 MΩ. Conversely the metallic electrodes operating in an AC mode have lower shunt capacities and thus are more sensitive to changing signal profile. These differences can have a direct impact on the performance of the electrodes for different applications (Gesteland *et al.*, 1959). For example, the electrolyte-filled electrodes will perform as low-pass filters. Therefore, they are most suited for intracellular recording of relatively slowly changing potentials. As noted above the metallic electrodes act as high-pass filters, indicating their use for more rapidly changing signals. The impedance of the electrode,

determined by the materials and geometry, and the impedance of the external path determine the amount of distortion of the recorded signal (Geddes 1972; Gesteland *et al.*, 1959).

The performance of an electrode is largely determined by the event under investigation (either rapidly or slowly changing signals) and, in the case of *in vivo* studies, by the anatomical location. Recordings can be made with the electrode inside or outside the cell. There are several drawbacks to extracellular recording that make intracellular recording such as patch and voltage clamp favoured by investigators. First, as noted previously, information gathered by extracellular sensing may not be exclusive to a single cell, as discussed below this is particularly valid when there is poor sealing between an electrode and the cell membrane. It is normal for the recorded signal to be an average of several cells in the locale of the probe. Second, extracellular probing does not provide information about DC conditions or slowly changing potentials across the cell membrane. Due to the capacitive nature of the cell membrane, typically $\mu F/cm^2$, only the time of occurrence of an action potentials can be recorded, not the details of their form.

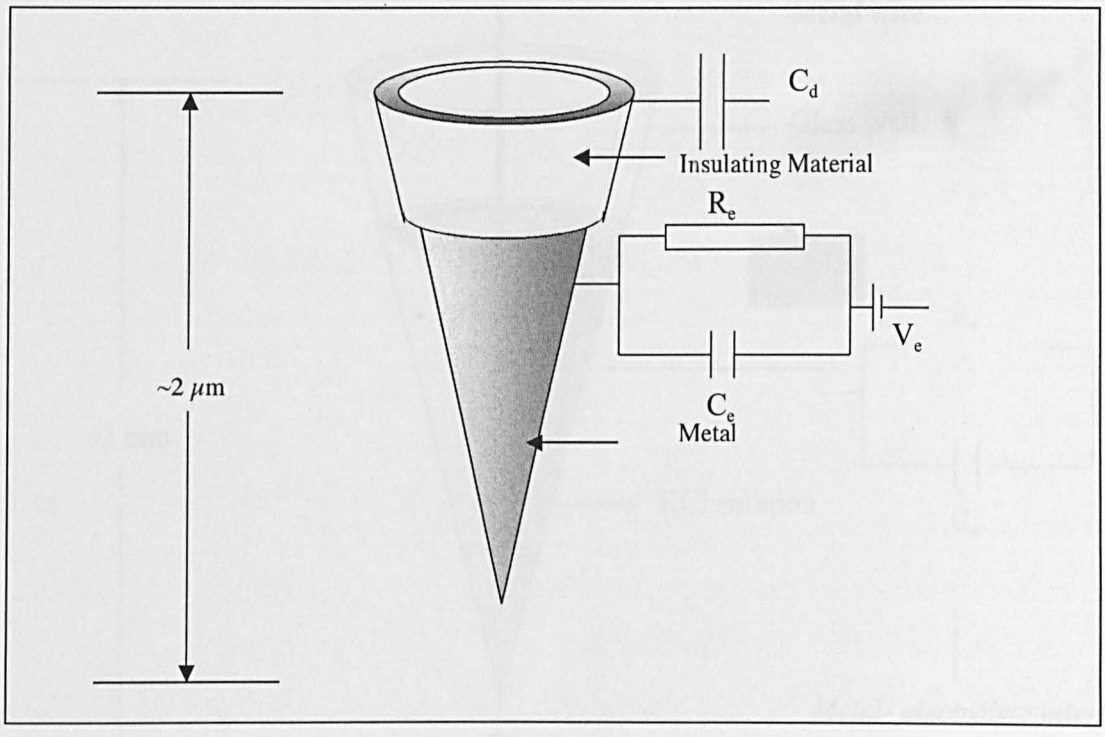

Figure 1.10 Electronic model of a metallic electrode.

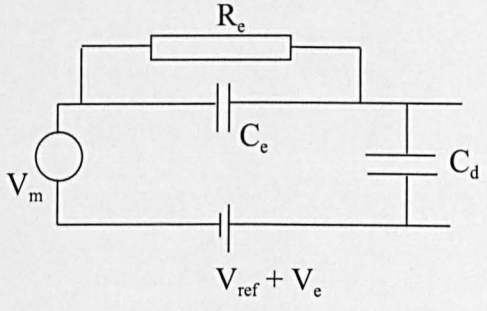

Figure 1.11 A simplified electronic model of a metallic electrode in electrolyte.

V_e = voltage source; V_{ref} = reference voltage; C_e = capacitor; C_d = Shank capacitor; R_e = resistor; V_m = voltmeter.

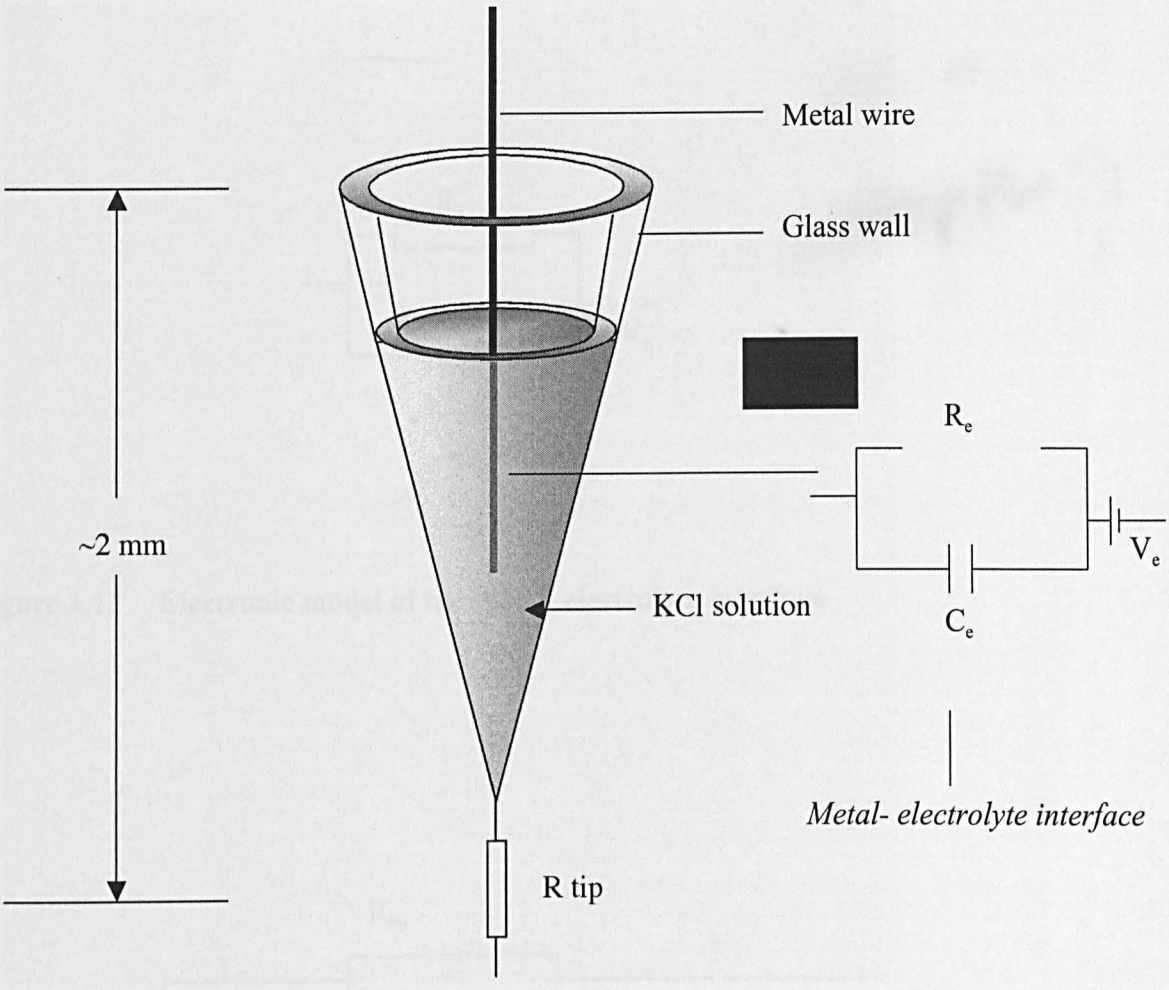

Figure 1.12 Electronic model of a filled glass electrode

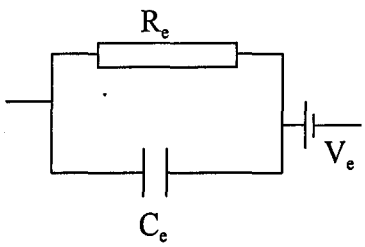

Figure 1.13 Electronic model of the metal- electrolyte interface

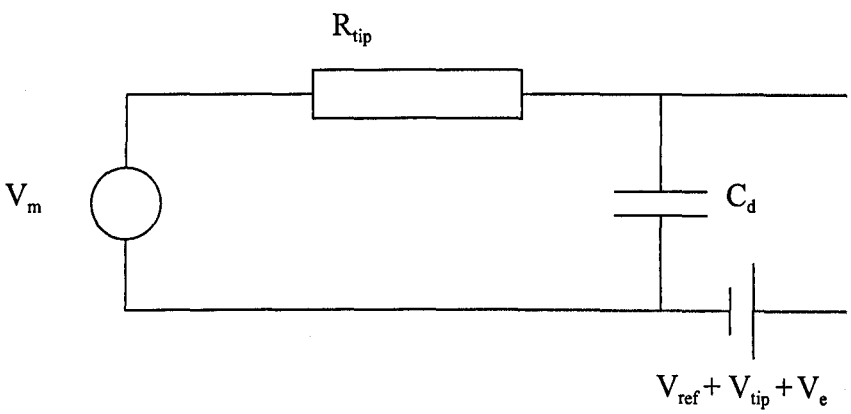

Figure 1.14. A simplified electronic model of a filled glass capillary electrode in electrolyte

1.7 THE USE OF SURFACE MODIFICATIONS FOR THE POSITIONING OF CELLS

1.7.1 Methods for cell positioning, adhesion cues and stimulation

Using planar micro-electrode arrays (MEAs) cells under investigation are required to be positioned with a high degree of accuracy on or adjacent to a recording point. Their relative position to an electrode or contact point must be controlled, due to the low levels of electrical activity in biological systems. Significant determining factors in the recording ability of a device for a single source are: (i) the strength of the original signal, (ii) the permittivity of the medium in which the cell is growing, (iii) the reciprocal of the squared distance between the recording and source, and (iv) any electrical interference generated by the device itself. As most MEAs are used for multiple sources then recording interference from other nearby cells must also be considered.

Neuronal plasticity is the ability of a cell or group of cells to move from their original position, or modify their shape to specific cues. Control of this and general growth is essential for both optimising the position of cells over electrodes and their processing capabilities. Several different methods have been employed to tackle this problem however they fall into two main categories, chemical and mechanical.

Systems for orienting the cells on specific substrates have been proposed: (i) printed chemical cues; (ii) modification of surface topography and (iii) mechanical forces - for instance holding a cell with a micropipette during patch clamp experiments. Heiduschka *et al.* (2001) suggested that the patterned adhesion of neurones and directed growth of neurites are prerequisites to establishing a meaningful *in vitro* model for the study of interactions and signalling between neurones. They propose two models for structured substrates. (i) Silicon, microstructured by etching, resulted in neurones that adhered preferentially onto the bottom of the resulting grooves and wells using polylysine and laminin to aid adherence. (ii) Platinum comb electrodes coated with laminin by electrochemical polymerisation resulted in an outgrowth of axons. This surface modification is cited as suitable for the creation of neuronal patterns with effective

growth of axons *in vitro*. Britland and co-workers (Britland & McCraig, 1996; Britland *et al.*, 1996) compared the relative effects of chemical cues and topography and demonstrated that an optimised topography was more effective, although a combination of the two methods gave improved control of neurite direction when compared to individual methods.

Groups obtaining extracellular recordings from single vertebrate cells have reported neuronal plasticity and neuronal size have affected development and final outcome of investigations, the use of neurones from leeches have provided some researchers with a modified system which provides a mechanism for simple arithmetic using neuronal firing rate encoding as a precursor for the development of a natural neurone language (Garcia *et al.*, 2002). Wilson *et al.* (1994) obtained recordings from large invertebrate neurones. Maher *et al.* (1999a) have reported success with hippocampal slices rat neonates. Groups such as those of Gross (Gross *et al.*, 1977), Jimbo (Jimbo *et al.*, 1992) and the early work by Thomas (Thomas *et al.*, 1972) have provided evidence that plasticity and neuronal selection need not adversely affect experimental procedure.

Fromherz and colleagues have recorded and stimulated invertebrate neurones on silicon electrode arrays (Fromherz & Stett, 1995; Fromherz *et al.*, 1991). A single Retzius cell connected to the open gate of a p-channel field-effect transistor (FET) was put forward as a suitable method for describing the junctions and proposes capacitive coupling of the plasma membrane and the gate oxide, thus accounting for variable resistance of the seal. Jenkner & Fromherz (1997), and Weiss & Fromherz (1997), proposed a method for the measurement of electrical transfer function by immobilising a cell with a glass micropipette on top of an FET (Vassanelli & Fromherz, 1999). This method approached the cell restriction and adhesion problem by adopting and modifying the patch and voltage clamp techniques and recording data directly using the FET. Although this method may be suitable for recording data for short periods (less than 1 hour), compromising the cell membrane results in rapid cell death deeming long-term recordings of the neurone-FET transfer function to be impossible. These investigations however demonstrate different interactions at the silico-neural junctions depending on certain criteria. Fromherz (1999) demonstrated that nearly all neurone-FET junctions

fell into two contrasting groups, with very few intermediates. Group 'A' junctions showed a weak, predominantly first derivative, coupling which equates more to a capacitive response. Fromherz' interpretation of this was that of low ionic conductance at the junction. Group 'B' junctions showed stronger ohmic response, i.e. direct coupling. A suggested explanation of this was voltage independent ionic conduction in the junction. However the physical basis for the two types is open to a number of interpretations, for example Fromherz (1999) attributed type 'A' behaviour to a poor neurone-FET seal and type B behaviour to a leaky cell membrane immediately overlying the FET but not elsewhere. The latter could occur if ion channels were stimulated to open following adhesion of the cell, either due to mechanical neurone-FET contact, or due the accumulation of ionic charge in the small neurone-FET cleft, leading to opening of voltage-gated channels. These channels, either calcium or potassium, are complex proteins. Structurally the calcium channel consists of a pore-forming alpha1 subunit, and associated beta, gamma, and alpha2/delta subunits. There are at least 7 varieties of alpha1 subunit in mammals, and 6 beta subunits, leading to enormous structural and functional diversity within the gated ion channel families.

There are four different types of gated channels which are derived from Ohm's law:-

$$C_m dV/dt = -\sum_k I_i \qquad \text{(Equation 22)}$$

(i) The passive gate lets ions through at a rate proportional to the voltage drop, given by the equation:-

$$I_i = \bar{g}(V - \overline{E}) \qquad \text{(Equation 23)}$$

where g = effective conductance, V= channel potential, E = equilibrium potential

(ii) The persistent gate requires the 'm" activating gate to be open, given by the equation :-

$$I_i = \bar{g}m(t)^p (V - \overline{E}) \qquad \text{(Equation 24)}$$

where m is a dynamic voltage dependent variable that increases with applied voltage, t = time, p = subunit component for each channel (potassium has 4 subunits so p_K=4)

(iii) the transient or inactivating gate requires both the activating gate and the inactivating gate to be open, and is given by the equation :

$$I_i = \bar{g}m(t)^p h(t)^q (V - \overline{E}) \qquad \text{(Equation 25)}$$

where h is a dynamic voltage dependent variable that increases with applied voltage, t = time, q = subunit component for each channel (potassium has 4 subunits so p_K=4)

(iv) the anomalous or activated channel requires the inactivating gate to be open and is described by the equation (ref):

$$I_i = \bar{g}h(t)^q (V - \overline{E}) \qquad \text{(Equation 26)}$$

Such mechanisms are all plausible however it is normal for neurones, *in vivo*, to be in close proximity to other cells over their whole surface, without showing such leakiness. Furthermore, Fromherz and colleagues now report 60-100nm gaps between the silicon substrate and the neuronal membrane, making type A behaviour more difficult to explain (Braun & Fromherz, 1998).

If Fromherz and his colleagues are correct there is little possibility of obtaining the degree of coupling required for reliable recording from electrodes in a silicon substrate in contact with neurone cells. However, their findings on coupling contrast with measurements of the neurone – substrate gap by Interference Reflection microscopy and FTIR microscopy which suggest that the neurones are 10-30 nm from the electrodes (Curtis, 2000). Furthermore the separation of neurones from the substrate will be heavily dependent on the size and shape of any proteins used to adhere the neurones on to the surface.

Thomas and colleagues were able to record from embryonic chick heart cells grown on glass, with a passive electrode array of gold-plated, platinised and nickel contacts, provided that there was a confluent monolayer of cells over the electrodes (Thomas *et al.*, 1972). They stated however that efforts to record from electrodes underlying single,

contracting cells or small cell clumps failed. Regehr *et al.*, (1989) were able to stimulate and record from neurones of invertebrates (leech, slug and snail) on a passive array of platinised Indium Tin Oxide (ITO) electrodes on glass. They noted that the large size (40-200mm) of these neurones allowed them to form seals over the electrodes and when this occurred, they obtained a signal to noise ratio (S/N) up to 500:1.

1.7.2 Signal recording

Standard techniques for neural recording and stimulation using discrete microelectrodes require precise positioning, which is hard to achieve using more than 2 or 3 microelectrodes, maintenance of a recordable signal in the long term, greater than several days, *in vivo* is not commonplace. Electrode arrays have allowed extended recording periods from many neurones simultaneously both *in vitro*, (Boppart *et al.*, 1992; Egert *et al.*, 1998; Maeda *et al.*, 1995; Meister *et al.*, 1994) and *in vivo* (Della Santina *et al.*, 1997). However identification of events in single cells is difficult to obtain at present. To accurately separate and estimate the signal source without the knowledge of the characteristic of the transmission signal is not an easy task and such 'blind signal separation' has received a great deal of attention in recent years. This problem is not unique to the field of MEAs, multi-source and multi-sensor devices such as hearing aids also require discrete signal processing in order to function efficiently. All noise cancellation devices have the common problem of identifying an individual source from multiple signals plus noise, and production of the noise-free output relies on quantifying the source.

Many different approaches have been attempted by numerous researchers: output correlations (Van Compernolle & Van Gerven, 1994), higher order statistics (Thi & Jutten, 1995), array processing, (Bell & Sejnowski, 1995), adaptive noise cancellation (Al-Kindi & Dunlop, 1989) and electronic or artificial neuronal networks (Cichocki & Unbehauen, 1996), each claiming varying degrees of success. Despite the differing approaches, the fundamental idea is that the source signals are independent of each other and have an unique property such as frequency that can be isolated to aid the signal separation.

If the problems of culturing, cueing and signal separation can be overcome then neurones can be incorporated into a biologically interfaced device (BID) as described below. BIDs cover three main types:

(1) *in vitro* biosensors,
(2) intelligent implantable medical devices
(3) biologically interfaced neural networks.

The potential practical and industrial applications of BIDs include: screening of prospective pharmaceutical compounds, the bio-electronic nose (Göpel *et al.*, 1998; Ziegler *et al.*, 1998) and surgically implanted prostheses (Kovacs *et al.*, 1992).

(1) In vitro biosensors

These can be classified as those that quantitatively detect single compounds in complex biological matrices using immobilised receptors or enzymes, and those that sense the viability of intact living cells (viability sensors). The former type of sensor could be improved through the use of PS if the increased surface area of PS compared to conventional silicon substrates can be harnessed. This would result in an increase in sensitivity *via* the immobilisation of a greater amount of receptor or enzyme per unit of surface area. The biotechnology industry represents the main market for viability type sensors. As such the industry is in constant pursuit of sensors which could provide real-time viability determinations of living cells in bioreactors. In addition, the optoelectronic properties of PS could facilitate optical data transmission, hence removing the risk of electromagnetic forces affecting cellular function.

(2) Intelligent implantable medical devices

Most materials currently used in medical implants are bioinert and, as such, do not interact with living systems. This is ideal for mechanical substitutes for replaced body parts, such as artificial hips. However, the integration of a biological system and solid-state device requires information to be passed across the biological:non-biological interface in order to sense a change or effect. For these devices to be 'intelligent' they must also be able to respond to those changes and/or effects and this requires the transduction of information from the biological system to the solid-state device.

Biosensors that use silicon-based devices are currently available for *in vitro* applications. However, a lack of biocompatibility attributed to silicon has prevented its use *in vivo* (Bustemante *et al.*, 1997; Kopp *et al.*, 1996; Svesson *et al.*, 1997; Tanaka *et al.*, 1994). In contrast, PS has good biocompatibility, for example Canham has reported the growth of hydroxyapatite on porous silicon inferring the possible bone implantability of the material (Canham, 1995) and has now further reported manufacturing processes which enhance the biostability of PS (Canham *et al.*, 1999). Furthermore Bayliss *et al.*, 1997a; 1997b) reported the ability of Chinese Hamster Ovary cells (CHO) to adhere to PS. Again, using the optoelectronic properties of PS, optical datalinks to the biomaterial sensor or implant could be employed, removing the risk of electromagnetic forces affecting cellular function. This material could thus facilitate the realisation of devices to replace damaged tissues in the ear, eye, skin or nasal cavity.

(3) Biologically interfaced neural networks

Pine and colleagues at CalTech have developed "the neurochip", a device micromachined on silicon with a 4 x 4 array of metal electrodes, each of which has a caged-well structure designed to hold a single neurone and allowing outgrowth of neural processes (Maher *et al.*, 1999a; 999b). This has only been partly successful, as constraining cells in this way has proved difficult due to the plasticity of the neurones and their tendency for movement. The driving force for this work was the realisation of a biologically interfaced neural network. This technology could lead to the development of parallel processing units capable of positive reinforcement and learning, consisting of a network of living cells receiving and passing computational signals to and from a solid state device.

1.7.3 The realisation of BIDs

The majority of these applications could be realised if it was possible to interface PS-based devices directly with living cells. In order to achieve this the cells must adhere to the solid-state device in a pattern appropriate to the circuitry. Also, a quantifiable signal must be able to travel across the solid state:biological interface and back. Work by Bayliss and co-workers has demonstrated that living transformed cells could be cultured

directly onto PS without an intermediate treatment being applied to make the cells adhere to the surface (Bayliss *et al.*, 1997b; 2000). Significantly, this finding indicates that the interaction is governed by the surface structure and chemistry of both the biological species and its prospective substrate (Curtis & Wilkinson, 1998). Cells are sensitive to the topological, chemical and electrical properties of surface substrates on which they are grown. Knowledge of these factors is crucial to the ability to direct cell growth to a predetermined pattern. Cells cultivated on microstructures made by semiconductor technology grow normally on silicon surfaces covered with microelectrode arrays, as well as on microperforated silicon membranes with square pores (5, 10 or 20 μm edge length at the top and 1.2, 6.2 or 16.2 μm at the bottom (Maher *et al.*, 1999b). The cells spread over the 5 and 10 μm pores, but mostly fail to cover the 20 μm pores. This is a crucial consideration when interfacing a semiconducting material to a cell. Cell growth must be targeted to semiconducting points on a device using an appropriately engineered surface. Cells cultured on titanium surfaces demonstrate that the surface chemistry of biomaterials can selectively regulate the cellular behaviour at the molecular level and, conversely, that molecular biological techniques provide sensitive indicators of the molecular biocompatibility of implant materials (Nordsletten *et al.*, 1996). Anchorage dependent cells (mouse fibroblasts L929 and 3T3) successfully cultivated on microstructures made by semiconductor technology were able to pass through pores in the silicon substrate to the underside of the membrane. Small pores (about 1 μm^2) impeded but did not prevent cells crossing the membrane, whereas medium and large pores were freely crossed (Larrson *et al.*, 1996). In order to quantify the effect of the substrate surface topography on cellular behaviour, planar and micro-textured silicon substrates were produced and made suitable for cell culture by radio frequency glow discharge treatment. These substrates possessed parallel surface grooves with a groove and ridge of varying widths and a groove depth of approximately 0.5 μm. Cell counts proved that neither the presence of the surface grooves nor the dimension of these grooves had any effect on the cell proliferation. Finally, it was observed that the cells on the micro-textured substrates were capable of spanning the surface grooves (Desilva *et al.*, 1995).

The ability of a surface to influence cell adhesion depends upon both the surface and the cell type. In 1996, Grattarola and co-workers investigated the adhesion properties of human red blood cells to silicon dioxide (SiO_2) layers of differing depths, and the effect of doping in comparison with glass (Grattarola *et al.*, 1996). As a result it was suggested that SiO_2 was a possible candidate for future developments towards the functional coupling of living cells to microelectronic integrated circuits. Mrksich and co-workers reported using microcontact printing to pattern the attachment of mammalian cells to self-adhesive monolayers of alkanethiols on transparent films of gold and silver (Mrksich *et al.*, 1997). Contact printing of a methyl terminated monolayer followed by assembly of oligo (ethylene glycol)-terminated monolayers on non-printed regions resulted in cell growth on the printed regions of a gold substrate. This technique has yet to be tried on PS substrates. Webb *et al.*, (1995) investigated the effect of substratum topography on guidance of oligodendrocytes and their progenitors. Chrome-plated quartz discs were used to present ridges and toughs to the primary neuronal cells. The patterned substrata were produced by a modification of the processes used to make integrated circuits, as described by Wood (1988); the etched area consisting of an array of six 3 mm^2 squares, patterned with regular and parallel grooves of consistent dimensions. The use of MEA technology takes advantage of micro-fabrication techniques to construct a wide variety of small electromechanical, chemical and biological devices (Regehr *et al.*, 1989). Silicon-based planar microelectrode arrays were developed with the forethought to allow both *in vivo* and *in vitro* multiple site recording. These devices support the combined capabilities of silicon integrated-circuit processing with thin-film micro-electrode sensing. The pioneering work by Meister *et al.* (1991) has been followed by numerous studies that exploited integrated-circuit technology to build neurological microelectrodes. These devices typically consist of metallic electrodes, such as iridium (Boppart *et al.*, 1992) gold (Egert *et al.*, 1998; Maeda *et al.*, 1995), and platinum (Della Santina *et al.*, 1997), which are photolithographically patterned on passivated silicon substrates. The interconnects are passivated by a dielectric layer. The *in vivo* designs include a release process that separates needle-shaped devices from the silicon wafer. For a review on the design and realisation of thin-film microelectrodes, see Vassanelli & Fromherz (1999). An additional benefit of micro-electro-mechanical systems (MEMS) devices is the wide

variety of additional sensors or effectors that can be integrated with the recording electrodes. With such elements neuronal recording can be linked with chemical stimulation using fluidic channels and valves (Papageorgiou, 2001), or temperature control using micro-heaters (Chen, & Wise, 1997).

Thin-film microelectrodes are produced using standard micro-machining processes. Even though most of these techniques were originally developed for the silicon microelectronics industry, and may include the use of some very harsh chemicals, completed devices made of silicon, noble metals, and dielectric layers, such as silicon dioxide, nitride, or polyamide, are not toxic and can be successfully used to interface with biological elements. A detailed study by Kristensen *et al.* (2001) demonstrated that the coupling between brain tissues and silicon-based chips had little effect on the tissue under investigation. However, the overall compatibility of devices with the biological environment includes several other factors that have to be considered. Bio-compatibility is a very common term to describe a proper interface between a biological system and a foreign element but this is a very broad and often a very poorly defined concept.

To avoid ambiguity, a discussion follows of several specific issues that relate to the interaction between implants and biological systems. The first issue is bio-fouling, i.e. the strong tendency of proteins and organisms to adsorb physically to synthetic surfaces (Horbett, 1982). Bio-fouling by bacteria is a major source of failure for scores of devices, including macroscopic-scale elements such as metal piping (Costerton & Stewart, 2001). Bio-fouling is a very challenging issue and adsorbed proteins are known to clog MEMS devices with small constrictions, such as bio-capsules (Zhang *et al.*, 1998). The driving mechanism for bio-fouling in live organisms is protein attachment. This process may affect various devices such as pH (Auerbach *et al.*, 1994) and glucose (Yang *et al.*, 2000) sensors. In these cases, the adsorbed protein layers directly affect the operation of the sensor. Protein layers are also responsible for various biological responses, such as cell attachment and activation (Choi & Callow, 1994). Cell attachment may interfere with the optimal operation of the device by, for example, reducing its life span or increasing its power consumption (Stelzle *et al.*, 1997). Protein and cell attachment to a device surface may trigger the response of the immune system,

which in turn may result in inflammation. It is therefore important to consider not only the short-term effects of the biological environment on the device (the effects of protein adsorption on electrode performance are known to occur during periods of hours (Auerbach *et al.*, 1994) or days (Choi & Callow, 1994) but also the longer-term effects of the device on the hosting environment. It is important to note that these effects may vary for different applications and biological systems.

Clogging of micro-pipette intracellular electrodes over several hours suggests that protein adsorption may interfere with the recording. In the case of metallic intracellular electrodes, the tips are exposed to protein adsorption. This may affect the recording stability. The components of the device outside the cell are also susceptible to cell attachment. To resolve these problems, surface modification techniques (Hanein *et al.*, 2001; Zhang *et al.*, 1998) can be integrated with standard MEMS processes and can dramatically reduce protein and cell attachment. It has also been shown that a thin non-fouling coating may provide protection to coated electrodes from protein adsorption and cell attachment without compromising their conductivity (Hanein, *et al.* 2001).

Another major problem related to the interface between artificial devices and biological environments is corrosion. Direct contact between the device and the biological system exposes the surface of the device to corrosive aqueous media. The durability of the device is therefore strongly dependent on the properties of the passivation layer and the quality of the adhesion of the different coatings on the device. Passivation layers used in microelectrode fabrication, such as silicon dioxide, silicon nitride, or polyimide, were originally developed as dielectrics for non-corrosive environments and therefore may perform very poorly (failure after several minutes or hours) in electrolyte solutions. The use of these passivation materials for corrosive environments requires special attention. By studying a large number of common barrier materials as a passivation layer for silicon-based microelectrode devices, Faßbender *et al.* (2000) and Schmitt *et al.* (1999) demonstrated that by a careful choice of material and preparation the corrosion resistance of the passivation layer can be maintained for several months. It was shown that by adequate control of deposition conditions and process cleanliness, effects such as stress, pinholes, and particle inclusion were avoided. In return, effects including

buckling and swelling were dramatically reduced and the overall corrosion resistance of the devices was improved.

A major consideration in the design of microelectrodes is their geometric interface with the environment. As previously mentioned, a tight seal between the electrode and the cell membrane is favourable for good extracellular recording. These conditions are very hard to reach with flat electrode designs and a special effort was made, in *in vitro* setups, to improve the sealing by shaping the electrode sites into a cup structure (Regehr *et al.*, 1998). Action potential simulations based on the equivalent electric circuit of neurone-to-electrode contact show significant signal distortions due to inadequate sealing (Buitenweg *et al.*, 2000; Grattarola & Martinoia, 1993). Clearly, good sealing is very hard to realise *in vivo* with thin-film microelectrode devices and therefore, despite their many appealing advantages, their recording capabilities are limited to applications where the understanding of synaptic interactions is important. It is important to note that complete sealing between the recording electrode and the cell membrane may not always be a major problem. This may depend on the level of detail that one requires from the recording and also on the exact experimental setup, ie. whether the recording is performed with brain cells, such as astrocytes, or other nerve cells. MEMs surface electrodes, even without complete sealing, can be used to study brain activity of intact and freely behaving animals (Buzsaki & Kandel, 1998; DellaSantina *et al.*, 1997). The signal-to-noise level is sufficient to allow spike detection and sorting. Improvement of the signal-to-noise ratio and higher signal amplitude can be achieved by fabricating three-dimensional tip-shaped electrodes, tips extending from the two-dimensional surface of the wafer into either the brain slice. Such designs allow electro-physiological recording from inside a cultured tissue (Campbell *et al.*, 1991; Kristensen *et al.*, 2001). Campbell *et al.* (1991) used thermomigration to define p-doped columns in n-doped substrates. A dicing saw was used to define pillars in the p-doped regions. This process permitted the formation of electrically insulated pillars. The pillars were sharpened by a chemical etch consisting of 5% hydrofluoric and 95% nitric acid. Gold and platinum were deposited on the tips with a metal foil used as a protection mask for the base of the electrodes. Thiébaud *et al.* (1999) exploited the anisotropic etching characteristics of silicon in KOH to form 47 μm tall tips. These tips were coated with platinum. As in the

planar microelectrode case, the metal is passivated with an additional dielectric layer. A thick photo-resist was patterned and used as a mask to expose the electrode tips.

Conductors, photo-lithographically deposited on a glass substrate and insulated with polyimide, polysiloxane, silicon nitride or sapphire except at active sites, have been used successfully to stimulate and record electrical activity in cultured neurones in several laboratories (Gross *et al.,* 1993; Jimbo & Kawana, 1992; Meister *et al.*, 1991; Robinson *et al.*, 1993; Wilson *et al.*, 1994). The transparency of these arrays is of great value in monitoring the growth and, using optical probes, the activity of neurones grown on them, but precludes on-chip electronic interfacing. ITO has the advantage that the electrodes are transparent but as long as the surface surrounding the electrodes is transparent recognition of the precise position of cells in relation to the electrodes is fairly easy.

Methods of chemically constraining mammalian cells to a specific site on a substrate have been reported previously (Curtis *et al.*, 1996). For example, laminin and the associated neurotrophins such as ciliary neurotrophic factor (CNTF) and brain-derived neurotrophic factor (BDNF) have been used for guidance. These compounds were selected as they are important in the formation and maintenance of the axons and dendrites of vertebrate neurones. The addition of chemical species to the surface of any substrate will change both its electrical and physical properties. This physical modification is used in optically based *in vitro* biosensors based on PS, where the interaction of an analyte with a receptor gives rise to variations in the Fabry-Perot interference fringes (Janshoff *et al.*, 1998).

The superposition of the constructive and destructive interference of light reflected at the interface can be described by the equation:

$$m\lambda = 2nL \qquad \text{(Equation 27)}$$

where m is the spectral order, λ is the wavelength at which the maxima or minima occurs, n is the refractive index, and L is the physical thickness of the layer. The

principle by which the biosensor works assumes that the PS is pure and has a refractive index (n) = 3.9. The porosity-weighted index would be :

$$n_{eff} = (1-P)n_{si} + Pn_{med} \qquad \text{(Equation 28)}$$

where n_{eff} is the weighted average (effective medium approximation) refractive index of the sensing layer, P is the porosity of the PS matrix, n_{si} is the refractive index of silicon n_{med} is the refractive index of the substance occupying the matrix. The device response is calibrated by introducing molecular species of known refractive index to the PS layer. There have been several methods employed to physically 'entrap' neurones on the surface of their respective substrate, including the creation of shuttered and capped wells and troughs. However as the cell is not adhered to the surface, contact is weak and the cells remain motile (Maher *et al.*, 1999a). This motility causes problems with reproducibility of same-cell recordings. Following the targeted attachment of neurones to the substrate, the ability of the cell to receive a signal must be quantified. This can be achieved experimentally using dyes specific to the movement of an ion such as calcium or a change in voltage. Voltage-sensitive fluorescent dyes can be used for noninvasive multicell recording of electrical activity, and could therefore be useful for studying the synaptic interactions of small networks of cultured neurones. Using voltage-sensitive dyes, Fromherz has suggested that it is, in principle, possible with high temporal resolution to observe the spread of electrical signals in a dendritic tree at all points simultaneously (Fromherz & Lambacher, 1991). Currently available dyes enable a resolution of approximately 10 μm and 0.5 ms on linearly grown cables of leech neurones. The electrical response to somatic stimulation is observed as a time-resolved map. Using dendrites originating from pyramidal rat hippocampi (Meyer-Franke *et al.*, 1995) Lambacher & Fromherz, (2002) reported a resolution of 9μm at a time constant of 0.4ms without signal averaging. The data was interpreted in terms of a tapering cable using the Hodgkin & Huxley equation as a model (1952).

The biotechnology industry currently runs perfused reactors for a number of weeks in the enzymatic production of medicines to which real-time sensors would be of great economic use. Therefore if this technology is to be implemented in *in vitro* sensors the viable period of the cells will have to be increased to periods of weeks. If *in vivo*

implantation is to be achieved the interfaced cells will need to remain viable for the lifetime of the recipient organism. Therefore non-invasive interfaces need to be developed for sending signals between the solid state and living elements of devices. Because of this some groups are now moving towards the use of self-organised cultures and sampling signals at fixed points beneath the culture (Maher *et al.*, 1999b). Even this approach will have its problems as cells adhere to a surface using a sticky extracellular matrix consisting of proteins and sugars. It is predicted that the gap between the cell and the semiconductor surface filled by the matrix must be less than 10nm for an electrical signal to be transduced (Fromherz *et al.*, 1991). This gap is increased if adhesion factors, such as laminin or fibronectin, are coated on the semiconductor surface (Braun & Fromherz, 1998). However, such factors are not required on PS surfaces, and this is one of the great advantages of using PS cell culture substrates.

1.7.4 Passing signals across the silicon:cell interface

Biological signalling can take a number of forms, for example chemical signals, such as the hormones that regulate growth and development, or the electrical signals that travel through the nervous system. The brain consists of a complex network of neurone cells that process information by transmission of electric potentials: the brain is a fast 'biological computer'. Interfacing living neurones in a bio-neural network with silicon-based devices possess a number of problems. Silicon devices operate between +5 and 0 volts while neurones operate between –60 and +40mv. Silicon devices are serial processors that have a 'hard-wired' fixed architecture, in contrast neuronal networks are parallel processors that are plastic and self-organised. The biological requirements of neurones make them intolerant to large variations in temperature and pH, and in constant need of nutrition. Mammalian cells in culture require constant contact with pH-controlled nutrient media (solution) and must be maintained at 37°C. Nutrient media contains electrolytes, sugars, amino acids, vitamins, growth factors and dissolved gases, all of which may interfere with the passage of an electrical signal across the silicon:cell interface.

1.8 AIMS OF THE INVESTIGATION

The initial aim of this investigation was to produce a device which would enable the growth of neuronal cells on various substrates, in particular porous silicon. Porous silicon as a material exhibits the properties of photoluminescence in both air (Canham, 1990) and aqueous solutions (Uosaki *et al.*, 1996), and has a high surface area per square centimetre (Thust *et al.*, 1996). These properties have been used to develop biosensors (Thust *et al.*, 1996) and chemical immobilisation for the identification of various analytes (Sailor, 2001). Furthermore, previous work in this laboratory has demonstrated that porous silicon is non-cytotoxic to B50 cell line (Bayliss *et al.*, 1997a; 1997b).

Brain tissue slice and single cell stimulation are well-accepted techniques for *in vitro* neurophysiology research. The slice preparation provides an excellent access for physiological investigations, the hippocampal slice model being one of the most popular systems for such studies (Andrew *et al.*, 1996; Duong & Chang, 1998; Gluckman *et al.*, 1996; Johnson *et al.*, 2000; MacVicar & Hochman, 1991; Muller & Somjen, 1999; Polischuk & Andrew, 1996; Snow *et al.*, 1983; Turner *et al.*, 1995). Patch clamping and cell entrapment enable specific investigation of the single cell. Traditional research involves electrophysiological measurements with the help of extracellular (field potentials) or intracellular (transmembrane potentials) electrodes. However, these methods suffer from rapid deterioration of the living cell, and/or from lack of compatibility with conventional electronics technology.

The aims of the project and the criterion used were to:-

A. Examine the effect on growth of cells under investigation by:-
    a. Different substrates glass, silicon and porous silicon.
    b. Modification of the substrate surface topography by:-
        i. KOH etch of silicon.
        ii. HF anodic etching to produce differing pore size for differing applications.

c. Distribution and position of cells under investigation relative to the porous silicon substrate.
d. Stimulation of cells grown on glass substrates.

This series of results are discussed in chapter 1

B. Design a device utilising the data obtained in chapter 1 by:-
   a. Identifying a suitable substrate for cell growth
   b. Identifying a suitable conductive layer gold or ITO and a method of modification.
   c. Developing the integration of two or more layers onto the glass substrate to produce a multilayered structure.
   d. Quantify the toxicity of the constructed device and each of its components using established cytotoxicity assays (MTT and NRU).

This series of results are discussed in chapter 2.

C. Test the device produced using equipment currently available.
D. Identify future directions of the developed technology.

CHAPTER 2

CONTROL OF CELL GROWTH ON SILICON AND ITO SUBSTRATES

2 CONTROL OF CELL GROWTH

2.1 INTRODUCTION

2.1.1 Control of cell growth

The interaction of cellular processes such as adhesion, migration, growth, secretion and the expression of genes do not occur randomly, as under normal development they are the result of many factors including their three dimensional position within the developing and mature brain construct. It is this position which triggers, controls and influences each and every cell growth and function. The complexity of this situation means that it cannot be fully reproduced in the laboratory. Cells not only respond to their macro environment, their position in the brain, cerebral blood flow and temperature, for example, but are in many instances more acutely affected by localised specific changes in the micro environment. The latter includes local concentrations of ions, growth factors, molecules on the surface of adjacent cells or the substrate on which the cells are cultured. Modifying the local substrate, using microfabrication techniques on a nanometre scale, enables us to examine the effects of surface modification with respect to neuronal plasticity. Neuronal plasticity is the ability of a cell or group of cells to move from their original position, or modify their shape to specific cues. Control of this plasticity and general growth of cells is essential for both optimising the position of cells over electrodes and their processing capabilities. Several different methods have been employed to tackle this problem however they fall into two main categories: mechanical and chemical.

(1) Mechanical

Since Harrison (1912) reported that the linear arrangement of cells in a spider's web was dependent on the morphological topography of the underlying structure, the substrata have been of interest in the mechanics of cellular control. Loeb & Fleischer (1917) suggested the theory of stereo-tropism, whereby the direction in which cells move and grow is governed by direct contact with solids, fibres or fibrin. Weiss (1934; 1941) termed this "contact guidance". The development of fibroblast type cells was demonstrated to be affected by the topography of patterned substrates (Rovensky *et al.*

1971; Rovensky & Samoilov, 1974). The use of extra-cellular material, fibrils, to orient the growth of cells has been reported by several groups (Gallin & Quie 1978; Clark *et al.* 1990; Curtis & Clark, 1990), concluding that chemotaxis was the leading force of directional cell movement, although topography can be utilised to enhance this response. Multiple grooved substrata have been used by several research groups to manipulate cell growth, with differing cell types and differing degrees of success (Brunette, 1986a; 1986b; Clarke *et al.*, 1991; Dunn & Brown, 1986). This work suggests that topology does indeed play a role, however the depth of channels or grooves used and the cell types chosen, mainly fibroblasts, gives only an indication that topographical modification would work with neurones. Influencing the control of neuronal cells includes cell containment by confining the cell in a cage. For example, Maher *et al.*, (1999) developed a micro-array to trap the cell bodies of individual neurones in close proximity to a recording electrode. This method has also been used by groups such as Jerome Pine's at Caltech and has additionally been modified by Peter Fromherz's group at the Max Planck Institute for Biochemistry, Munich (Fromherz, 1996; Weiss *et al.*, 1996).

(2) Chemical

The chemical methods developed to overcome this specific problem range from patterning the surface of glass or substrate with poly-D:L-lysine to control neuronal attachment, to control of the availability of nutrients and proteins required for normal cellular development (Martinoia *et al.*, 1999). There are seven types of proteins that directly control cell growth: growth factors, growth factor receptors, signal transduction proteins, transcription factors, pro- and anti- apoptotic proteins, cell cycle control proteins, DNA repair proteins. The cell cycle is controlled by proteins called cyclins that regulate the function of cyclin-dependent kinases. The concentrations of these proteins increase and decrease with respect to the phase of the cell cycle. cyclin-dependent kinases thus regulate the activity of other proteins by activating or deactivating them.

2.1.2 Development of the growth cone

The main areas of movement in an immature cell are the areas of growth, specifically the growth cone. Growth cone motility involves adhesion to the respective substrate, membrane flow, and force generation via the cytoskeleton. Lin & Forscher (1995) postulated that adhesion between the growing axon and its substrate might be linked to the actin cytoskeleton. The retrograde flow of actin generates force to move the growth cone forward; the growth cone movement being directed by external cues and regulation of the coupling between cell surface adhesion molecules and the cytoskeleton. Theoretical models and experimental studies of motile cells indicate that a relaxing or programmed failing of the adhesion mechanism is required for cell movement. Rapid movement of the growth cone away from the site of cellular synthesis in the soma suggests that there is only localised transport of synthesised surface molecules and the cytoplasmic machinery involved in movement.

Lauffenberger & Horwitz (1996) modelled simulations describing fibroblast migration via integrins based on cellular experimental findings and mathematical models. The authors suggested that cell migration on a flat homogeneous substrate follows a cyclic process, supporting the observations of Di-Milla *et al.* (1991). The proposed mechanism follows the profile:

(1) Initially, there is forward extension at the front of the cell of a thin piece of membrane and cytoplasm, called a lamellipod.

(2) From this extended cytoplasm receptors adhere to the substrate via specific ligand interactions and stabilise the lamellipod thus preventing its retraction.

(3) Adhesion to the substrate occurs preferentially at the front of the cell; extension of the forming lamellipod requires local polymerisation of actin filaments and their appropriate organisation in order to generate protrusion of the membrane.

It is unclear how polymerisation of the actin cytoskeleton occurs, however two models, the Brownian ratchet model (Mogilner & Oster, 1996; Peskin *et al.*, 1993) and the cortical expansion model (Condeelis *et al.*, 1990), have been proposed. The lamellipod contains actin fibres forming a lattice network that provides mechanical strength. Following lamellipod formation and adherence to the substrate, myosin II-based

contraction of the actin cytoskeleton, together with a disproportionately large number of adhesion receptors towards the front (direction of travel), results in forward movement. Some bonds between adhesion receptors and the substrate then break due to a stronger attachment to the contracting cytoskeleton than the substrata (Palecek *et al.*, 1996). This forward movement causes adhesion receptors to be removed from the surface, which requires that mechanisms exist to replace them at the leading edge; endocytic mechanisms may participate in this replenishment (Lawson & Maxfield, 1995). As the adhesion receptors redistribute, some remain clustered and travel forward to readhere, while others are internalised into intracellular vesicles which move toward the perinuclear region.

Bretscher (1992) and Forscher *et al.* (1992) suggested a reintegration into the membrane followed by forward trafficking via cytoskeletal mechanisms; both groups investigated the effects of physical and chemical cues in order to elucidate this question. As described in the above model, control of migration is dependent upon either controlling the modification molecules, by suspension of the ability of the molecules to unbind, or by providing an insurmountable physical barrier to the advancing cell. Chemically, the control of movement can be, to a limited degree, achieved by modification of the growth factors that the cell is exposed to. The physical constraint approach is dealt with by the hypothesis that the cell will refrain from moving from a preferential substrate to a less favourable one, with the provision that the environmental conditions such as temperature, chemical and growth factors are at optimal levels.

2.1.3 Aims of the investigation

(1) Topographical modifications

In the data presented in this chapter, physical and chemical modifications are examined with respect to both surface modification of the silicon surface and chemical modification of the cellular growth media. As discussed in Chapter 1, silicon wafers can be modified in a number of ways, including etching the crystalline structure with solutions containing KOH. The pattern of etch can be modulated using masking, photolithographic techniques, or doping (by increasing or decreasing the level of ions such as Boron, the dopant, in an area affects the rate at which the substrate is

susceptible to etching). Silicon can also be etched with HF to produce porous silicon (PS). This is done either with or without a potential difference, and combinations of these techniques can also used. The silicon wafers used in this series of experiments were modified to produce ridges, troughs and transitions, each with differing levels of roughness and porosity in order to ascertain the level of surface modification required to produce an area which would prove advantageous for adherence and also inhibit migration.

(2) Dissociated neuronal cells and immortalised cell lines

Mammalian neurones can be mechanically and enzymatically dissociated from brain tissue and grown in culture for months. The longevity of the neuronal culture is dependent upon maintaining sterility, temperature, pH, osmolarity and oxygenation, and providing a supply of the required growth supplements. This technology, reviewed by Banker & Goslin (1998), although not new is still being modified and developed. During the first week in culture the neurones extend many dendrites, form synapses and begin to develop spontaneous activity (Basarsky *et al.*, 1994; Gross *et al.*, 1993; Ramakers *et al.*, 1991). The activity patterns in these cultures continue to develop in the following weeks, the changes in the firing patterns being accompanied by morphological changes and greater and more elaborate dendritic and axonal junctions and connections (Corner, 1994). It is more common to have terminally differentiated neurones cultured. Glial cells, if they have not been removed, will continue to differentiate and only tend to be limited by contact inhibition, unless exogenous inhibitors of division are used (Banker & Goslin, 1998). Glial cells provide essential trophic factors for the cultured neurones (Meyer-Franke *et al.*, 1995); Pfrieger & Barres (1997) reported that the presence of glial cell trophins are crucial for neuronal survival and are also required for the development of synaptic process systems. Mammalian nerve and muscle cells can be distinguished from glia, and most other cell types, by their electrically excitable membranes (Kuffler & Nicholls, 1966).

Work in this area has, in the past, used leech neurones - these cells are approximately 500μm in length which makes them relatively easy to handle, enabling their direct positioning onto recording devices, and they are also well-profiled as a cell type

(Fromherz, 1996; Weiss *et al.*, 1996). As the concept behind the development of the device was to enable the recording of mammalian neuronal cell types, both the scale of a device developed for leech neurones and the electrical characteristics would be unsuitable for this function. Thus, B50 cell line, which are much smaller (approximately 30μm in length), have been used in the present experiments. This ethylnitrosourea induced tumour cell line is reported to have sodium channels I and II, a spontaneous regenerative action potential and an ability to grow on the surface of the culture dish (Baines *et al.*, 1992). The level of adherence is weak compared to other cell types, although a lower level of secretion of protein containing hydroxy-proline is suggested as a probable reason for this (Schubert *et al.*, 1974).

The reasons for using a specific neuronal cell line rather than culturing cells from neonate donor rats were two-fold:

(1) Validation of the theory required that the substrates were able to support neuronal cell growth from a cell line that possessed an ability to regenerate an action potential, either spontaneous or induced, the B50 cell line fulfils this requirement.

(2) The profile of the cells used in the investigation should remain constant, as the cell type is to be used as a tool to investigate other variables. Unlike neurones, B50 cell lines have the ability to divide whilst maintaining many characteristics present in neurones such as regeneration of action potentials.

2.2 MATERIALS AND METHODS

2.2.1 Cell culture and preparation for imaging

(1) Source of the cell line

The original B50 cells were obtained from the European Collection of Animal Cell Cultures (ECACC; Porton Down, UK) and supplied in dormant state under liquid nitrogen. The cell line was cultured and then frozen in liquid nitrogen according to the protocol described below. These passaged cells were then used as the initiator cells over the period of the study, and thus were as close to the original profile as possible.

(2) Initial passage

Cells were grown in Dulbecco's Modified Eagle Medium (DMEM) supplemented with 10% foetal bovine serum (FBS), 1% L-glutamine, and 1% penicillin–streptomycin. Cultures were grown at 37°C in an atmosphere of 100% humidity and 5% CO_2. The cells were cultured for four passages prior to storage in liquid nitrogen.

(3) Cell freezing

Freeze medium was freshly prepared, by adding FBS (10% v/v) and DMSO (dimethyl sulphoxide; 10% v/v; 25% stock) to DMEM.

Cells, as cultured in supplemented DMEM, were harvested and centrifuged at 15,000 rpm for 4 min. The supernatant was discarded and the pellet resuspended in 5 ml freezing DMEM, at a density of $1x10^7$ cells ml^{-1}. 1.5 ml aliquots were dispensed into 2ml cryo-vials (Nunc), sealed and labelled. The cryo-vials were then placed in a container lined with sterile cotton wool and transferred to a -80°C freezer. After 2 hours the vials were transferred to liquid nitrogen for storage until required.

(4) Experimental passage

Two vials containing frozen cell suspensions were removed from liquid nitrogen storage and placed in a water bath (37°C) for 2 min. Following defrosting, the contents of each vial were transferred to separate centrifuge tubes and 5 ml supplemented DMEM (37°C) added. The tubes were then centrifuged (15,000 rpm, 4 min), the supernatant was discarded and the pellet resuspended in 5 ml supplemented DMEM. Cell viability and density were determined using the Trypan Blue exclusion test, whereby Trypan Blue (10 µl) was added to the cell suspension (10 µl), placed in a Thomas haemocytometer and viable cells (those remaining non-stained) counted. The cells were then seeded in a T75 tissue culture flask (Steralin) at a density of $4x10^6$ cells per ml. The cell line was passaged once before being used for experimental work.

(5) Glutaraldehyde fixation

Cells were subjected to glutaraldehyde fixation prior to scanning electron microscopic imaging (see below). DMEM was removed from the culture plate wells, cells were washed twice with PBS, and then immersed in 3 ml PBS containing 25% glutaraldehyde for 1 h at 4°C. This was repeated for 50, 75 and 100% concentrations of glutaraldehyde. The cells were then washed in ethanol and dried under nitrogen.

(6) Incubation with fluorescent dye

(i) Prior to imaging via confocal microscopy (see below), cells were cultured on the silicon substrates for 30 h in supplemented DMEM. Once 70% confluency was achieved, samples were washed in PBS and then incubated for 30 min in PBS containing 1 $\mu l\ ml^{-1}$ Ca OG488 dye (Molecular Probes).

(ii) Prior to investigation of signal propagation (see below), cells were cultured on glass coverslips (22 mm in diameter; Chance Proper Ltd., Wareley) for 30h in supplemented DMEM to form semi-confluent (70%) layers. The samples were then washed once in PBS (containing potassium chloride and calcium chloride) and then incubated for 30 min in PBS containing 1 $\mu l\ ml^{-1}$ Fura 3 dye (Molecular Probes).

2.2.2 Substrate preparation

(1) Mask production

Masks DMU1a through to DMU2d were prepared by photographing a laser-printed image (1200 dpi) as the patterned template onto a 4" x 4" plate camera. Masks DMU3 and above were designed using Adobe Photoshop and Freehand and printed onto a lithographic acetate sheet using a RIP4000 assembler at a pixel size of 10.34μm.

(2) Photoresist masking

A p-type silicon wafer (20 Ωcm), with surface orientation 100, was dried at 180°C for 35 min. Positive Photoresist (Kodak; 2ml) was applied to the centre of the wafer, which was then spun at 200 rpm for 30 s, followed by 400 rpm for 3 min. The wafer was baked at 85°C for 1 min and then placed in the mask aligner. The required mask was

selected and the wafer exposed to UV light for 17.5 s to polymerise the exposed photoresist. The photoresist was developed by immersion for 1 min in developer 1, followed by 2 min in developer 2, both under constant agitation. The wafer was then flushed in RO water for 15 min and dried under a nitrogen stream.

(3) Silicon etching

Following masking, the p-type silicon was either:

(i) Placed in a PTFE cell and exposed to KOH (0.1M) for 15-20 s. Each sample was then washed in RO water for 5 min. This process resulted in the production of troughs and ridges.

(ii) Placed in a PTFE cell containing a platinum counter electrode. The wafer was then exposed to an HF etch solution (HF:ethanol; 1:2) and anodised with a current density (J) of 20 mA cm^{-2}, for 10-30 min. Each sample was then washed in RO water for 45 min. This process resulted in the production of photoluminescent porous silicon.

2.2.3 Microscopic imaging of cells cultured on silicon substrates

(1) Scanning electron microscopy (SEM)

To determine a standard growth profile the B50 cells were cultured for five days on glass coverslips until a 70% confluent layer was present. The cells were then fixed by immersion in sequential glutaraldehyde concentrations (see above). The fixed cells were then coated with a 15nm layer of gold which was sputtered onto the coverslip (Edwards sputter coater S150B) and imaged via SEM (Leica S430). This procedure was repeated for both *n*-type silicon and porous silicon, optimising the protocol from Banker & Goslin (Banker, 1998) for each of the substrates.

(2) Confocal microscopy

Following incubation with Ca OG488 fluorescent dye (see above), imaging was carried out using the SYCLOPS confocal microscope (Station 13.1a, Daresbury Laboratory, Warrington, UK). The light source was either a HeCd nitrogen laser for continuous beam (offline) or the Synchotron (for pulsed beam, using single-bunch mode online).

The recordings produced a 100 x 100-μm (X x Y) image. The Z plane 'slices' were collected at height separations of 5μm. The data collected were stored in TGA format for subsequent analysis.

2.2.4 Analysis of cell distribution on microstructured substrates

SEM was used to examine cellular distribution, following glutaraldehyde fixation and gold coating (see above). A grid was applied to the SEM micrographs, enabling cell counts to be performed which related to the positions of the cells on the substrates (NIH Image for Macintosh; http:\\NIH.gov.org). The count was then calibrated to determine the number of cells per available unit area. Areas were thus designated either ridge, trough or plateaux.

2.2.5 Signal propagation

Cells cultured on coverslips were incubated with Ca Fura 3 fluorescent dye (see above), the samples were then positioned above the photodetector (Station 13.1b, Daresbury Laboratory) and stimulated mechanically by depressing a glass rounded end rod onto a small group of cells. The recordings were collected as a data file of light intensity against time, using a Canberra data collector. The data analysis was carried out at De Montfort University.

2.3 RESULTS

2.3.1 Profiling the B50 cell

Cell morphologies were determined on glass (Figure 2.1), *n*-type silicon (Figure 2.2) and porous silicon (Figure 2.3). Alignments of cells on all substrates were random, the cells being approximately 25 to 40μm in length and 5 to 25μm in width. The growth cone was noted as being flat with many projections. The body of the cell also had projections of an extracellular matrix (ECM; Figures 2.2 and 2.3); these indicate points of attachment between the cell body and the surface.

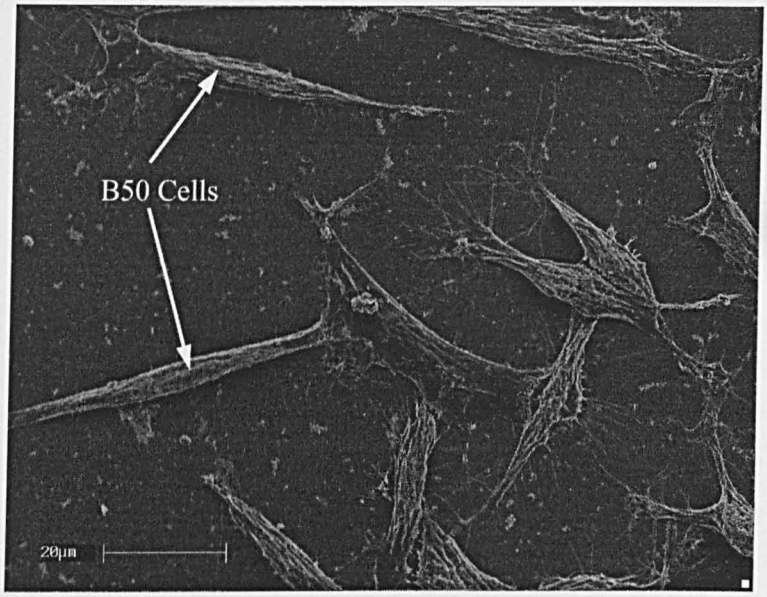

Figure 2.1 **B50 cells cultured on glass coverslips, fixed in glutaraldehyde 72 h post seeding, coated in 10nm gold and imaged using a Leica S430 SEM.**
Scale bar represents 20µm

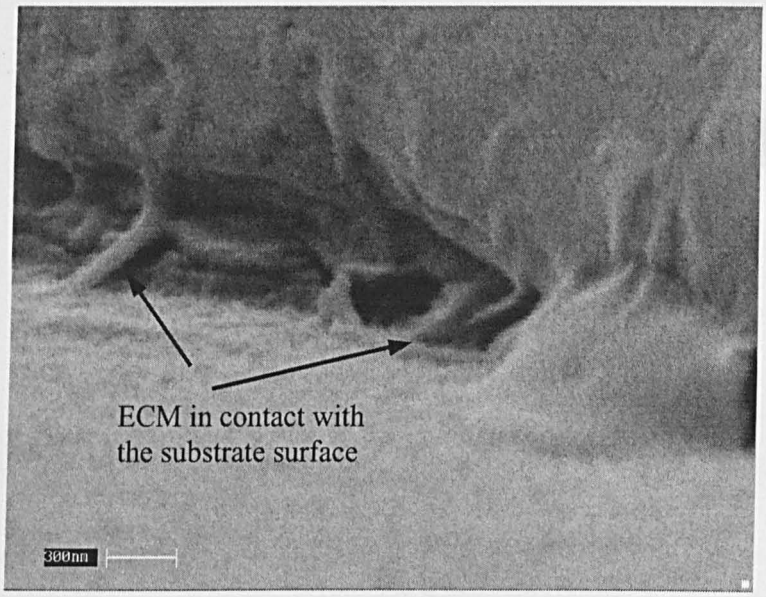

Figure 2.2 **Extracellular matrix (ECM), on the surface of the B50 cells, in contact with the substrate (*n*-type silicon). Scale bar represents 300 nm**

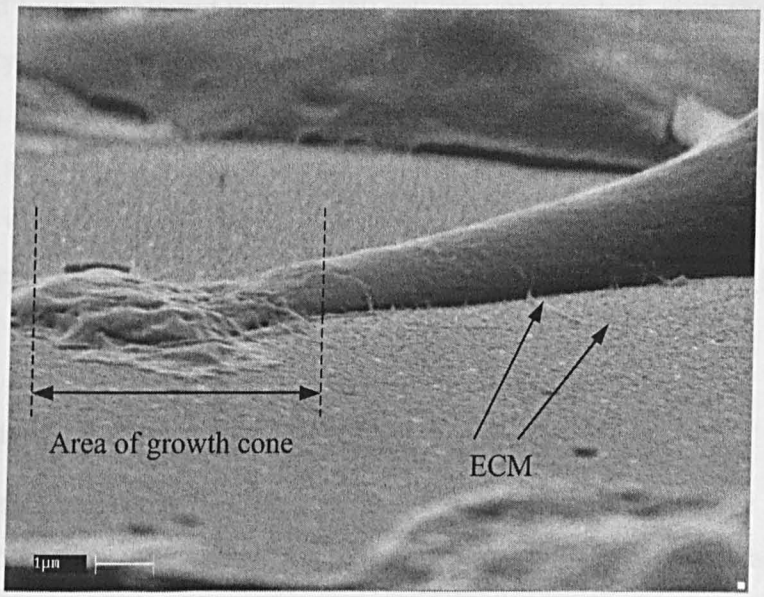

Figure 2.3 **Axon of B50 cell cultured on PS, 72h post seeding, showing the ECM and the growth cone.**
Scale bar represents 1 µm

2.3.2 Substrates

Once it had been established that the B50 cell line grew on both glass and the various silicon subtypes the next stage was to investigate the etching of silicon and any effect on cell growth. P-type silicon wafers were etched according to the KOH etching protocol to produce a profile as shown in Figure 2.4. The effect of an HF etch directly on the photoresist was also investigated to measure the level of detail that could be achieved using conventional HF and photolithographic techniques. The results are presented in Figures 2.5 –2.8, and discussed below.

2.3.3 Photolithography

The photolithography technique requires the deposition of either positive or negative photoresist onto the substrate which is then fixed using ultraviolet light. The resolution achieved with this technique is governed by the wavelength of the light used (the optics of any such system is accurate to half the wavelength of the light used), grain size of the photoresist and, for each of the photoresists, different post exposure processing techniques and annealing.

(1) Negative photoresist

Application of the Kodak negative photoresist resulted in the production of rounded edges (Figure 2.6). These feathered edges would make the design of small tightly interfaced junctions more difficult. Figure 2.7 shows the effect of reversing the mask to produce dots on the surface of the silicon however, as can be seen, the resolution was not maintained and bleeding of the dots occurred, producing a wavy line. The transition areas formed (Figure 2.8), also proved to be susceptible to erosion during HF etching, thus weakly attached photoresist was prone to damage.

(2) Positive photoresist

The positive photoresist contained a smaller grain size and consequently produced an improved resolution compared to the negative photoresist. This, together with easier removal (using isopropanol), made it a better candidate for the masking of the device.

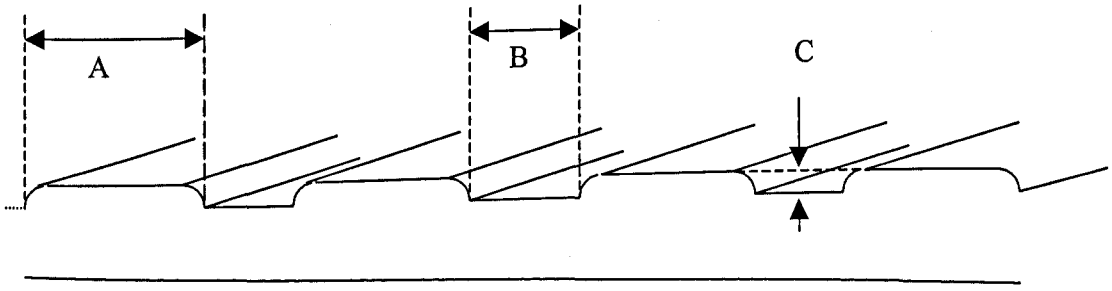

Figure 2.4 **Etch profile**
A = 97μm, B = 80μm, C = 6μm

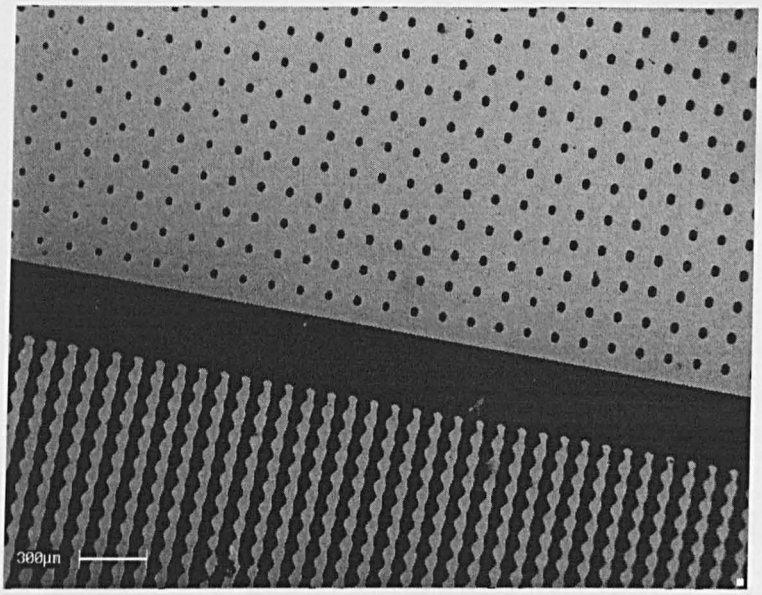

Figure 2.5 **Results of photolithographic deposition of the DMU1a mask on silicon using negative photoresist. Exposure time 15 s. Scale bar represents 300 µm**

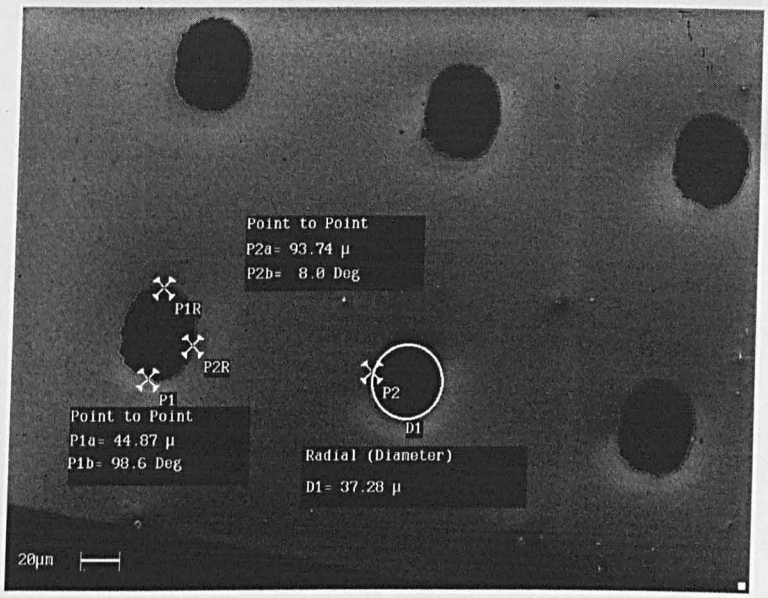

Figure 2.6 **The negative photoresist produced a mask with approximately circular areas of 40µm size however, as can, be seen the edges produced are feathered and are likely to be susceptible to erosion by HF.**
Scale bar represents 20µm

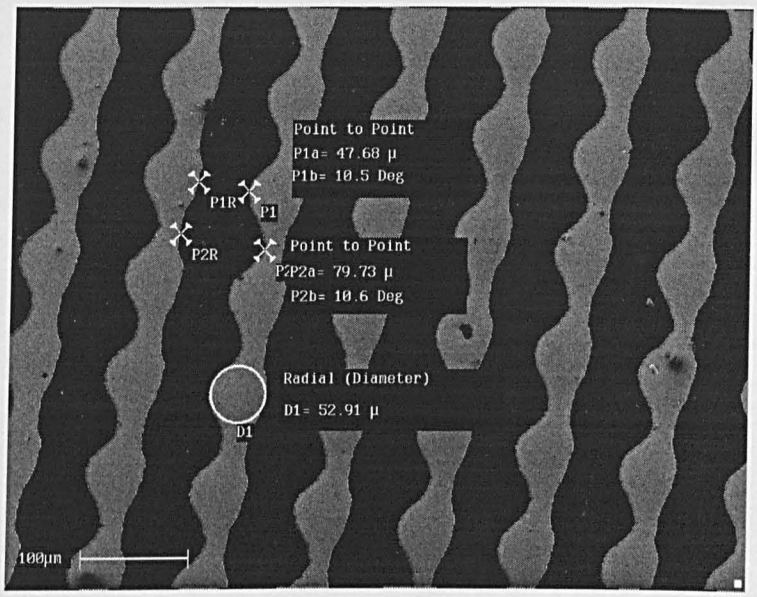

Figure 2.7 **Using a negative of the original image to produce individual spots of photoresist on the surface of the silicon produced a wavy line at the 50µm scale, indicating that achievable resolution was inadequate for this project.**
Scale bar represents 100 µm

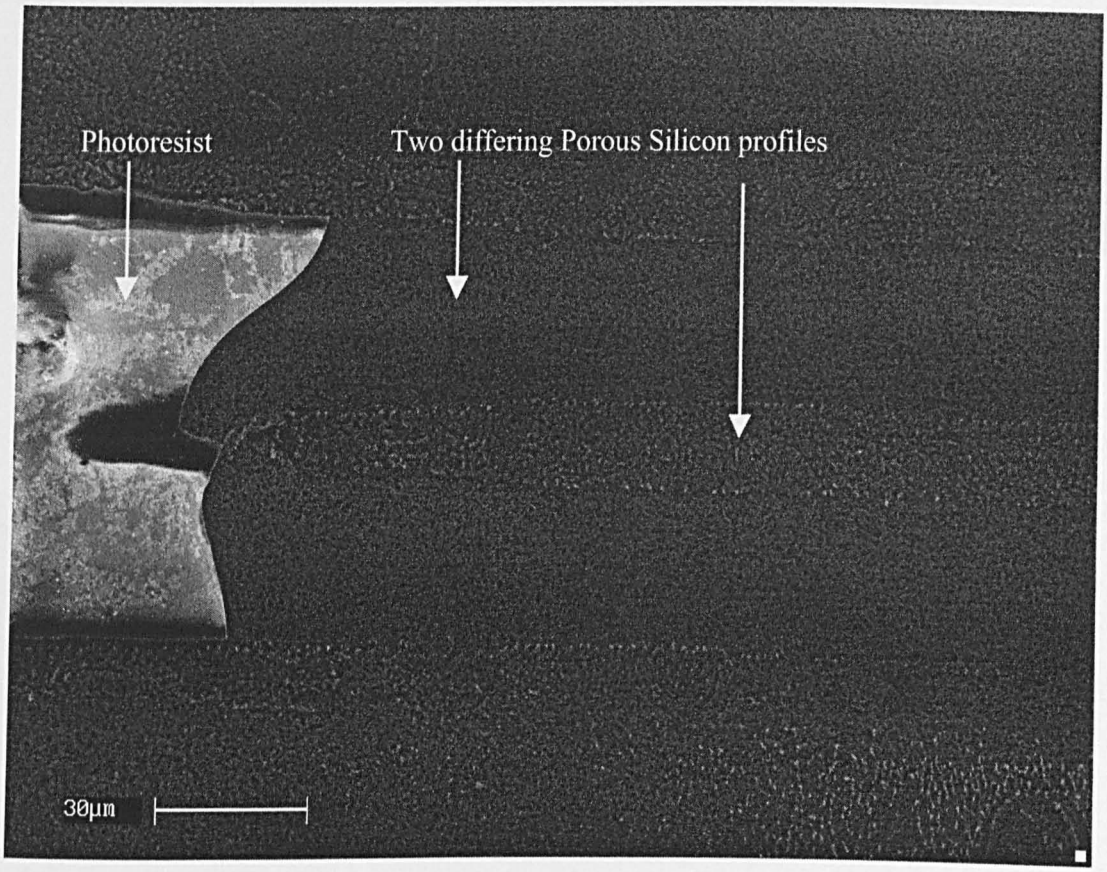

Figure 2.8 **Differing porous silicon profiles achieved by a sacrificial layer of photoresist.**
Scale bar represents 30 µm

Once a technique for producing a mask, and its subsequent removal, had been established then the development of a protocol for anodic etching to form a porous substrate was required.

2.3.4 Macrostructure

To investigate the preference of B50 cells for a specific macrostructure profile an analysis was carried out of cell distribution on differing topographies following surface modification (section 2.2.4). The relative cell counts on plateaux, troughs and ridges were 65, 32 and 98 respectively. The results of this series of experiments indicated a profile which was etched with both KOH and HF, producing an area that was heavily eroded and porous (Figure 2.9), providing anchorage points for cell growth. Figure 2.10 shows cells grown on this region, contact being predominately in the ridge areas (Figure 2.11).

Figure 2.12 demonstrates the effect of differences in localised current densities during anodic etching. The microporous (< 1 μm) structure is visible in area A, which is revealed following the electropolishing and subsequent removal of a layer of silicon. The mesoporous (1 - 2 μm) structure can be seen in area B and macroporous (> 2 μm) structure in area C.

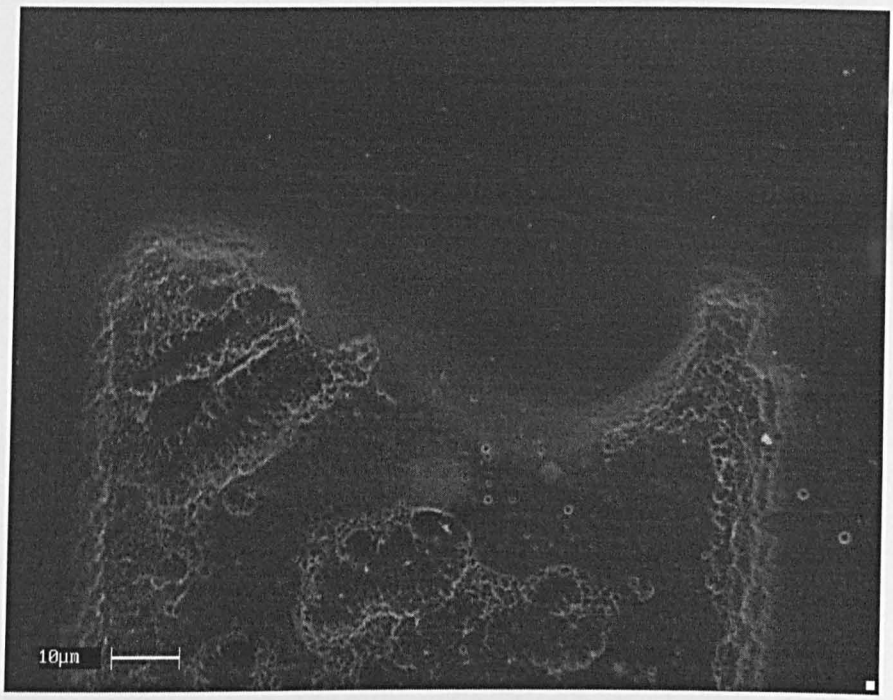

Figure 2.9 **Pre-seeding SEM view of KOH etched porous silicon. Scale bar represents 10 µm**

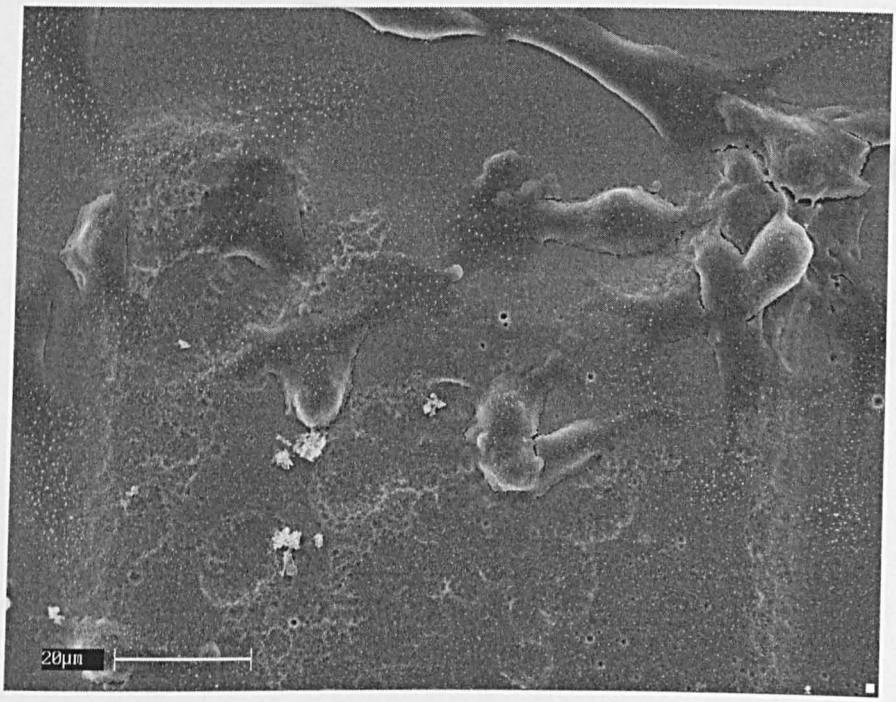

Figure 2.10 **SEM view of KOH etched porous silicon 48 h post seeding.**
The same area as Figure 2.10, showing B50 cells attached on ridges.
Scale bar represents 20 µm

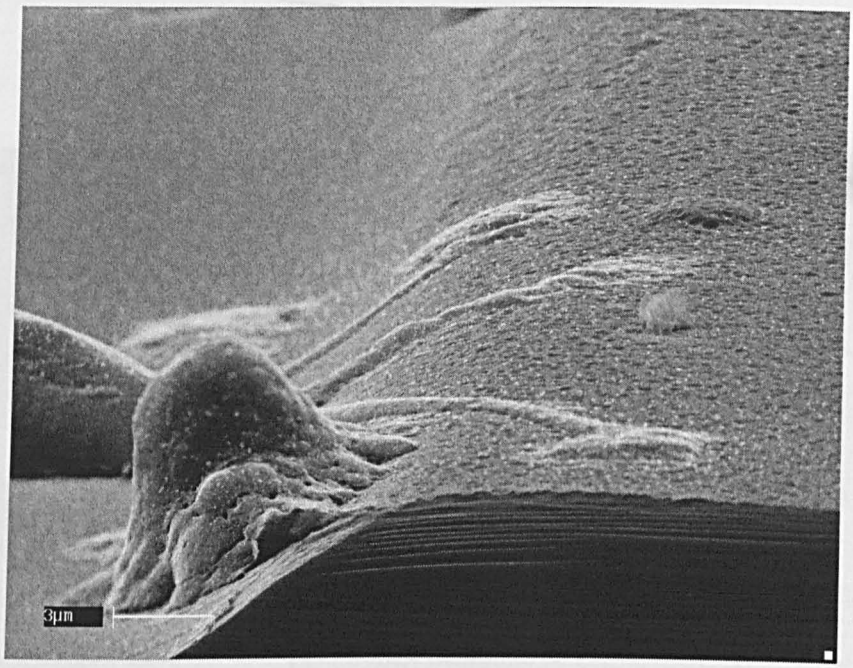

Figure 2.11 SEM image of B50 cells cultured on porous silicon patterned with 100 µm lines separated by 100 µm.
Scale bar represents 3µm.

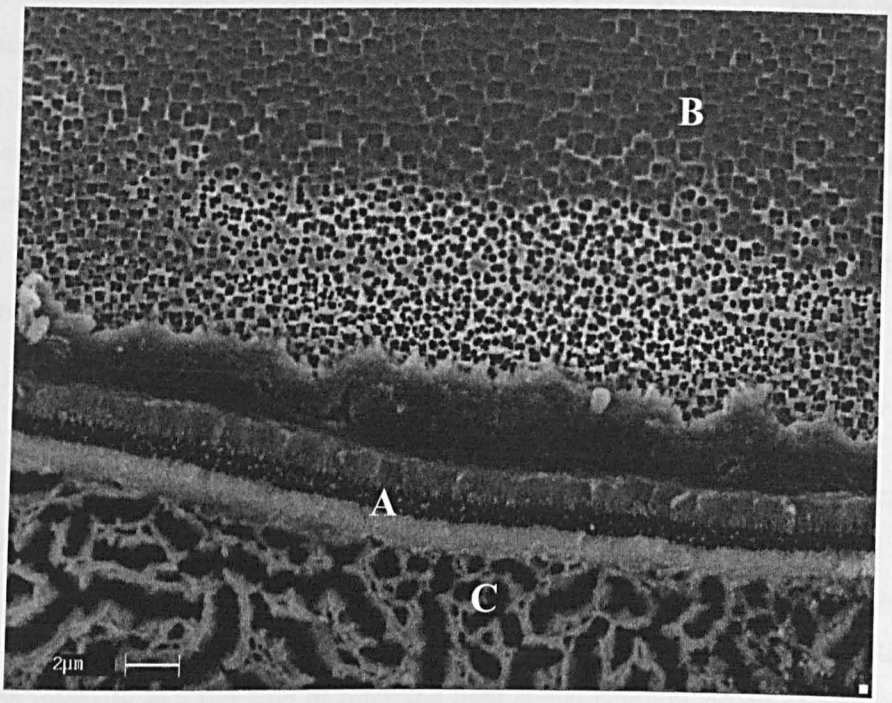

Figure 2.12 **An example of porous silicon demonstrating differing pore sizes, generated by modification of local current density.**

A: microporous < 1 μm;

B: mesoporous 1 - 2 μm;

C: macroporous > 2 μm.

Scale bar represents 2 μm

2.3.5 Anchorage

The use of SYCLOPS (station 13.1a, Daresbury) enabled investigation into the depth at which the extracellular matrix penetrates the porous silicon structure. In the current study, sequential z plane images of a B50 cell cultured on a porous silicon surface were produced following development of the method reported by Löster & Hortstkorte (2000). A composite of two z plane images shows a porous silicon substrate and B50 cells artificially coloured in brown and green respectively (Figure 2.13). Sequential data was collected as a series of images (Figure 2.14); these were then assembled to give a 3D image of the cell and its relationship to the PS layer. The position of the cell appeared to follow the contours of the PS substrate.

2.3.6 Signal transduction

Signal transduction in the cellular matrix was also investigated using Fura3 calcium dye. Mechanical cell stimulation and signal propagation studies were carried out (station 13.1b, Daresbury) using the setup shown in Figure 2.15. The results of these studies are shown in Figure 2.16. This graph shows the variation in Ca^{2+} dye light emission intensity as a function of time, the light signal being recorded 15 mm from the stimulation point. Although there is a loss in signal in one time region, the response shown is the best signal:noise measured.

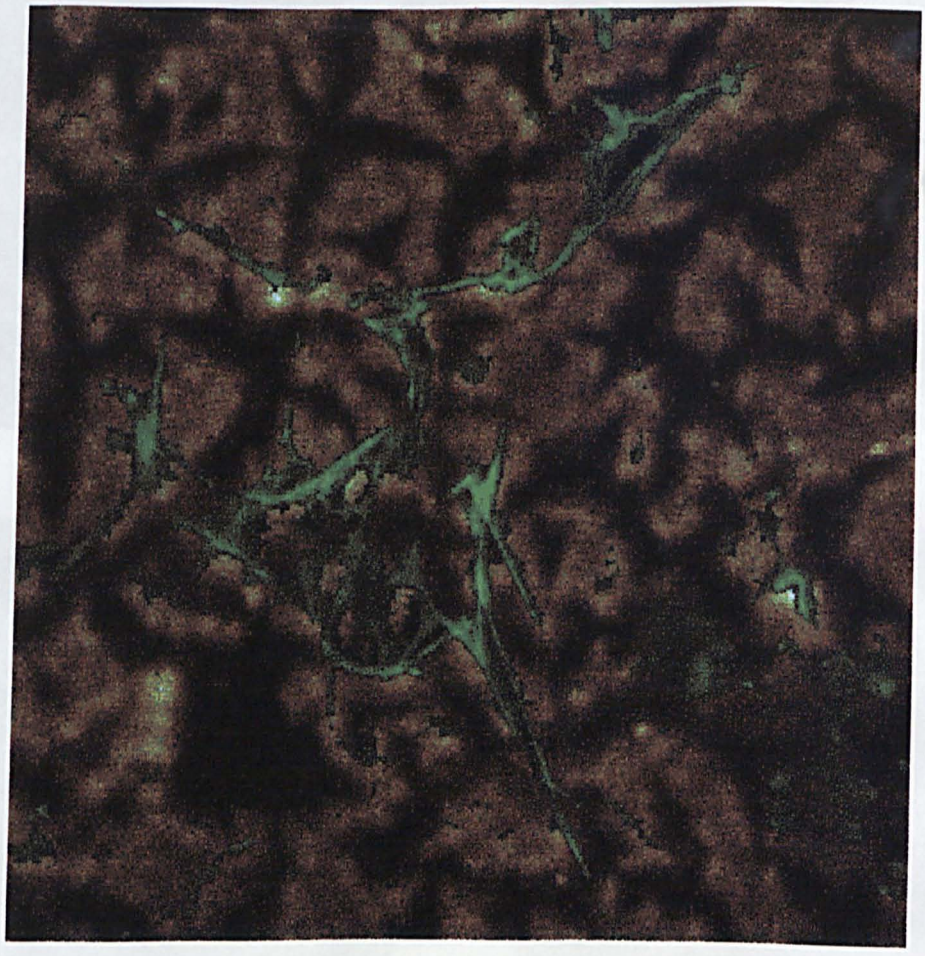

Figure 2.13 OG488 dye image of a B50 cell superimposed on the image of the substrate.
The same area was recorded for both images, and the height separation was 30 µm. The image size is 100 x 100 µm, and was obtained using SYCLOPS, (station 13.1, Daresbury).

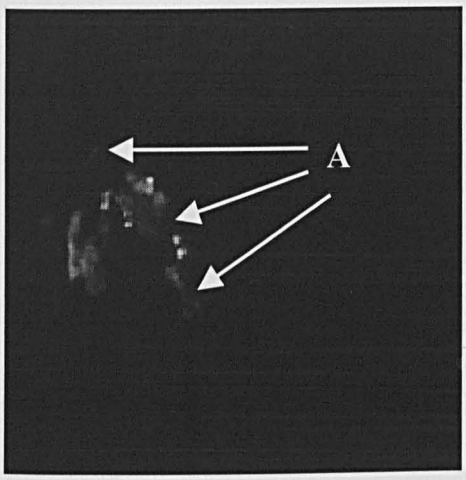

Frame 1

Frame 2

Frame 3

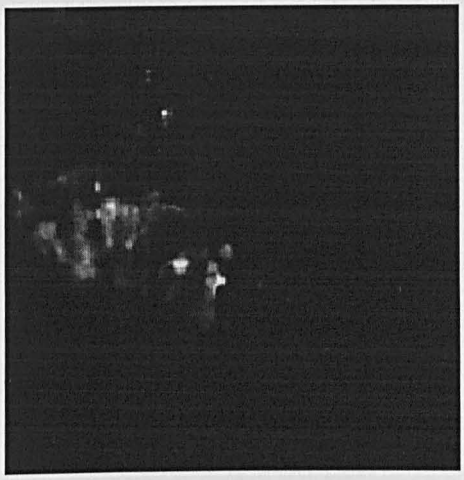

Frame 4

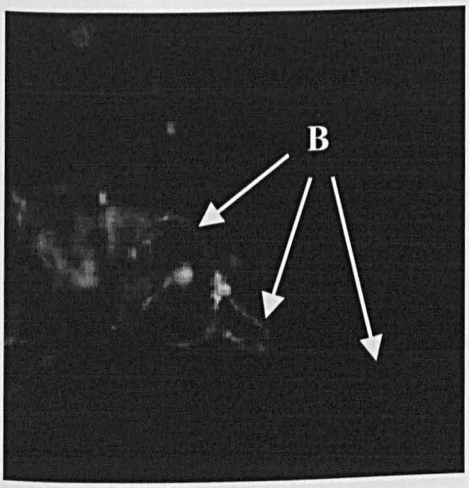

Frame 5

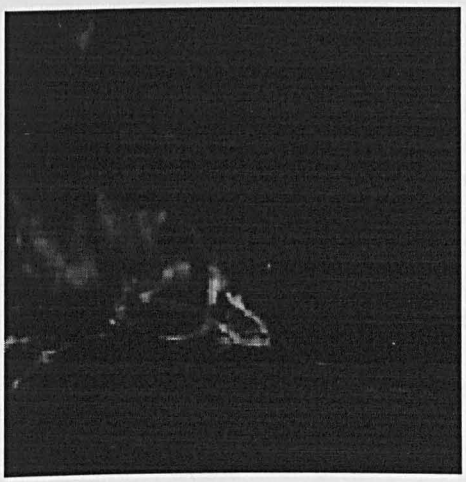

Frame 6

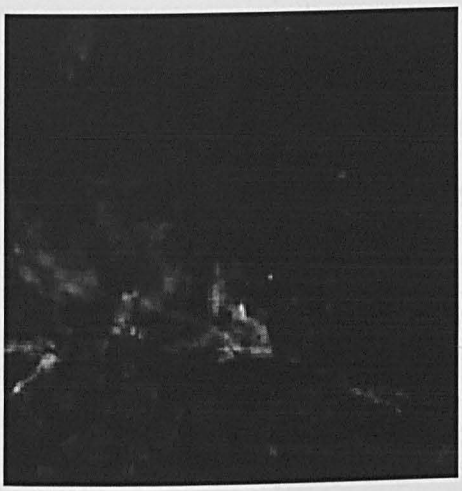

Frame 7

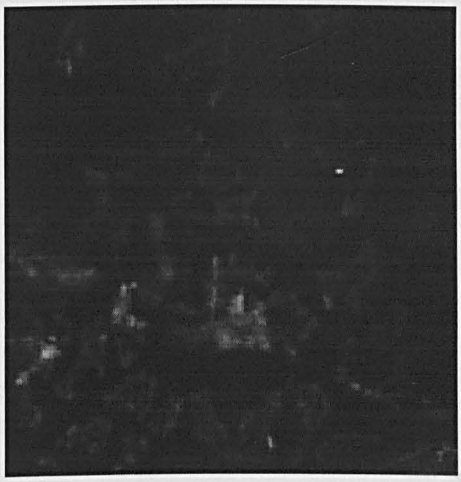

Frame 8

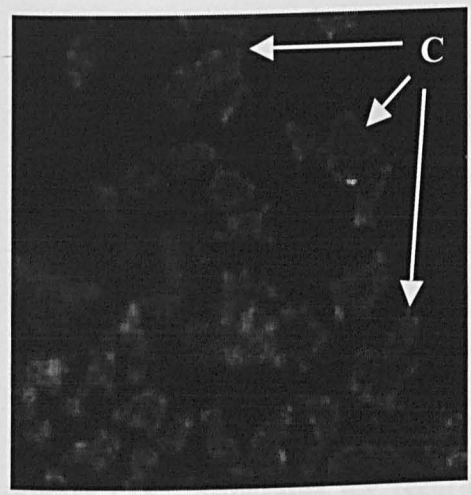

Frame 9

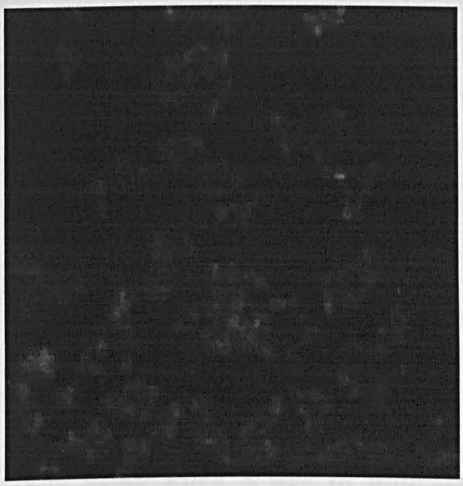

Frame 10

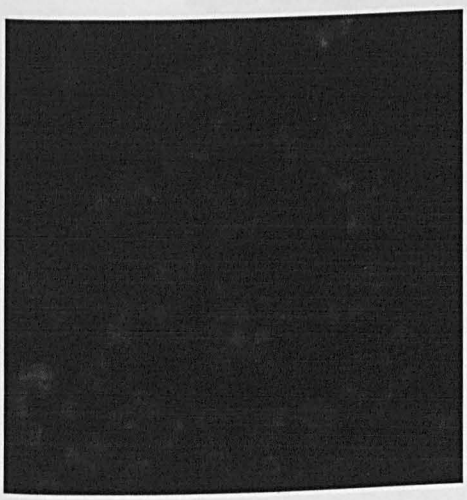

Frame 11

Figure 2.14 Composite frames.

Sequential frames from the confocal microscope (Daresbury) in the z plane. Frame 1 is collected at the upper surface of the cell (A), as the in focus plane travels through the z plane the cytoskeleton (B), can be seen in frames 5, 6 and 7. The substrate, PS (C), can be seen from frames 6 through 11.

Each frame 100 x 100 μm

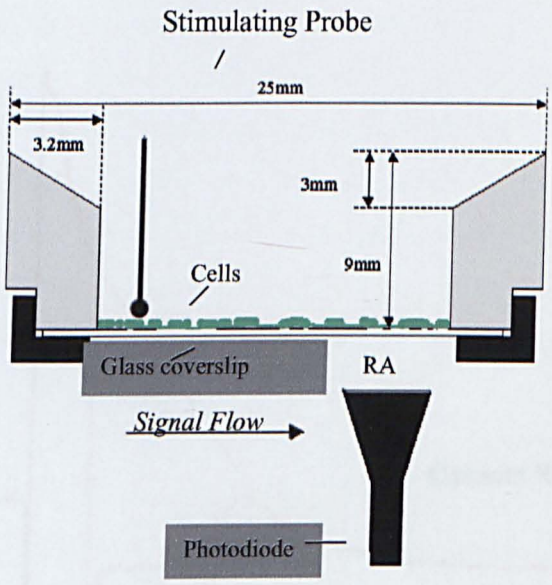

Figure 2.15 Apparatus for recording Ca^{2+} flow using Fura 3 dye to indicate signal through a confluent layer of B50 cells.

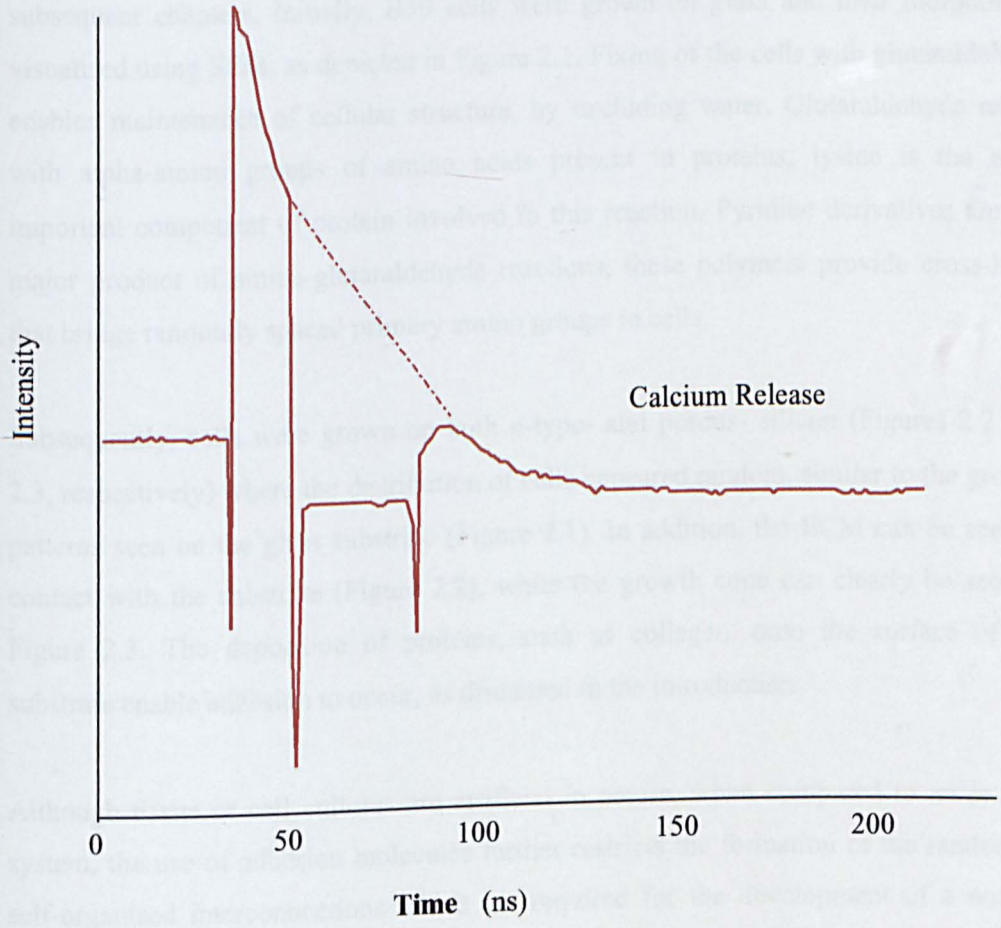

Figure 2.16 Signal progression across a network.

Intensity of light emitted by Ca^{2+} dye in a living neural network as a function of time, measured 15 mm from a cell stimulation point. For these studies, cells were cultured on a coverslip, stimulation was provided mechanically, and the optical signal recorded from underneath.

2.4 DISCUSSION

The data obtained from this series of experiments laid the foundation for work in subsequent chapters. Initially, B50 cells were grown on glass and their morphology visualised using SEM, as depicted in Figure 2.1. Fixing of the cells with glutaraldehyde enables maintenance of cellular structure, by excluding water. Glutaraldehyde reacts with alpha-amino groups of amino acids present in proteins; lysine is the most important component of protein involved in this reaction. Pyridine derivatives are the major product of amine-glutaraldehyde reactions, these polymers provide cross-links that bridge randomly spaced primary amino groups in cells.

Subsequently, cells were grown on both *n*-type- and porous- silicon (Figures 2.2 and 2.3, respectively) where the distribution of cells appeared random, similar to the growth patterns seen on the glass substrate (Figure 2.1). In addition, the ECM can be seen in contact with the substrate (Figure 2.2), while the growth cone can clearly be seen in Figure 2.3. The deposition of proteins, such as collagen, onto the surface of the substrate enable adhesion to occur, as discussed in the introduction.

Although tissue or cell cultures are artificial in nature, when compared to an *in vivo* system, the use of adhesion molecules further restricts the formation of the random or self-organised interconnections which are required for the development of a normal cellular network. Previous studies have indicated that molecular printing with tethered neurotrophins, or other adhesion molecules, is a prerequisite for the growth and attachment of cell lines onto silicon and its derivatives (Curtis, 1996; 2000). However, the current study has demonstrated the ability to culture the B50 neuronal cell type on various silicon substrates without the need for adhesion molecules. With the addition of adhesion molecules a bridge is formed between the substrate and the cell, e.g. Poly-lysine, ~15nm; laminin, ~70nm; Arg-Gly-Asp (RGD) ~20nm (Sorribas, 2001). If the adhesion molecules are used for preferential transduction via these contact points, then a prerequisite for the surrounding area would be that it was electrically insulated, however this would be difficult to achieve using conventional techniques. Hammerbach & Letourneau (1996) provided evidence that fine filopodia can extend across 'non

adhesive' surfaces in an exploratory manner. This exploration, they suggested, leads to more permanent adhesions, often at the nearest edge of the substrate covered with adhesion promoting molecules. This would suggest that the receptors remain functional and do not result in prolonged receptor occupancy. However, with transient receptor occupancy two problem areas for the usefulness of these applied adhesion molecules can be identified:

(1) Meisenhelder *et al.* (1989) suggested that maintenance of protein phosphorylation is dependent upon continuous occupation of these surface sites. Thus, if the binding was transient then the functional properties of the cell would be compromised.

(2) The deposited layer becomes redundant as a guide layer, however it is still on the surface and is able to act as a conductive strip.

The direct contact of the cells to specific zones or areas by non adhesive topographical modification thus overcomes the problems associated with additional adhesion protein printing. Gundersen (1987) reported that growth cones respond to substrates patterned with laminin and fibronectin, however Hammarback *et al.,* (1988) suggested that this guidance is not limited to the control of the position of the cell but also mediates growth cone development thus movement is an on going process. Mediation of growth cone control also leads to modifications of normal cell morphology (Hammarback *et al.,* 1988), whereas the use of a patterned topography shows little or no difference in morphology while exposed to these various substrates.

The exclusion of surface modification by applied trophins is important when considering the electrical properties of any manufactured device. In a device the construction of critical areas for signal propagation also function as transduction points, at these points a signal travels from one media to another. It is the type and mechanism or mode of transduction at such points that will determine the profile of the recording device. ITO based devices are normally capacitively coupled, however the integrity of the electrical properties of the device will be compromised with artificial patterning. Planar MEAs with or without patterning have been widely used with increasing success for long term recording from, and stimulation of, neural networks in culture (Gross *et*

al., 1993; Van Pelt *et al.*, 1996; Canepari *et al.*, 1997; Rutten *et al.*, 1999; Jimbo *et al.*, 2000).

For selective stimulation a well-characterised and reliable neurone electrode contact is required prior to performing long term recording. As discussed in Chapter 1, during culture development both growth and mobility of neuronal and non-neuronal cells are likely to affect the stimulation thresholds for individual neurone-electrode contacts. The role of sealing resistance in the electrical contact has been identified as a key component in the long term recording from neuronal cultures (Regehr *et al.*, 1989; Grattarola and Martinoia, 1993; Bove *et al.*, 1995; Fromherz and Stett, 1995; Vassanelli and Fromherz, 1998). Sealing resistance refers to the point at which the neurone covers, or seals, an electrode completely; at this point there is only the narrow sealing gap between membrane and substrate that mediates transfer of electrical signals for both stimulation and recording. Due to current density distributions, generated by the neuronal membrane or the electrode, potential distributions arise in the sealing gap, which modify the membrane potential (stimulation) or can be probed by the electrode (recording). As these potential distributions are proportional to the resistivity of the sealing gap, sealing resistance is an important measure for the neurone electrode contact. Impedance spectroscopy together with an impedance model enables information as to the linear properties of the neurone electrode contact, including the sealing, to be determined (Buitenweg et al., 1998). Regehr *et al.* (1989) reported that, in these situations, the level of recording is increased from microvolts to tens of millivolts and can be close to intracellular profiles for the shape of the recording. In addition, the threshold level required for stimulation is significantly reduced (Fromherz, 1999).

As reported in the results section, photolithography was dependent upon its integrity and performance under HF and KOH etching conditions. The low resolution and formation of feathered edges (Figures 2.6 and 2.7), together with reactivity to KOH, meant that negative photoresist was unsuitable for use in this device manufacture. The removal protocol for negative photoresist following masking and etching is normally achieved by submerging the substrate in KOH (0.5M; 5 s), however this is also the method for removal of "sacrificial" PS layers in MEMS production, thus any PS

produced is removed whilst removing the photoresist. The use of positive photoresist enabled the production of sharp lines, and excess positive photoresist was easily removed with isobutanol.

The current study has demonstrated that B50 cells grow preferentially on the roughened areas of micro-machined silicon and porous silicon, as compared to amorphous silicon. Figures 2.9 and 2.10 show the same area of PS before and after 48 h incubation with B50 cells, respectively, where cell attachment can be seen to occur on the roughened areas. These structures were possibly caused by bubbles forming under the mask during the anodic etching; these bubbles initially form an insulating layer, thus changing the local current density, and causing either a relative increase or decrease in the etching rate. This data, together with the evidence provided by cell count studies, demonstrates that porous silicon is an ideal candidate for cell growth, while its topographical modification by etching enables the patterning of contact points without the need for additional molecular printing (Figure 2.11). The large separation between ridges (100 μm) was selected to prevent the entrapment or impaling of cells during cell growth, as entrapment has been reported to increase neuronal migration (Pine, 1999).

Once cell growth on both glass and silicon substrates had been demonstrated, it was necessary to investigate the effects of surface modification by different etching techniques. Thus KOH etching of *p*-type silicon and HF etching to produce porous silicon were performed. The dimensions of pores generated during electrochemical etching of PS have been shown to display a complex relationship between, for example, current density (*J*), electrolyte composition and dopant concentration and type (Herino, 1997; Cullis *et al.*, 1997). In the current study, PS was produced with differing pore sizes, an example of which can be seen in Figure 2.12. The requirement for the PS was that the structure would enable promotion of cell growth, be stable, easily manufactured, exhibit photoluminescent properties and, ideally, have a structure in which nutrients could be delivered to the cell from all sides. Thus for all subsequent studies, nanoporous silicon (pore size: 480 - 750 nm) was used, as this provided optimal conditions for cell growth and was also less susceptible to shearing forces during both manufacture and use.

Confocal microscopy studies (SYCLOPS) further elucidated the interaction between the topography of the PS and cell positioning. Collagen is a major component of the extracellular matrix and, in vertebrates, constitutes approximately 25% of total cellular protein. Its function is not only structural, but is also important in cell adhesion and migration, as discussed earlier. Specific collagen receptors, such as fibronectin, and a number of other proteins involved in cell–cell and cell–surface adhesion have been demonstrated to bind collagen. In addition, cell adhesion can be detected using fluorescence-based assays (Löster & Hortstkorte, 2000). In the current study, OG488-labelled cells were imaged using synchrotron microscopy. Figure 2.13 is a composite image showing two frames with a separation of 30μm in the z-plane. In both this image and Figure 2.14, the cell cytoskeleton can clearly be seen to follow the substrate profile. These data are in concurrence with the results of investigations into the effects of topography on cell growth (see above). The extra-cellular matrix is seen to extend into the PS layer (Figure 2.14), although an exact depth of this intrusion is difficult to ascertain due to the resolution of the optics of the microscope. Depth of field, the area in focus on an image, is the limiting factor within optical systems and is inversely proportional to the size of the pre-objective aperture. For example, in this series of experiments, the high power of the laser required an aperture to constrain the energy available to 0.1% of the original power. A consequence of this, is that the area in the z plane in focus is increased, thus reducing the accuracy of the collection method. The image z plane accuracy was estimated to be 5μm.

The ability for neuronal systems to propagate signals is required if the system is to survive. Cell to cell signals, and even the exchange of cytoplasm, occur in many systems across tight junctions. Neuronal and muscle cells, however, both exhibit the ability to conduct electrical signals along their cell membranes. To enable the device to be developed as a tool in neuronal research, stimulation of the cells by several means would be an advantage. For example, optical stimulation of non-photoreceptive cell lines via PS, mechanical stimulation via embedded quartz oscillators, chemical stimulation using thin membrane separation of channels, or electrical stimulation via ITO electrodes. The current study has demonstrated that the B50 cell line can be mechanically stimulated; signal transduction was initiated by the stimulating probe

(Figure 2.14) and visualised as fluorescence of the Fura 3 indicator dye, thus showing that calcium release had occurred (Figure 2.15). To ensure that the signal was propagating through the cells, as opposed to through the medium, an artificial breakage was made in the cellular network. No signal was recorded by the photodiode under these conditions, thus indicating that the signal was, in fact, passed through the cellular matrix and not through the media. This work suggests that direct signal transduction by the cell is feasible through the contact media, axon and/or dendritic interface. Utilising the phototonic properties of PS suggests that optical transduction of signals via the axons would enable data collection using contact, capacitive coupling via the cell body, thus isolating the signal paths.

In conclusion, these studies have demonstrated that a neuronal cell line can be successfully cultured on silicon substrates, in particular demonstrating adhesion to ridges in the silicon surface. The ability to control the position of the cell with respect to the contact points will be essential for the development of a microelectrode array device. This may be achieved by selective masking and etching areas of the substrate to enable the positioning, recording of electrical information and independent stimulation of a neuronal culture.

CHAPTER 3

DEVICE DEVELOPMENT

3 DEVICE DEVELOPMENT

3.1 INTRODUCTION

3.1.1 The development of a multi-electrode array (MEA)

Since the development of planar multi-electrode arrays (MEAs) neuroscientists have utilised this technology for the study of the network activity of excitable cells (Thomas *et al.*, 1972; Gross *et al.*, 1977). The majority of reports concerned measurements of electrical activity from a significant number of cells within either a small network of cultured neurones or an organotypic preparation. Cells cultured on an MEA are able to establish tight seals between the cell membrane and the electrode surface. Electrode coupling, the tight seal resistance between the tissue and the electrodes, is often difficult to achieve in organotypic slices due to a layer of dead cells formed at the surface of the slice during slice preparation. Cell culture systems are also sensitive to their environment, showing tissue modification, a reduction in their synaptic arrangement, and a resultant reduced signal to noise ratio (Wheeler & Novak, 1986; Novak & Wheeler, 1988; 1989).

Stable recordings of excitatory post-synaptic potentials (EPSPs) and population spikes over several hours have recently been described (Novak & Wheeler, 1988; Oka *et al.*, 1999), however the amplitudes of these evoked responses are significantly smaller, by one order of magnitude, than responses obtained using glass microelectrodes. The active cells producing EPSPs or spikes are at least one or two cell layers above the measuring electrodes of a conventional planar MEA. MEAs based on glass substrates that are able to penetrate the dead cell layer(s) and record the EPSPs would provide a useful tool in neuroscience. A first stage to this is the development of a device based on a planar MEA incorporating silicon as the substrate for cellular growth. Silicon deposited onto a glass substrate could then be etched to elicit closer contact with the active cell layer in organotypic hippocampal slices.

Non-invasive and specific stimulation of the neurones is required to simulate external inputs. The effect of these stimuli on the mapping of the closed network system and its

effect on the connections and plasticity of the system (i.e. changes in the connections between the neurones based on the activity patterns over a specific time) were the primary goals of the current project. The multi-electrode array is a layered micro-machined device upon which cultured mammalian neurones can be continuously monitored and with the use of specific signal separation techniques, stimulated either *en masse* or in isolation. MEA devices were therefore developed as part of this project to investigate the effects of changes in environmental criteria on the growth and development of cultured mammalian neurones.

One of the most widely used MEA for recording signals from cultured cells is produced by the laboratory of Professor GW Gross at the department of Biological Sciences, University of North Texas (see Figure 3.1 for a diagrammatical representation). This device has a 5 x 5 cm x 1.1 mm glass base with a series of conduction strips of indium tin oxide (ITO). The strips are 1200 Å thick and have a resolution of 10 μm. They are arranged in a pattern of 4 rows separated by 200 μm, and 16 columns, with a separation of 40 μm between these columns giving a 0.8 x 0.8 mm recording matrix. This is then covered by a 2 μm insulating layer of the hydrophobic polymer polysiloxane (DC 648). Contact through the polysiloxane is achieved by etching using a nitrogen laser (337 nm, 2 $\mu J\ \mu m^{-2}$) pulse. The resulting ablated area is approximately 50 μm in diameter. Therefore, the actual substrate for neuronal growth is the polysiloxane. The Texas device has a 64 channel array of electrodes, each of which is designed to record and excite a single mature cell without adversely affecting normal neural development.

During this project, the development and manufacture of a device capable of maintaining a viable cell population, together with electrodes that can both record and stimulate electrical activity in individual cells, have highlighted problems which can be divided into two categories: (1) the practical construction of a device depends upon the ability of the composite materials to bond to each other and the affect, if any, that any of these materials has on the growth or function of the cells, or on device performance; (2) the ability to consistently produce devices with predictable electrical properties and a known topographical profile. As both gold and ITO film were to be used as contacts, knowledge of these materials and their deposition had to be gained.

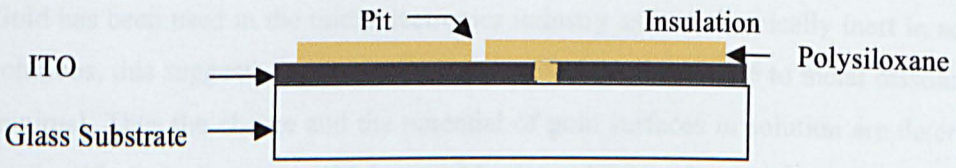

Figure 3.1 The layered structure of the Texas MEA.

Using the polysiloxane array as a base comparative material, neurones cultured on a selection of substrates, together with cytotoxicity assays, support the validity of silicon and PS as substrates for multi-electrode arrays.

3.1.2 Gold

Gold has been used in the microelectronics industry as it is chemically inert in aqueous solutions, this suggests that in the build-up of surface charge due to metal dissolution is minimal. Thus the charge and the potential of gold surfaces in solution are determined by specific ion adsorption which is highly dependent on the solution composition and presence of any impurities. Impurities can be introduced into the system during preparation and cleaning procedures, thus affecting the surface chemical properties (e.g., presence of oxide layers). Gold surfaces readily adsorb contaminants from the air which may be a reason why there are few literature references and practically no consistent data on the potential of gold surfaces. Values reported for the surface potential of gold in neutral solutions of low salt concentration vary from +30 to -70 mV (Ducker, 1992; Biggs & Mulvaney, 1994; Hu & Bard, 1997; Ederth, 2000).

Bos *et al.* (1994) found that when an applied potential was applied the adsorption kinetics and adsorbed amounts of various proteins on indium tin oxide (ITO) are hardly affected. This contrasts to the effect of the pH-determined equilibrium potential of the ITO surface on the adsorption. Bos *et al.* suggest that there may be various causes for this difference, one of these being that the applied potential difference between the ITO electrode and reference electrode is for the most part realised in the semiconductor phase and not in the solution. The applied potential is only noticeable at the electrode/solution interface.

3.1.3 Indium Tin Oxide (ITO)

Transparent conductors were first reported in 1907 when conductive cadmium oxide (CdO) films were introduced. Throughout the following decades there has been an increase in technological interest in materials with such properties. Non-stoichiometric and doped films of oxides of tin, indium, cadmium, zinc and their various alloys exhibit high optical transmittance and nearly metallic conductivity is achievable (Chopra, 1983). Tin-doped indium oxide (ITO) is currently the most widely used transparent-conducting material. Such transparent-conducting thin films are in widespread use as electrodes in a variety of optoelectronic devices, such as heat-mirror coatings in 'smart windows' for buildings, in car and airplane windshields, incandescent light bulbs, flat-

plate and concentrating solar collectors, and in a wide range of other applications (Chopra *et al.*, 2000; Dawar & Joshi, 1984; Granqvist, 1994). ITO is a wide-bandgap oxide semiconductor (E_g =3.75 eV), which absorbs UV radiation (due to band-to-band transitions) and reflects in the IR region (due to free-electron oscillation). In between these two limits it has a transparency window covering the visible spectrum and near-IR. Transition between the transmitting and reflecting regions takes place at a wavelength (λ_p) called the plasma reflection edge. The location of λ_p in an ITO film depends on the free-electron concentration n_1; as n_1 is increased, λ_p moves towards shorter wavelengths.

Modification of the surface and tailoring the bulk properties of ITO to specific areas of research is of considerable importance to the manufacture and design of display devices, as well emergent technologies such as organic optoelectronic devices and biological electrodes. Changing the work function of the material, for example, is a requirement in controlling the charge injection properties of light emitting diodes fabricated on organic semiconductors (Pankove & Johnson, 1991). The free-electron density in ITO films is normally ~10 cm^{-3} but the drift mobility (~10–70 $cm^2 V^{-1} s^{-1}$) is much lower than that of conventional semiconductors such as silicon. Hence electrical conductivity of ITO is significantly lower than that of a typical metal (Dawar & Joshi, 1994). The reason for the low drift mobilities is the presence, in large concentration, of structural defects such vacancies, interstitial atoms and grain boundaries in these films. These defects act as scattering and trapping centres in ITO films. Successful post-depositional modification of high resistance films deposited by radio frequency (r.f.) sputtering should enable the production of optically clear, in the visible spectrum and near-IR spectrum, films with resistances in the order of 50 – 100Ω cm^{-1}. The production of such films, together with a suggested low cytotoxic profile, make it an ideal candidate for biological applications such as MEAs. The transparent nature of ITO enables use of inverted microscopy for positioning the array on the stage. In addition, molecular dyes used in monitoring signal propagation can be observed at the same time as making electrical measurements. Differing production techniques for ITO result in widely differing optical and electrical properties. Thus control of the deposition parameters and post-deposition modification is required to produce a film specific for this task.

(1) Physical structure and properties of ITO

Indium tin oxide is formed by substitutional doping of In_2O_3 with Sn. This replaces the In^{3+} atoms from the cubic bixbyte structure of indium oxide. Sn forms a bond with oxygen and exists either as SnO or SnO_2, depending on its valency of +2 or +4 respectively. It is this valency state that has a direct relation to the final conductivity of ITO. The lower valency state results in a net reduction in carrier concentration, since a hole is created which acts as a trap and reduces conductivity. Conversely, the predominance of the SnO_2 state means that Sn^{4+} acts as an n-type donor releasing electrons to the conduction band. However, in ITO both substitutional tin and oxygen vacancies contribute to the high conductivity and the material can be represented as $In_{2-x}Sn_xO_3^{-2x}$. ITO in thin films has a lattice parameter close to that of In_2O_3, lying in the range 10.12 to 10.31 Å (Fan & Goodenough, 1977). A summary of electrical and optical properties of typical ITO films deposited using various techniques is shown in Table 3.1. Variations in film are attributable to both pre- and post-deposition treatments as well as the techniques themselves.

Transmission electron microscopy and electron diffraction studies of r.f. sputtered ITO films on glass substrates by Sreenivas *et al* (1985) suggest that films grown at room temperature have large stacking faults and represent an amorphous structure; increasing this temperature to 200°C leads to the formation of a polycrystalline structure and, finally, annealing above 600°C results in near single crystallinity with uniform grain size and thus increased conductivity. It is also suggested that deposition of ITO on single crystal substrates, rather than amorphous glass, can enhance the grain growth process. The refractive index of ITO is reported to be 1.96 at 550nm (Szczyrbowski *et al.*, 1983), although this figure is influenced by surface- and optical-roughness causing scattering in the direction normal to the film surface as previously discussed.

Deposition Technique	Thickness [Å]	Hall Mobility m H [cm2V-1s-1]	Carriers N [cm-3]	Resistivity r [Ωcm]	Transmittance Tr [%]	Reference
r.f. Sputtering	7000	35	6.00E+20	3.00E-04	90	Fan 1977
r.f. Sputtering	5000	12	1.20E+21	4.00E-04	95	Sreevnivas 1985
r.f. Sputtering	4000	25	3.00E+20	8.00E-04	-	Szczyrbowski 1983
Magnetron Sputtering	800	26	6.00E+20	4.00E-04	85	Buchanan,1981
d.c. Sputtering	1000	35	9.00E+20	2.00E-04	85	Higuchi,1994
Reactive Evaporation	2500	30	5.00E+20	4.00E-04	91	Balasubramanian 1988
Ion Beam Sputtering	600	26	2.00E+20	1.20E-03	-	Bregman, 1990
Spray Pyrolysis	3000	45	5.00E+20	3.00E-04	85	Haitjema 1991

Table 3.1 Typical electrical and optical properties of ITO deposited by various techniques

The production of dark brown (effectively translucent) metallic films of ITO are attributed to unoxidised tin metal grains on the ITO surface as a result of instability due to absence of sufficient oxygen during deposition (Fan & Goodenough, 1977; Sreenivas *et al.*, 1985).

(2) ITO Deposition Techniques

Sputtering, in one form or another, is by far the most extensively used technique for the deposition of ITO. This is closely followed by thermal evaporation - which can also be achieved using several different techniques. ITO has also been prepared by other methods such as spray pyrolysis and screen printing. The choice of deposition technique is dictated by a number of factors such as quality and reproducibility of the ITO film, homogeneity over a wide cross section, capacity, ease and cost of use as well as detrimental side effects and limitations specific to each technique. In addition, since the properties of ITO depend strongly on the microstructure, stoichiometry and the nature of the impurities present, it is inevitable that each deposition technique with its associated controlling parameters should yield films with different characteristics.

3.1.4 Sputtering

The technique used in the course of this work is magnetron d.c. sputtering in an Ar/O_2 plasma. Sputtering involves ejecting an atom or molecule out of a target material by accelerated ions from an excited plasma and condensing it on the substrate, either in its original or in a modified form (Figure 3.2). Most ITO sputter sources consist of hot pressed 90% In_2O_3: 10% SnO_2 compound targets. Sputtering can be achieved in a number of ways which include accelerating the plasma ions by a d.c. field (Higuchi, 1994) or a d.c. field combined with a magnet (to direct the high velocity emitted electrons away from the substrate). If the modification is induced by a chemical reaction during the transit from the target to the substrate, the process is referred to as reactive sputtering. Hence r.f. sputtering (with its self induced bias), ion beam (Bregman *et al.*, 1990), magnetron (Buchanan *et al.*, 1981) and reactive r.f. (Fan & Goodenough, 1977; Sreenivas *et al.*, 1985) sputtering reflect on the process that has been used for the deposition of the ITO film. R.f sputtering produces a uniform, highly conducting and

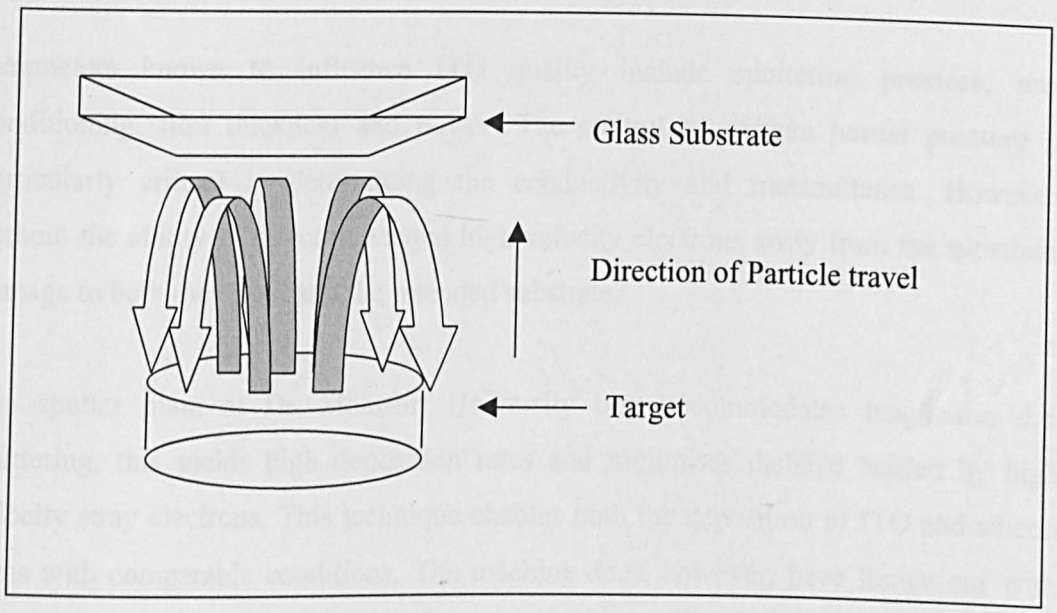

Figure 3.2 **Schematic representation of the particle field in a sputterer, indicating the importance of the position of the sample within the chamber relative to the plasma field**

highly transparent film, however this technique is not currently available at De Montfort University.

Parameters known to influence ITO quality include sputtering pressure, pre-conditioning, film thickness and power. The control of oxygen partial pressure is particularly critical in determining the conductivity and transmittance. However, without the ability to direct unwanted high velocity electrons away from the substrate, damage to both the target and the intended substrate.

The sputter plant at De Montfort University best accommodates magnetron d.c. sputtering, this yields high deposition rates and minimises damage caused by high velocity stray electrons. This technique enables both the deposition of ITO and silicon films with comparable conditions. The machine does, however, have limitations with control of deposition rates and problems associated with clearing gases and flushing, when running two or more gasses in the system; control of some of these parameters are discussed by Sreenivas & Mansingh (1985) and Sreenivas *et al.,* (1985). Sreenivas also highlights the need for post depositional modification of the surface to improve the conductivity of the sample.

3.1.5 Aims of the investigation

The information gained from both the control of cell growth studies (Chapter 2) and analysis of the Gross MEA device provided a framework for this series of experiments. The aim of this study was thus to design and develop a multi-electrode array device that would enable a direct comparison of electrical signal output from cells grown on several substrates. Data recorded in this situation is attributed to a model system. The development of comparative MEA devices included:

(1) Gold electrodes, silicon surface - MEA DMU-Si-Au

(2) ITO electrodes, silicon surface - MEA DMU-Si-ITO

(3) ITO electrodes, porous silicon surface - MEA DMU-PS-ITO

These devices were also compared to a sample device manufactured by Gross *et al.*, which is currently used in microelectrode array experiments (Sokal, 2000).

To examine the electrical properties of the deposited ITO, it was decided that substituting gold for ITO would provide a suitable baseline. There are two in-house methods for deposition of gold contacts onto glass substrates; evaporation and sputtering. Of the requirements for an optimal device, as listed earlier, the ability to pass light through it was one of the most important, thus any silicon deposition must be translucent (less than 1500nm). The device was envisaged as a sandwich and, as such, the relationship between the differing layers, the individual processing techniques and any post-deposition modification had to be defined. In order to achieve this aim each stage of development had to be thoroughly investigated and the study followed the layered construction of the device, developing methods and protocols at each stage:

(1) Gold and ITO were investigated as possible contacts with the amplification rig, on either a silicon wafer or a glass substrate.

(2) Once ITO had been established as the optimal contact material then its masking and modification was investigated.

(3) Once the ITO had been successfully modified a layer of silicon (650 – 900nm) was added, this was then masked and selectively etched to expose the contact points.

The device would be of little use if it were toxic to the cells under investigation, thus MTT and NRU assays were used to determine toxicity of the compounds present in the device. MTT provides information as to the ability of the cell to convert MTT [3-(4,5-dimethylthiazol-2yl)-2,5 diphenyltetrazolium bromide; thiazolyl blue] by mitochondrial dehydrogenases into formazan, a dye insoluble in aqueous solution but soluble in DMSO or propanol. Production of formazan is quantified against a zeroed control. The assay is actually an indication of mitochondrial activity, cell viability is extrapolated from this information. The neutral red uptake, NRU, assay provides information on the viability of cells by testing their ability to transport the dye across the cell membrane. Neutral red dye is presented to cells in phosphate buffer; the dye diffuses through the cytoplasmic membrane and accumulates in the cytoplasm of the living cells. The level of uptake is measured by absorbance, read at 540 nm, which is directly proportional to the number of live cells in the medium (Arechabala *et al.*, 1999). With both assays an

LD50, the amount of the material under investigation that must be presented in order that 50% of the cells cultured in its presence are nonviable when compared to a control, is normally recorded.

3.2 MATERIALS AND METHODS

3.2.1 Glass cleaning

(1) Method 1

Glass microscope slides or squares of glass (50 x 50 x 2.5mm) were sonicated for 15 min in a solution of Decon 90 surface action cleaner. The glass was then cleaned with ethanol followed by acetone. The glass underwent further sonication (15 min) in a solution of Decon 90, and was finally rinsed in double distilled water.

(2) Method 2

Squares of glass were cleaned as above (Method 1), prior to immersion in a solution of 1:1 concentrated sulphuric acid and hydrogen peroxide (15 min, agitation). The slides were finally rinsed in double distilled water.

3.2.2 Glass etching

(1) Stepping etch

Cleaned glass slides (as above) were lowered into a 48% HF solution in 1 cm steps, at a rate of 1 cm per 2 min. The slides were then rinsed in double distilled water and dried under nitrogen gas.

(2) Drop etch

Cleaned and dried glass microscope slides were spotted with a 1 ml drop of either:-

a) 48% HF

b) 48% HF : ddH_2O (ratios 1:1, 1:3, 1:5)

c) 48% HF : ddH_2O : glycerol (ratios 1:3:2, 1:5:3)

The slides were then rinsed in double distilled water and dried under nitrogen gas.

(3) Vapour etch

Cleaned and dried glass microscope slides were placed 15mm above the surface of 10 ml 48% HF in a *Fluororesist* Petri dish, for a period of between 15 s and 5 min. The slides were then rinsed in double distilled water and dried under nitrogen gas.

3.2.3 Gold deposition

Gold deposition was performed using the standard operating procedures as detailed below (see Figure 3.3 for a schematic representation):

(1) SEM sputter machine (Edwards S150B Sputter Coater)

- A cleaned glass slide was positioned in the sample chamber.
- The rotary pump was switched on and the chamber evacuated to a pressure of 1 x 10^{-1} mbar.
- Argon was then introduced into the system, resulting in a pressure of 3 x 10^{-3} mbar.
- The pressure was then reduced again to 1 x 10^{-1} mbar and argon re-introduced to achieve a pressure of 3 x 10^{-3} mbar.
- Coating time was set to achieve the required amount of deposit (fixed rate of 15nm min^{-1}).
- The high voltage and timer switches were simultaneously depressed to initiate sputtering.
- After the timer had automatically switched off, the high voltage supply was also terminated and the rotary pump disengaged.
- The vacuum was released slowly, by introducing argon into the system, and, once the pressure had returned to atmospheric, the sample was removed.

(2) Evaporator (Bazeley evaporation plant)

- The water supply for the cooler pump was switched on 20 min prior to loading the sample chamber.
- A cleaned glass slide was positioned in the sample chamber.
- The mains electricity supply, rotary pump and diffusion pump were switched on.

- The backing valve was opened, resulting in a pressure of 0.05 Torr (approximately 20 minutes).
- Once the correct pressure was achieved, the air admittance valve was closed, followed by closure of the backing valve.
- The roughing valve was opened, until the roughing pressure reached 0.1 Torr.
- Once the correct pressure was achieved, the roughing valve was closed and the backing valve re-opened.
- The baffle valve was opened slowly to achieve a pressure of 10^{-5} Torr (approximately 1 h).
- The high tension/low tension mains supply was switched on.
- The low tension switch was turned to the on position and the Ampere control output set at 206 amps.
- Thus, the sample was preheated for 3-5 min.
- The output current was increased to 400 amps, resulting in a change of state from solid to molten for the metal in the crucible.
- Once the metal was liquefied, the output current was decreased to 300 amps, and run for 5 min.
- The low tension switch and high tension/low tension mains supply were turned off and the sample allowed to cool 30 min.
- The baffle valve was closed and, after 5 min, the air admittance valve was opened.

3.2.4 Sputter deposition

The deposition of the silicon and ITO intermediate layers was performed using the CVC sputter plant according to the following protocols (see Figures 3.3 and 3.4 for schematic representations).

(1) Opening the chamber

- After ensuring that the DC power supply was in the 'off' position, the roughing valve and gate valves were switched off.
- The gas valve selector was turned to the vent position and the gas admittance valve opened slowly.
- The detector selector on the prani-penning 105 unit was switched to setting 1.

- Once the correct pressure was achieved (2.2 x10^3 mbar) following a further 2 min wait the seal around the hood was examined for a seal break gap.
- The orange release button was pressed to release the hood and the gas admittance valve was closed.

(2) Closing the chamber

- Once the samples were placed in the chamber, the orange release and back pressure buttons were depressed to release the hood.
- When the hood was almost completely closed, and whilst still pressing the back pressure release button the roughing valve was switched to the open position.
- When the seal was made the back pressure release button was released.
- Once the pressure had dropped to below 1.0 x 10^{-2} mbar (approximately 30 min) and the Butterfly Knob was in the vertical position, the roughing valve was closed and the gate valve opened.
- The detector selector on the prani-penning 105 unit was switched to setting 3
- When the pressure had reached 5x10^{-6} mbar (approximately 90 min) the butterfly valve was turned to 45 degrees and the high voltage power supply (MDX755) was switched on.
- The flow control valve regulator (URS 100.5) was set to the required settings for the sample (Table 3.2) and the flow tap was turned from the mid position to the gas unit position.
- The gas admittance valve was opened and the pressure steadied after 1 min to 8 - 9 x 10^{-5} mbar, the butterfly valve was returned to 10 – 15 degrees from vertical and the system permitted to settle for 10 minutes.

Settings	Silicon	ITO
Chamber Pressure	2.8×10^{-3} mbar	4.2×10^{-3} mbar
Baffle setting	65°	25°
Flow cell 1	0.0	30.0
Flow cell 2	47.5	38.5
Ramp time	1.1 min	2.5 min
Watts	100 W	120 W
Voltage	630 V	550 V
Pre burn	5 min	8 min

Table 3.2 **Instrument settings for silicon and ITO depositions.**

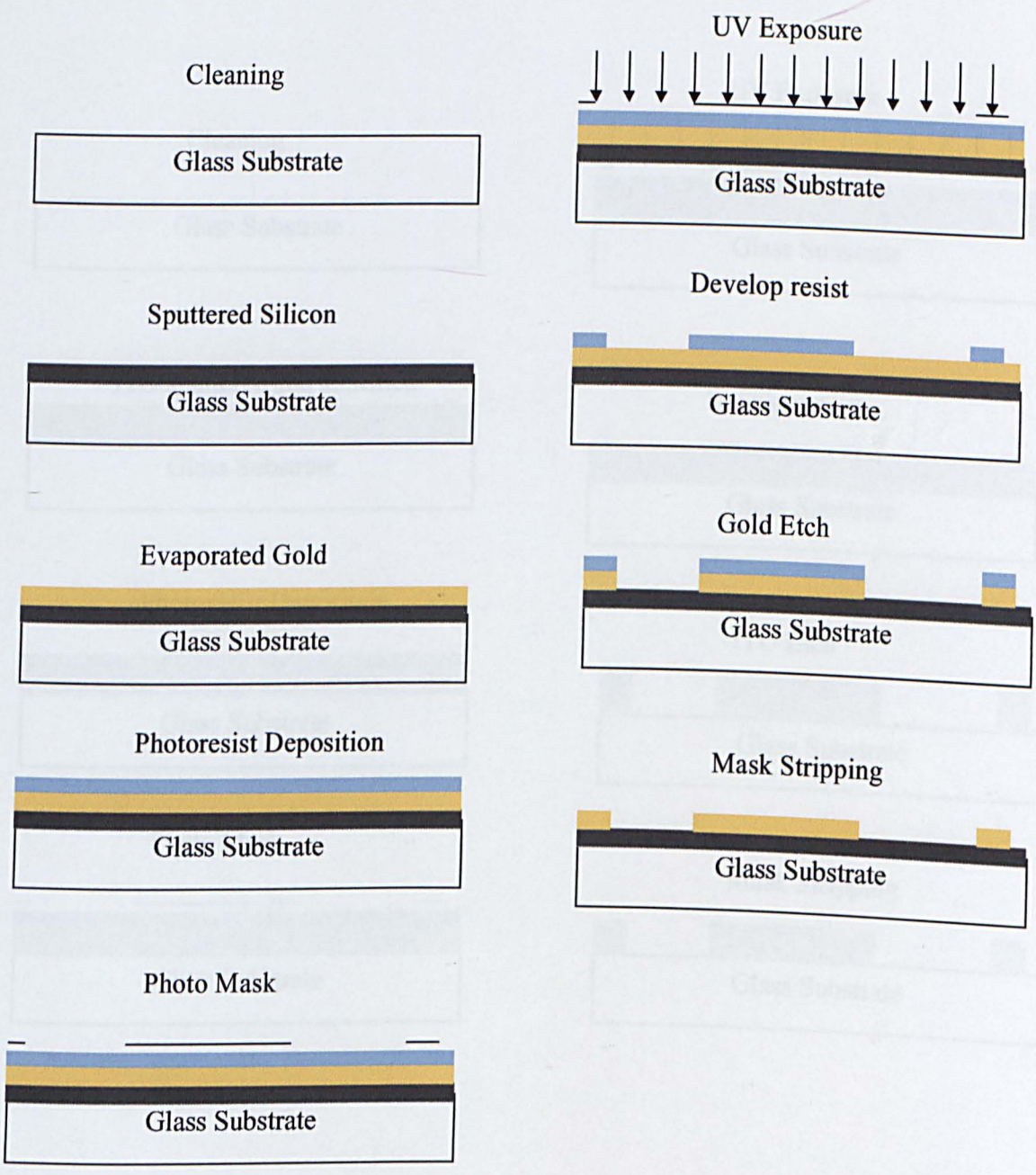

Figure 3.3 **Schematic representation of the process for the deposition of gold electrodes on silicon substrates.**

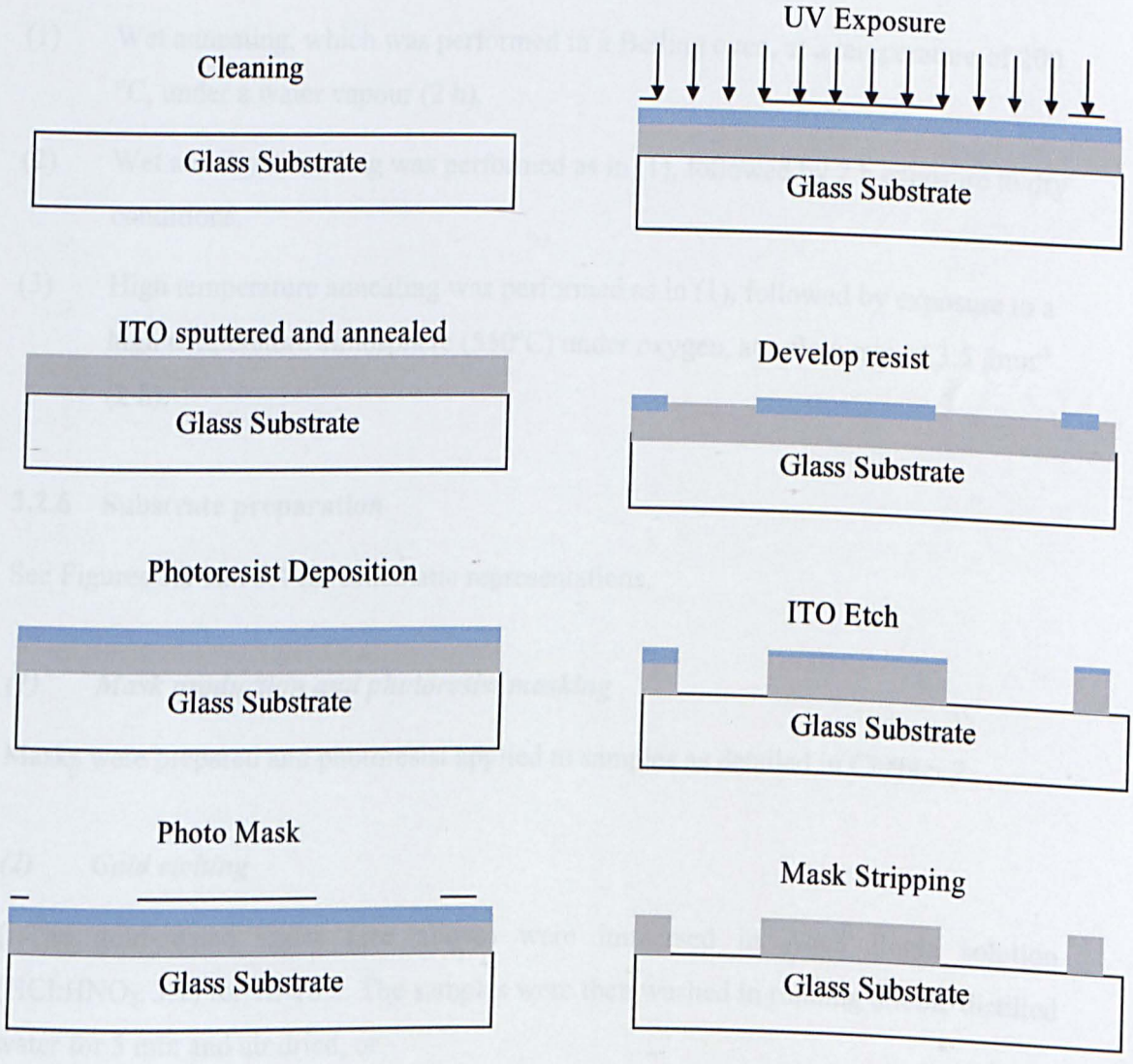

Figure 3.4 Process outline for ITO deposition and mask production on glass substrates.

3.2.5 Post-deposition modification - annealing

Post-deposition modification was achieved by:

(1) Wet annealing, which was performed in a Belling oven, at a temperature of 200 °C, under a water vapour (2 h).

(2) Wet and dry annealing was performed as in (1), followed by 2 h exposure to dry conditions.

(3) High temperature annealing was performed as in (1), followed by exposure to a high temperature atmosphere (550°C) under oxygen, at a flow rate of 3.5 $l\text{min}^{-1}$ (2 h).

3.2.6 Substrate preparation

See Figures 3.3 and 3.4 for schematic representations.

(1) Mask production and photoresist masking

Masks were prepared and photoresist applied to samples as detailed in Chapter 2.

(2) Gold etching

(i)The gold-coated slides (see above) were immersed in Aqua Regia solution ($HCl:HNO_3$; 3:1) for 12-18 h. The samples were then washed in running double distilled water for 5 min and air dried, or

(ii)The gold-coated slides were immersed in potassium iodide solution (30 g KI, 15 g I (sublimed) in 30 ml water) for 3 min. The samples were then washed in running double distilled water. If necessary, the samples were etched further, for periods of up to 30 s.

(3) ITO Etching

Masked patterned substrates (as above) were lowered into a $HCl:H_2O$:Glycerol (2ml:10ml:20ml) solution for seven minutes. The slides were then rinsed in double distilled water and dried under nitrogen gas.

(4) Silicon Etching

Masked patterned substrates (as above) were covered with 0.1M KOH for 15-20 s. The slides were then rinsed in double distilled water (5 min) and dried under nitrogen gas.

3.2.7 Holes in the silicon

In order to expose the ITO contacts to the cells a mask was produced to line up the tips of the electrode strips with the dots on the silicon surface. Marks on the DMU3a mask were used to align the points and the silicon was etched with NaOH (0.1M, 5 sec).

3.2.8 Sample preparation

The component compounds of the device were tin, ITO, silicon monoxide and silicon dioxide. As none of these metals are soluble in water, PBS, or media, the substrate samples were ground to form fine powders, using a pestle and mortar, then added to 100 ml double distilled water to form suspensions (Table 3.3). One week later, the sample solutions were aliquoted into 96 well plates prior to addition of the cell suspension (Table 3.4). The cells were cultured until 70% confluent (approximately 24 hrs), prior to implementation of either an MTT or NRU assay.

3.2.9 MTT cytotoxicity assay

A modified MTT assay (Arechabala *et al.*, 1999) was used to evaluate substrate toxicity. A 50 µL aliquot of MTT solution (1 mg/mL in DMEM), pre-warmed to 37°C, was added to each well containing the cell/substrate suspension (see above). After a 4 h incubation in a CO_2 atmosphere, the supernatant was removed and the formazan crystals dissolved by adding 50 µL of dimethyl sulphoxide (DMSO) to each well. After agitation for 5 min, absorption was measured at 540 nm using an ELISA plate reader. Background absorption was measured in wells containing the various substrates but no cells. Results were thus expressed as corrected optical densities (OD) (experimental OD - background OD). Standard curves were established using different cell concentrations. All experiments were performed in triplicate.

Substrate sample (powder)	Weight (g)
SiO	0.4632
SiO_2	0.6238
Sn	1.1334
ITO	2.2492

Table 3.3 Suspension of sample compounds.

Each compound was ground into a powder using a pestle and mortar, and suspended in 100 ml double distilled water.

		Volume (µl)		
Sample	**Sample**	**PBS**	**DMEM + B50 (cell suspension)**	**Total**
1	0	50	200	250
2	5	45	200	250
3	10	40	200	250
4	15	35	200	250
5	20	30	200	250
6	25	25	200	250
7	30	20	200	250
8	35	15	200	250
9	40	10	200	250

Table 3.4 Preparation of cell/substrate suspensions.

Increasing concentrations of sample suspensions were added to cell suspensions in 96 well plates.

3.2.10 Neutral red test

Similar to the MTT assay, 50 µl neutral red was added to the cell/substrate suspension and incubated for 4 hrs. Absorbance, at 540 nm, was measured using a Titertrek Uniskan II spectrophotometer and the reading was normalised using a standard of phosphate buffer. Toxicity was thus calculated by comparison of the mean optical density read for the concentration of the toxic compound with that of the standard.

3.3 RESULTS

3.3.1 Gold evaporation

Gold is deposited onto surrounding surfaces when the high current passed through a crucible containing gold wire causes the metal to evaporate. The gold-glass bonding achieved with this technique were initially inconsistent, with low conductivity and poor adherence. Cleaning pre-treatment of the glass (methods 1 and 2 as detailed above) resulted in little improvement in adherence of evaporated gold, when submerged in PBS for 5 min. The layer lifted from the corners and after 10 min 80% had been removed. To improve the stability of the gold/glass contact it was decided to modify the surface of the glass. Several etching mixtures were tried with differing levels of success (see below).

3.3.2 Surface modification

Direct etching of the surface using 48% HF solution or mixtures of HF, ethanol and H_2O or HF, ethanol and H_2O:glycerol proved to be ineffective in increasing the gold-glass bond. A method for vapour etching was developed in which the cleaned and dried glass microscope slide was placed 15mm above 48% HF in a Petri dish. The etching time was varied between 15 s and 5 min. These modifications improved the adherence significantly, the gold layer resisting immersion in DMEM or PBS (2 h) without being compromised.

3.3.3 Edwards Sputter plant

The gold sputtering achieved using the Edwards Sputter plant was removed both by 30 s submersion in PBS and by wiping (Figure 3.5). The modifications to the surface made little difference to the stability.

3.3.4 Silicon intermediate layer

The second method of depositing gold electrodes onto a surface involved the production of a glass/silicon/gold layered structure (see Figure 3.3). Silicon was deposited on the surface of the glass substrate using d.c. sputtering in the high volume sputter CVC plant. A layer of silicon was sputtered on to a cleaned glass slide with an initial sputter time of 20 minutes. This produced a predominately uniform layer which was 470 nm in thickness. However, in some areas, blisters formed in the silicon, probably due to debris on the glass surface (Figure 3.6).

The pre-treatment of the substrate, in this case the cleaning of the glass by sonication and subsequently acetone and ethanol, produced similar results. Figure 3.7 demonstrates the effect of 15s sonication; the silicon surface was disrupted, resulting in the removal of the film. To improve adherence, the glass was cleaned then immersed in a 1:1 solution of sulphuric acid and hydrogen peroxide. This method produced an even layer that resisted sonication for 30 minutes (Figure 3.8).

3.3.5 Deposition of gold

Deposition of a layer of gold on the surface of the silicon was achieved by evaporation. This produced a film approximately 1.1μm thick (Figure 3.9).

3.3.6 Photolithography

The glass-silicon-gold layered material was then prepared for the photolithography by cleaning with ethanol and the PT1 mask (Figure 3.10) was printed for use in the mask aligner.

Figure 3.5 **Gold sputtered on ethanol/acetone cleaned glass using the Edwards S150B Sputter Coater. Coating time 5 minutes at $3x10^{-3}$ mbar giving a 75nm thick film.**

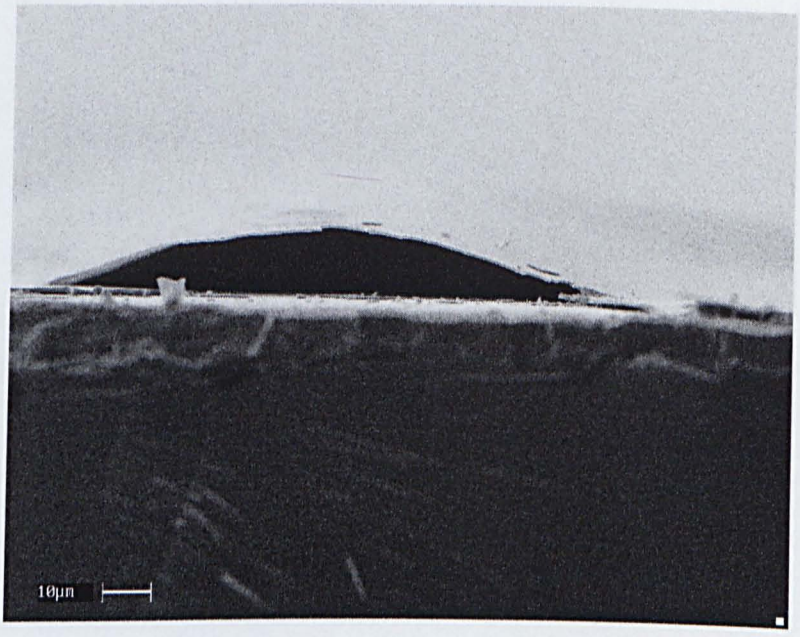

Figure 3.6 **Deposition blister on silicon after a 20 min. sputter at a pressure of $2.8x10^{-3}$ mbar.**
Scale bar represents 10 µm

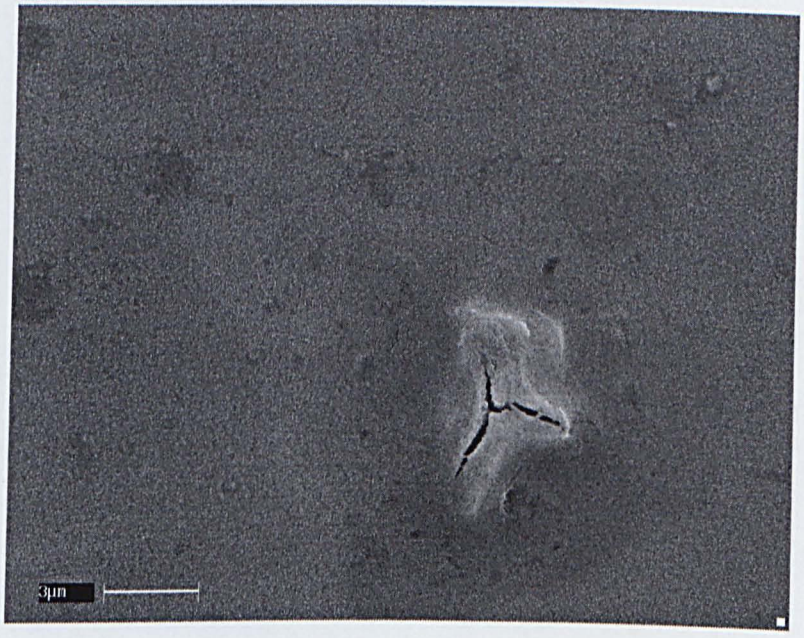

Figure 3.7 **Surface disruption following 15 second sonication.**
Scale bar represents 3 µm

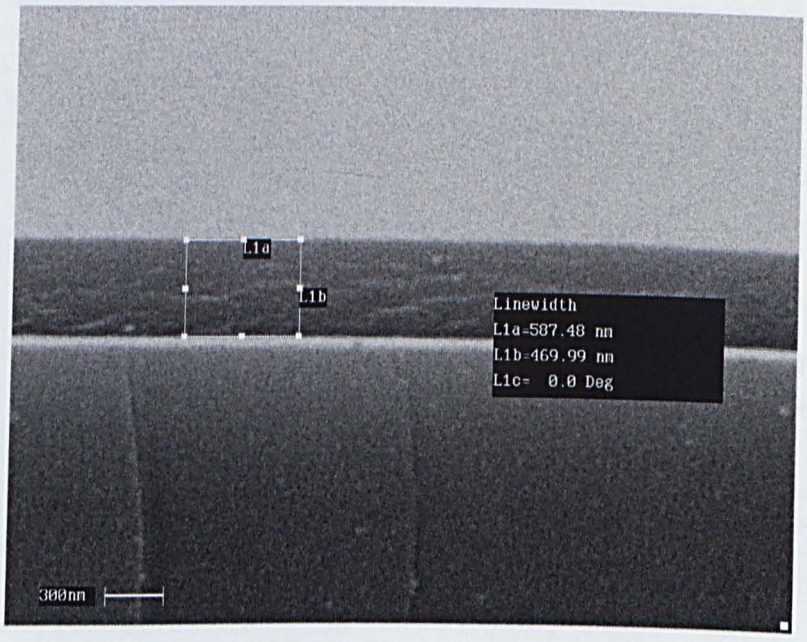

Figure 3.8 **SEM showing the layer of silicon deposited after a 20 minute sputter at a pressure of 2.8×10^{-3} mbar, following H_2O_2/H_2SO_4 pretreatment.** Scale bar represents 300 nm

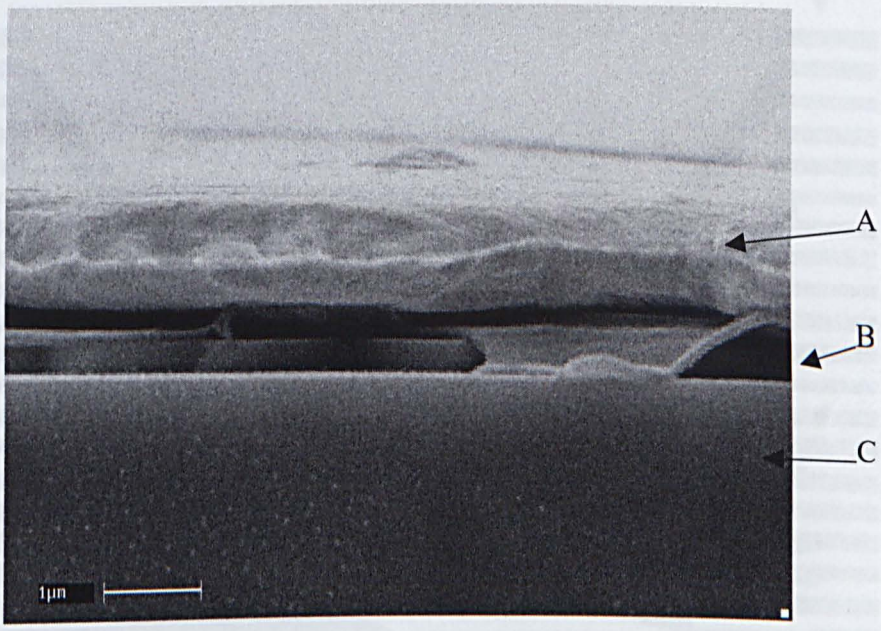

Figure 3.9 **SEM of a layer of gold 'A' evaporated onto a sputtered silicon layer 'B', the glass substrate, 'C'.**
Scale bar represents 1 µm

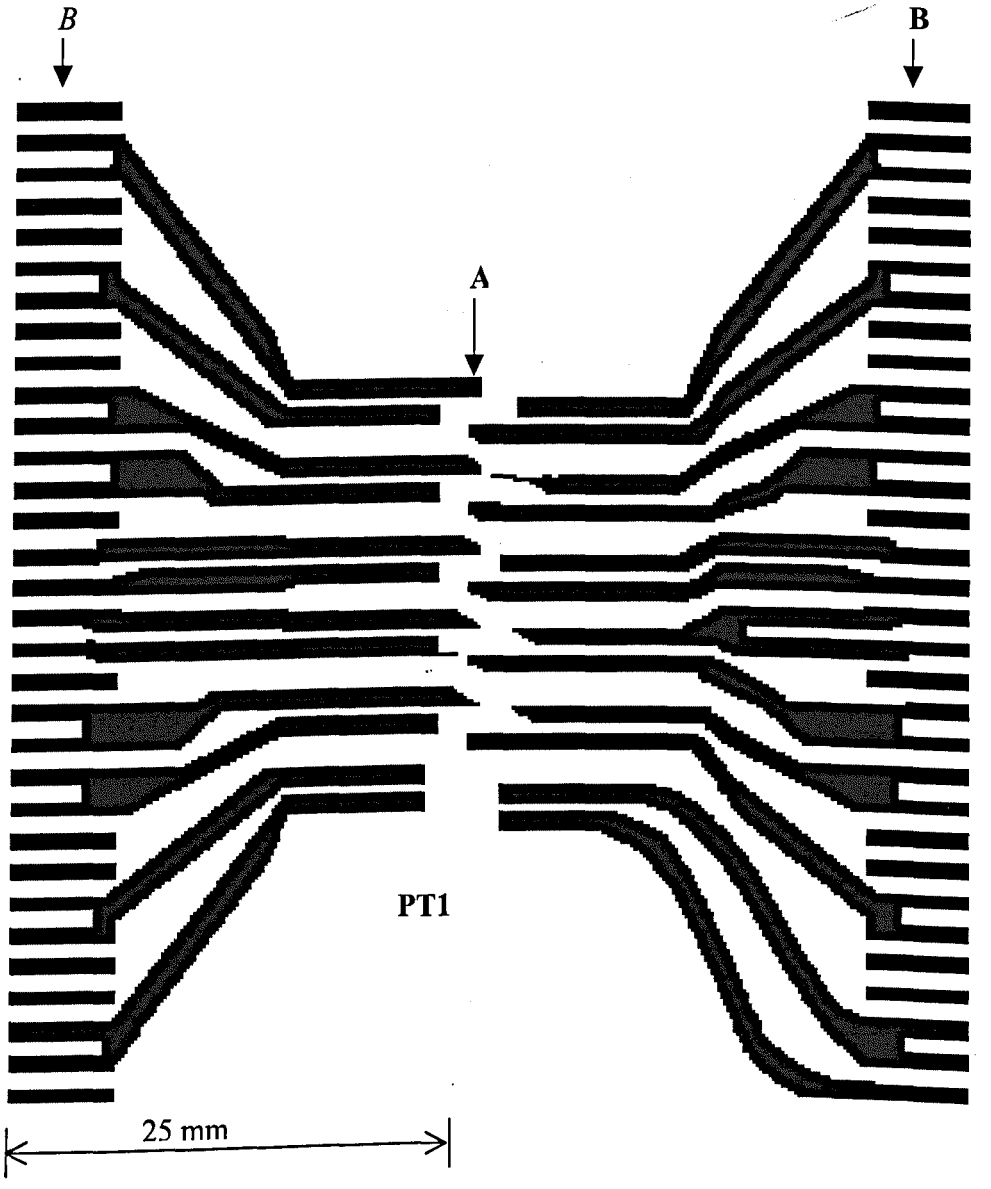

Figure 3.10 Mask "PT1" used for etching.

'A' represents electrodes with a 25μm separation at a resolution of 1200dpi. 'B' indicates the position of 32 gold contact points.

3.3.7 Gold Etching

(I) Aqua Regia

Once the mask had been applied to the gold layer the unprotected gold was removed using Aqua Regia. However as shown in Figure 3.11, electrodes were not individually defined. The figure shows the best resolution achieved following 18 h exposure time Aqua Regia; submerging for longer periods resulted in the edge contacts lifting and the whole sheet of deposited gold being removed.

(2) Potassium iodide

The use of potassium iodide solution gave a much quicker action time, of 6 min, together with an improved resolution.

The KI etched layer produced nearly vertical edges rather than tapered. The contact resistances produced with this technique were $2\Omega cm^{-1}$ compared with the resistances of $20M\Omega cm^{-1}$ or greater for the Aqua Regia etch.

3.3.8 ITO Deposition

The first samples to be sputtered using ITO (Figure 3.12), resulted in the production of uneven films with resistances ranging from $15K\Omega cm^{-1}$ to over $20M\Omega\ cm^{-1}$. An uneven layer of ITO was deposited, as indicated by the colour band that appears across the surface of the plate; the areas of similar resistances are also indicated.

3.3.9 Obtaining optimal resistance

By annealing at 200°C in the Belling oven, the resistance of the samples was reduced from 1159, 1300, 1254 Ω, to 31, 34 and 33.8 Ω, respectively (Graph 3.1). Figure 3.15 indicates the change in the surface morphology following annealing at 200°C for 35 minutes. Annealing for 12 h., in the presence of water vapour resulted in a reduction of resistance similar to that of the 35 min. annealing although there was deterioration in the sheet resistance after a 24, 48 or 120 hr period. However this deterioration was less than that seen in samples heated with no water vapour (Graph 3.2).

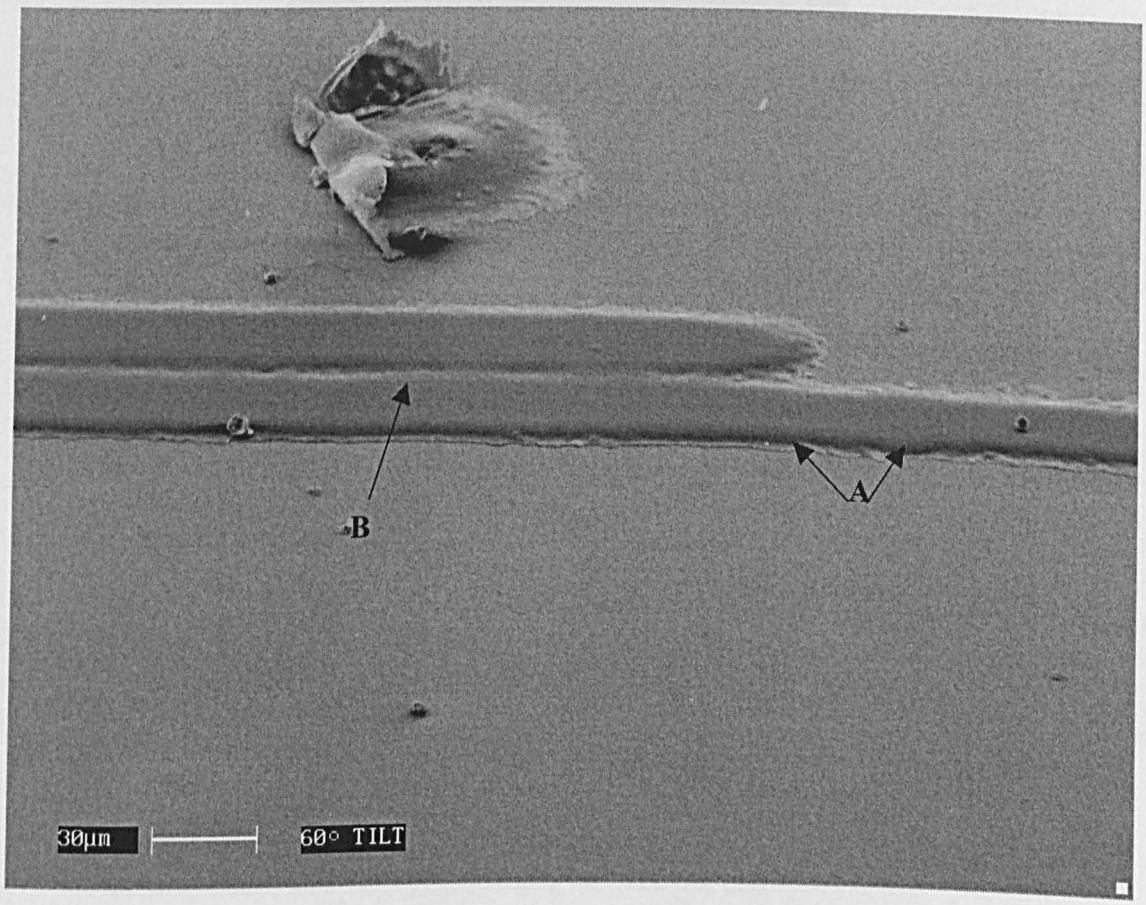

Figure 3.11 **SEM of an Aqua Regia etched device, showing the rounded edges 'A' and the low resolution, 'B', achieved with this process.**
Scale bar represents 30 µm

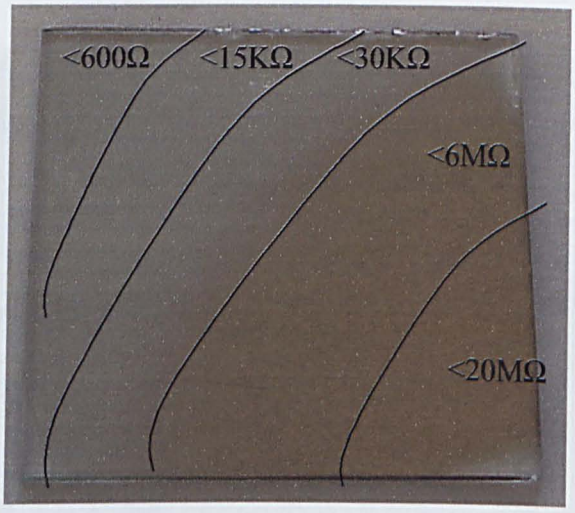

Figure 3.12 **Uneven ITO film deposition over the 49 x 49 mm glass slide indicating areas of resistance.**

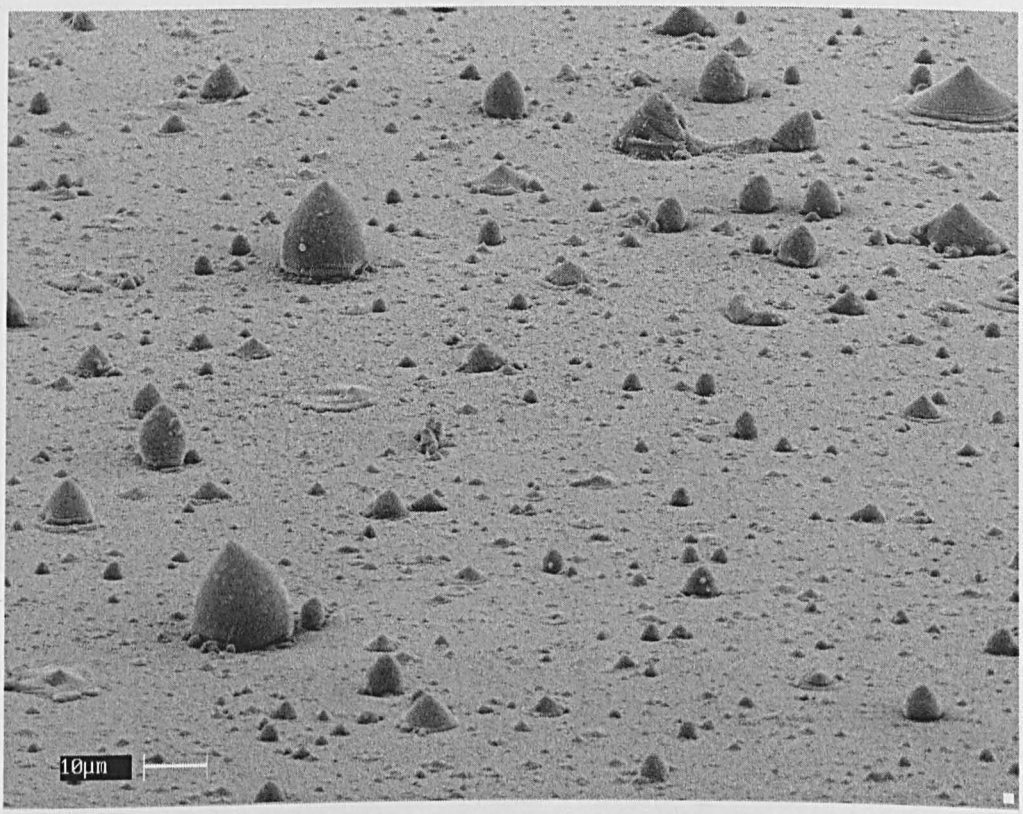

Figure 3.13 **ITO film on non-pretreated surface, viewed at a 70° angle.**
Scale bar represents 10 µm

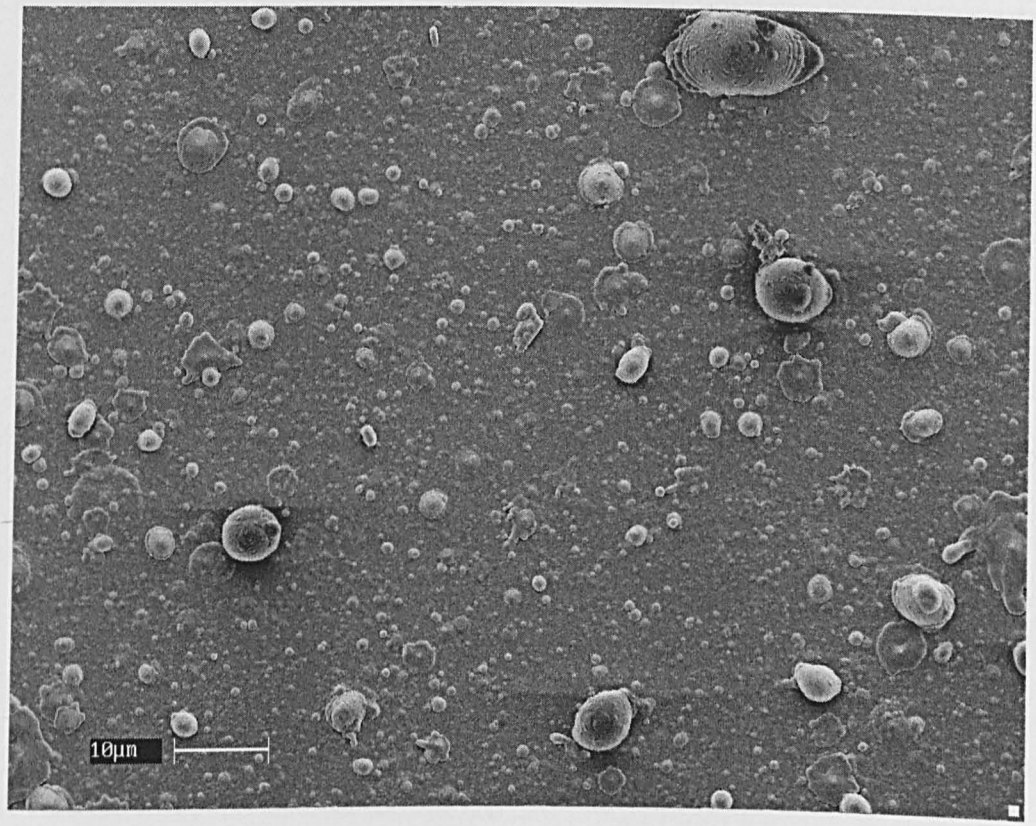

Figure 3.14 **ITO film on non-pretreated surface.**
Scale bar represents 10 µm

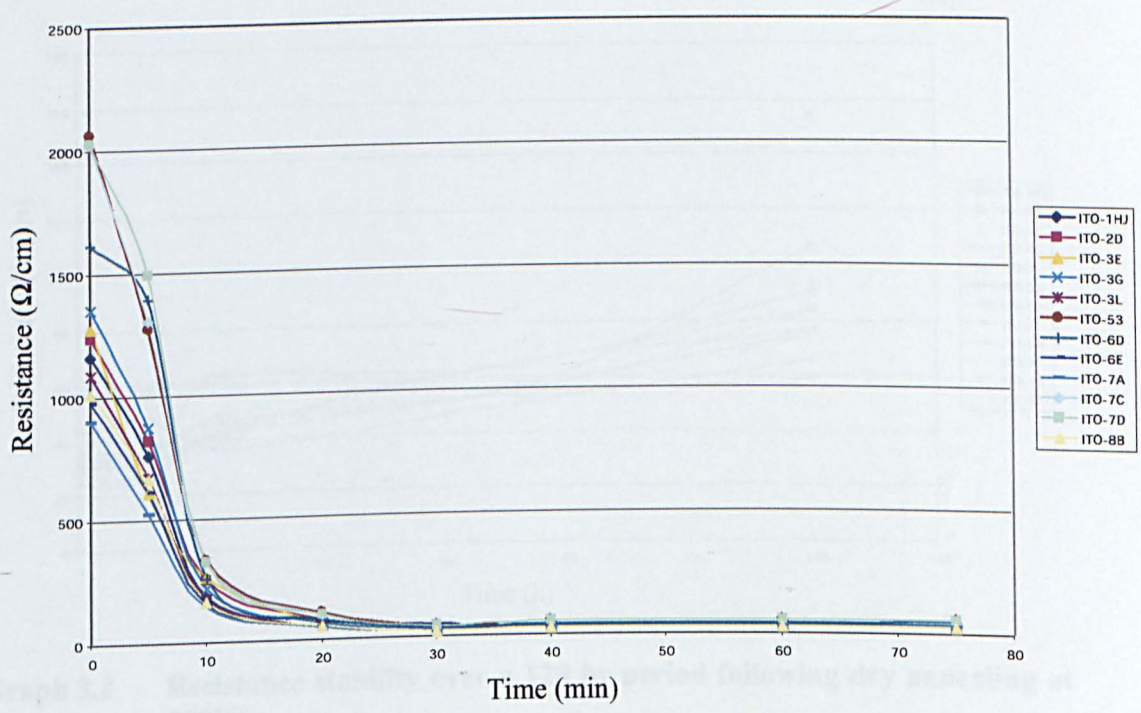

Graph 3.1 **The effect annealing at 200°C on the resistance of an ITO coating on a glass slide.**
Colours represent individual samples. n = 12

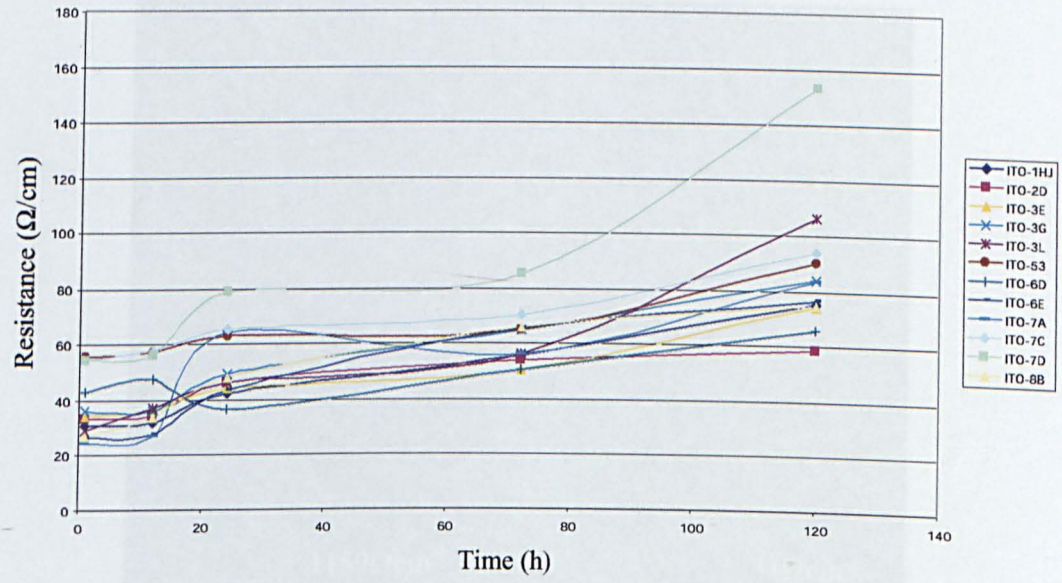

Graph 3.2 **Resistance stability over a 120 hr period following dry annealing at 200°C.**
Colours represent individual samples. n = 12

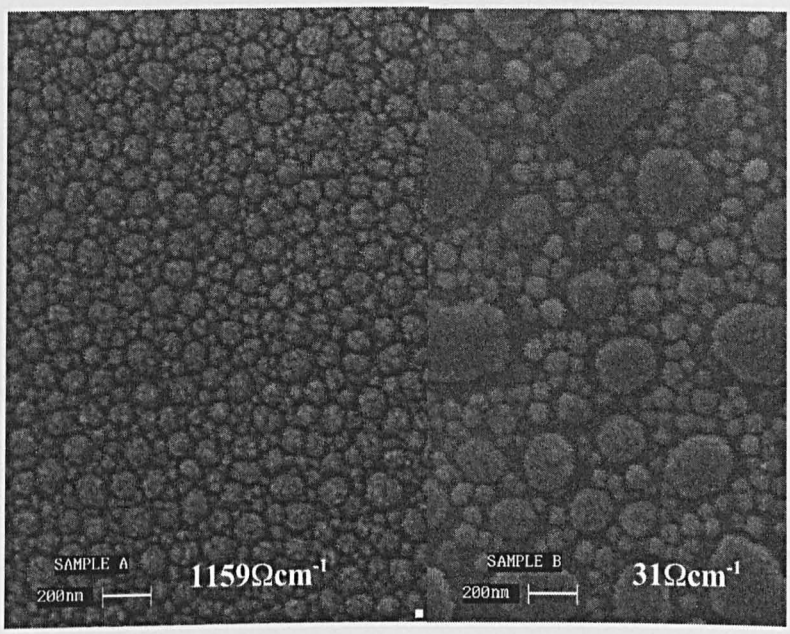

Figure 3.15 **The effect of a 200°C anneal on the surface morphology of an ITO coating on a glass slide together with their respective resistances.** Scale bar represents 200 nm

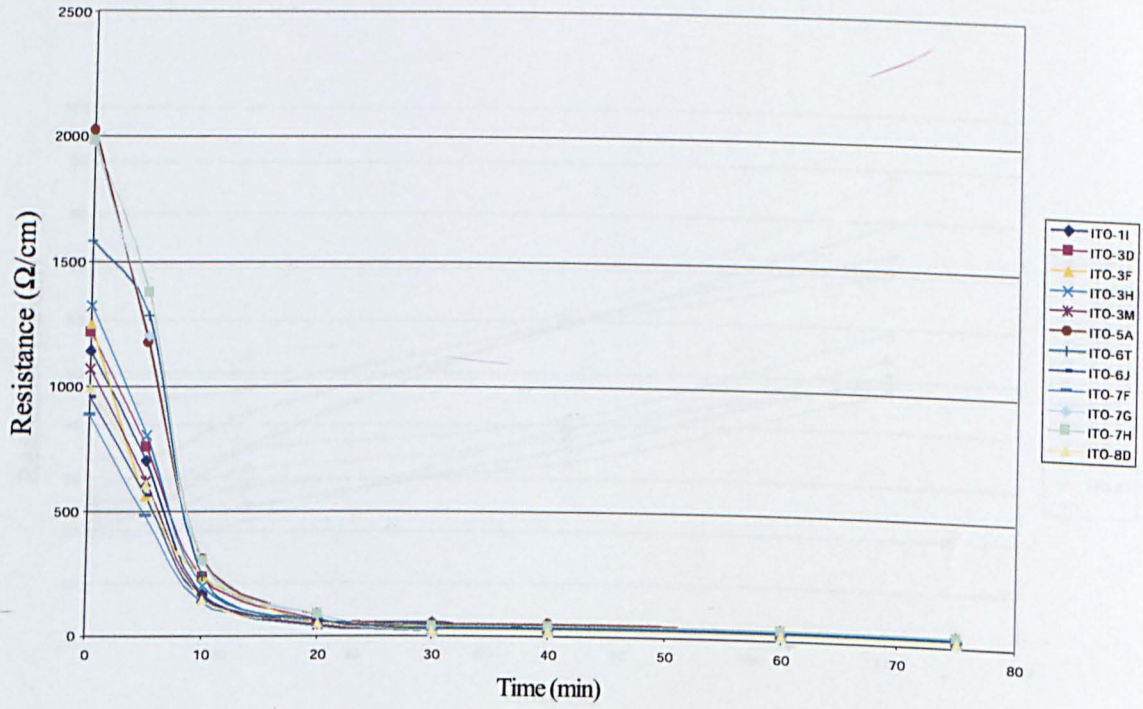

Graph 3.3 **The effect annealing at 200˚C on the resistance of an ITO coating on a glass slide wet atmosphere.**
Colours represent individual samples. n = 12

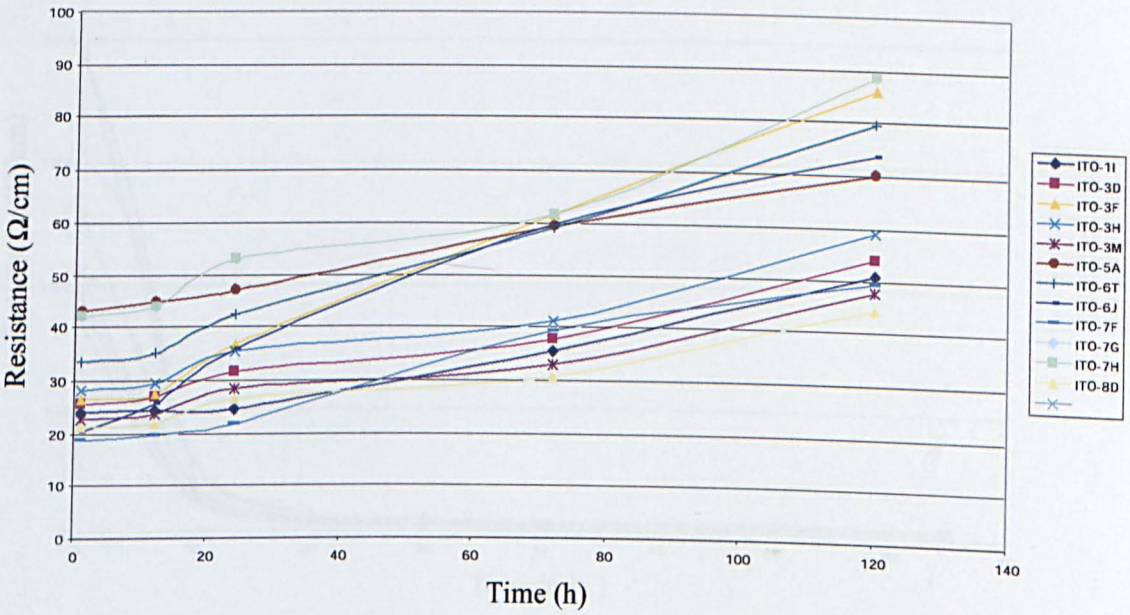

Graph 3.4 **Resistance stability over a 120 hr period following wet annealing at 200°C**
Colours represent individual samples. n = 13

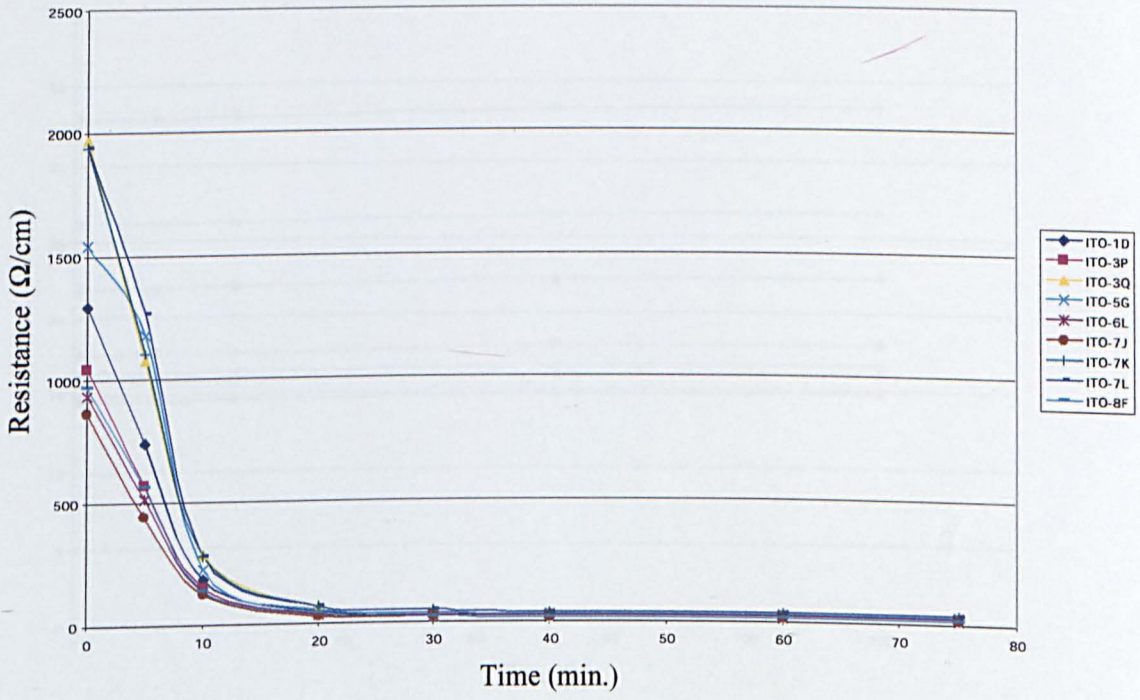

Graph 3.5 **The effect of annealing at 200°C on the resistance of an ITO coating on a glass slide in a wet atmosphere, followed by a period of dry annealing.**
Colours represent individual samples. n = 9

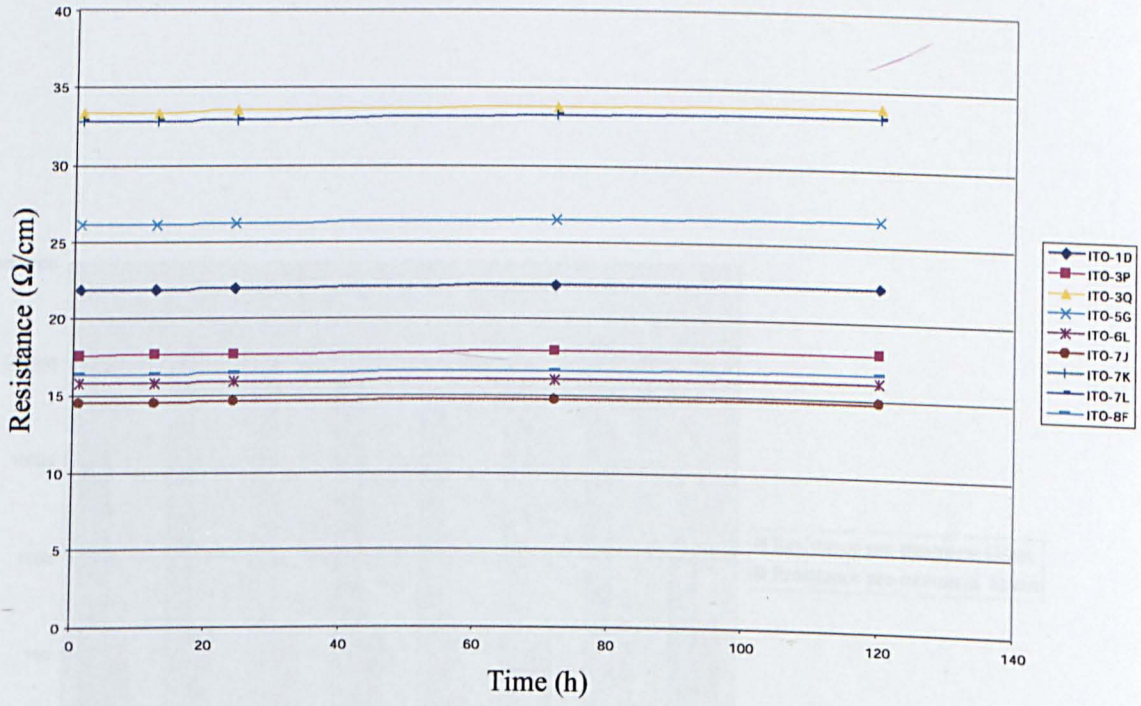

Graph 3.6 **Resistance stability over a 120 hr period following wet and dry annealing at 200°C.**
Colours represent individual samples. n = 9

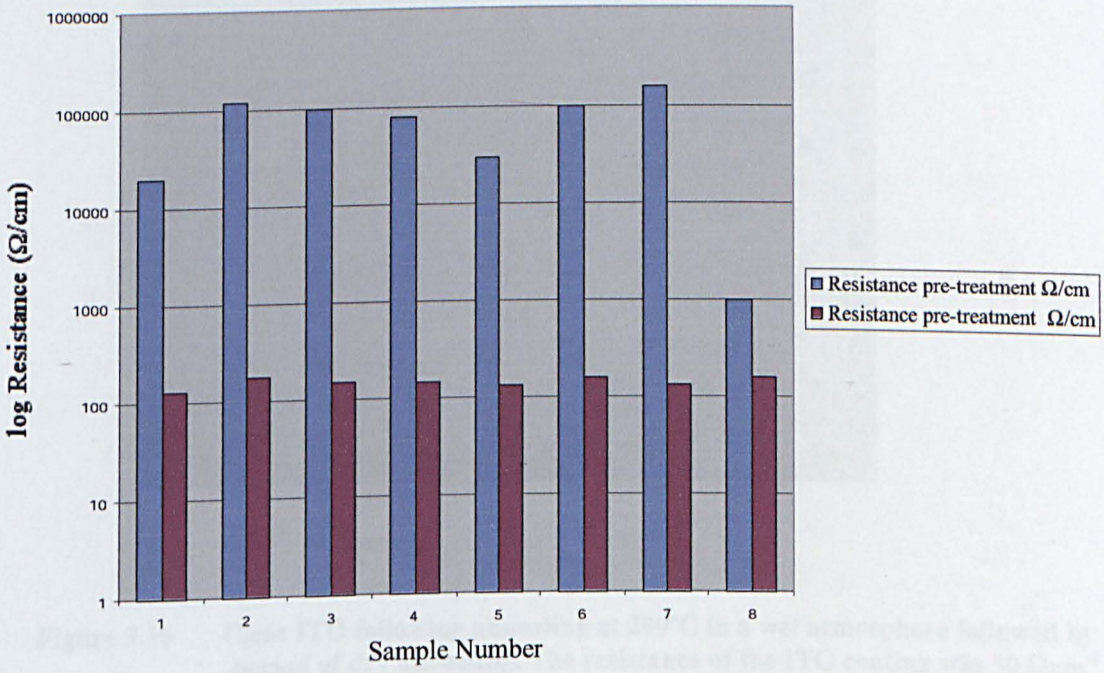

Graph 3.7 **Resistance drop following annealing at 550°C for 2 hours with an oxygen flow of 3.5 l min^{-1}, following wet annealing at 200°C for 2 hours.**

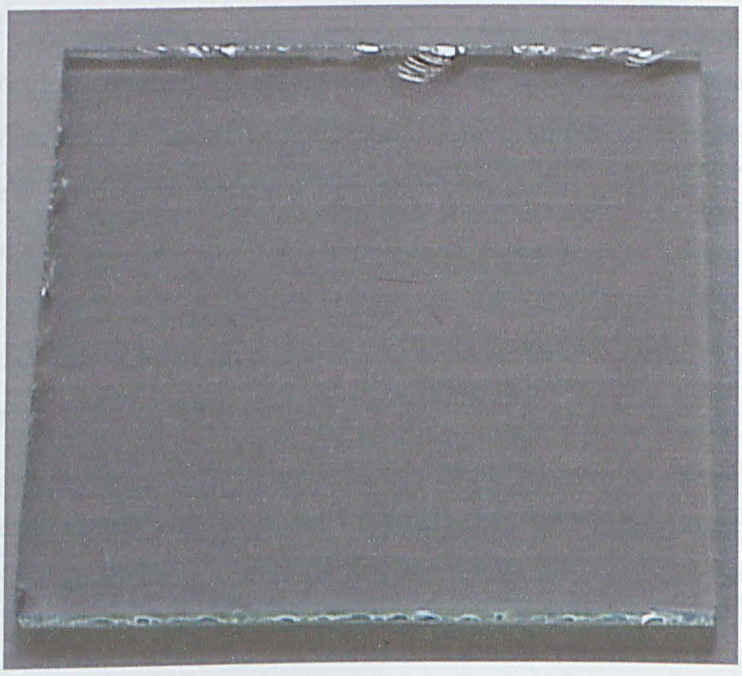

Figure 3.16 **Clear ITO following annealing at 200°C in a wet atmosphere followed by a period of dry annealing. The resistance of the ITO coating was 30 Ωcm^{-1}.**

The effect of higher temperatures, 550°C, under oxygen or argon (3.5 $l\ min^{-1}$) as the only method of post-depositional modification did not significantly alter the resistance. However, by pretreating the samples for 2 hours at 200°C, followed by exposure to an oxygen flow of 3.5 $l\ min^{-1}$ at 550°C produced a sample with much lower resistance, under these conditions, however the stability of the glass substrate was compromised, leading to samples with curved substrates.

The negative photoresist produced masks were difficult to remove and demonstrated a significant increase in resistances. Thus the use of negative photoresist was not pursued for this application. Positive photoresist, however enabled the production of clean masked areas which were resistant to the ITO etch (0.1M HCl), and also easily removed during post-etch cleaning with 0.1M NaOH.

3.3.10 Silicon surface layer

The deposition of a layer of silicon was required, to cover the ITO electrodes, acting as an insulator, and to produce a growth area for cells. Silicon was deposited on the surface of the glass / ITO substrate using d.c. sputtering, with an initial sputter time of 30 minutes. This produced a predominately uniform layer which was 630 nm in thickness.

Aside from cleaning, no pre-treatment of the prepared slide was required. Once the previous layer of mask had been removed with NaOH, the sample was washed thoroughly in double distilled water immersed in a 1:1 solution of sulphuric acid and hydrogen peroxide (0.01M), washed again with ddH2O and dried under a nitrogen stream. This method was seen to improve the adherence of the silicon without affecting the resistance of the ITO.

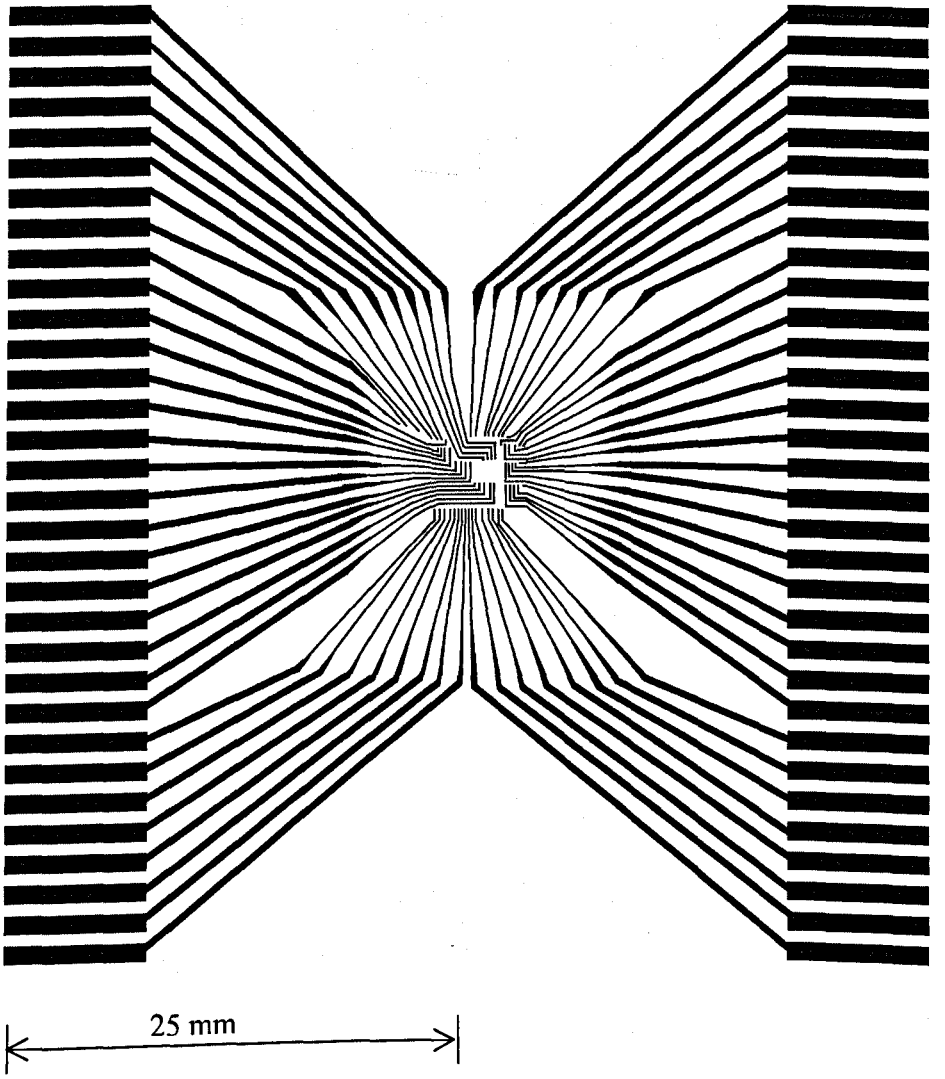

Figure 3.17 The mask DMU3d. This design is compatible with the 64 channel recording equipment at Nottingham University.

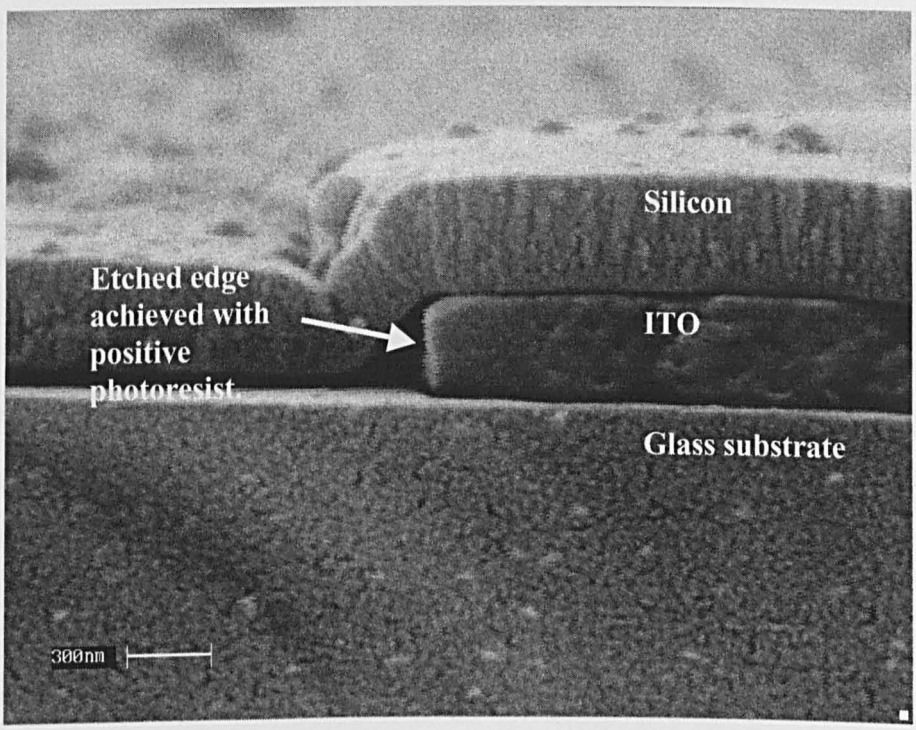

Figure 3.18 **Cross section of the device showing clearly defined lines produced using the positive photoresist.**
Scale bar represents 300 nm

3.3.11 MTT toxicity assay

The MTT assay was used to asses the cytotoxicity of SiO, SiO_2, Sn and ITO. Standard curves were established using differing cell concentrations to establish the optimal seeding density for the B50 cells for this assay. A growth curve was also plotted to obtain the optimal time point at which to inoculate the start cells with the MTT or neutral red dye.

3.3.12 Growth baseline

A profile of the growth, a growth curve, and a seeding density profile were plotted (Graph 3.8). Using the information provided an optimal time frame was decided, 24 h pre-inoculation followed by an MTT incubation of 4 h.

A seeding density of B50 cells of between 0.5 – 4 x 10^6 ml^{-1} was investigated. The value of 4 x 10^6 ml^{-1} provided repeatable results for the 24 – 30 h time period with a maximal reading at 30 h (Graph 3.9).

3.3.13 Neutral red uptake assay

The NRU assay followed the same basic protocols as for the MTT, however the post inoculation incubation period was 3 h, thus the pre-inoculation incubation period was amended to 25 h post-seeding. The results of this series of experiments are detailed in Graph 3.16.

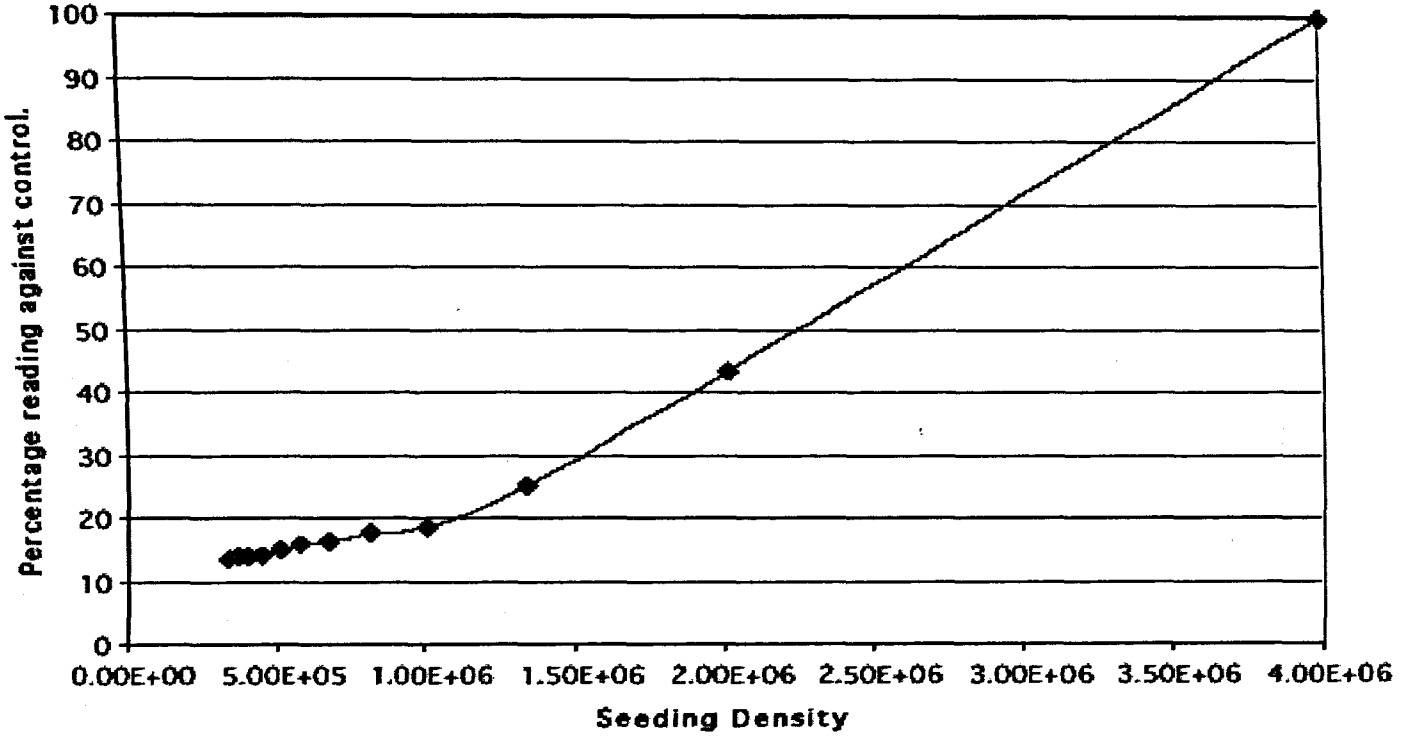

Graph 3.8 Seeding densities used in the MTT assay investigation, as measured 30 hr post seeding. 100% = seeding density of 4×10^6 cells per ml. (n=9-18)

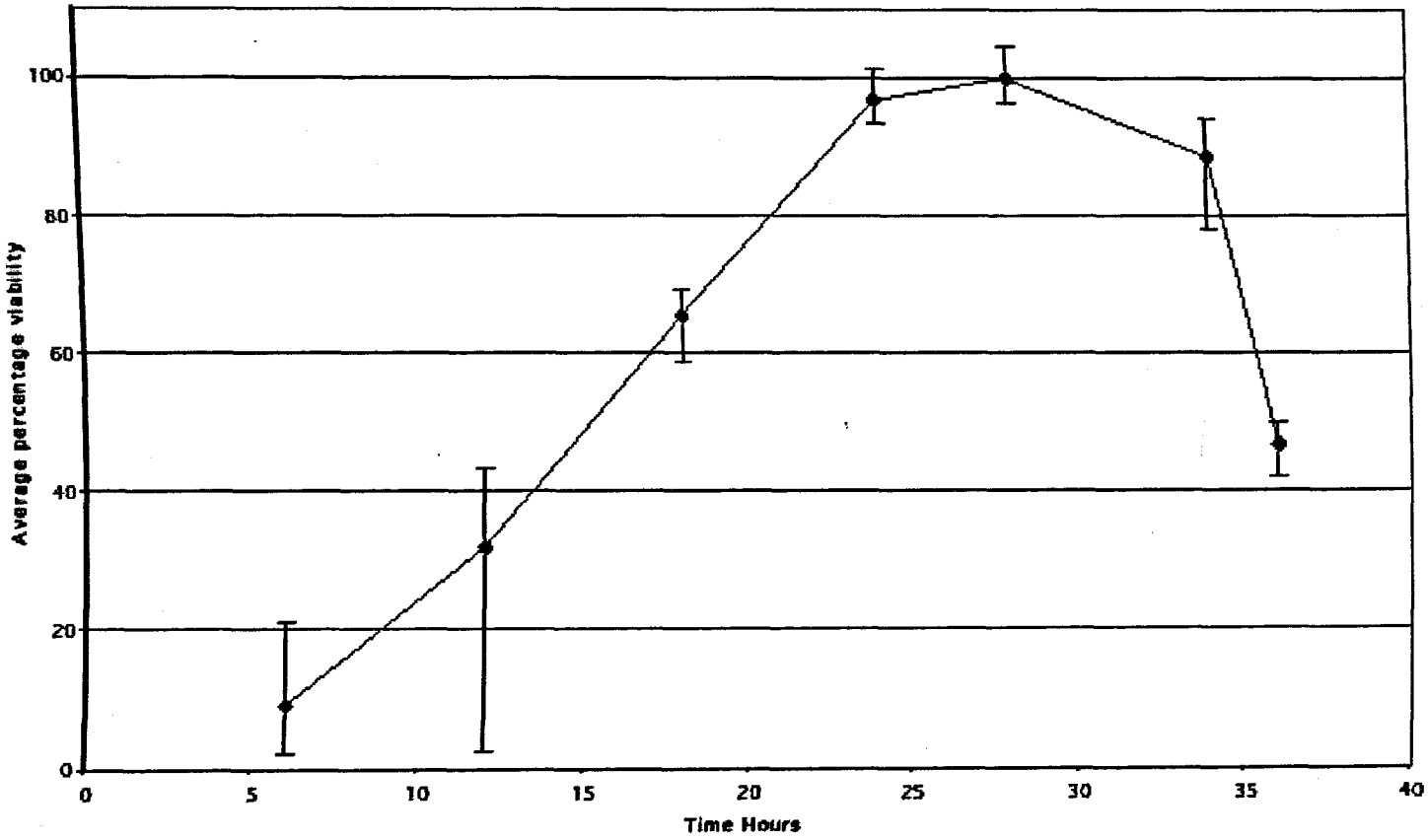

Graph 3.9 Growth curve for B50 cells grown under MTT test conditions. (n= 9-18)

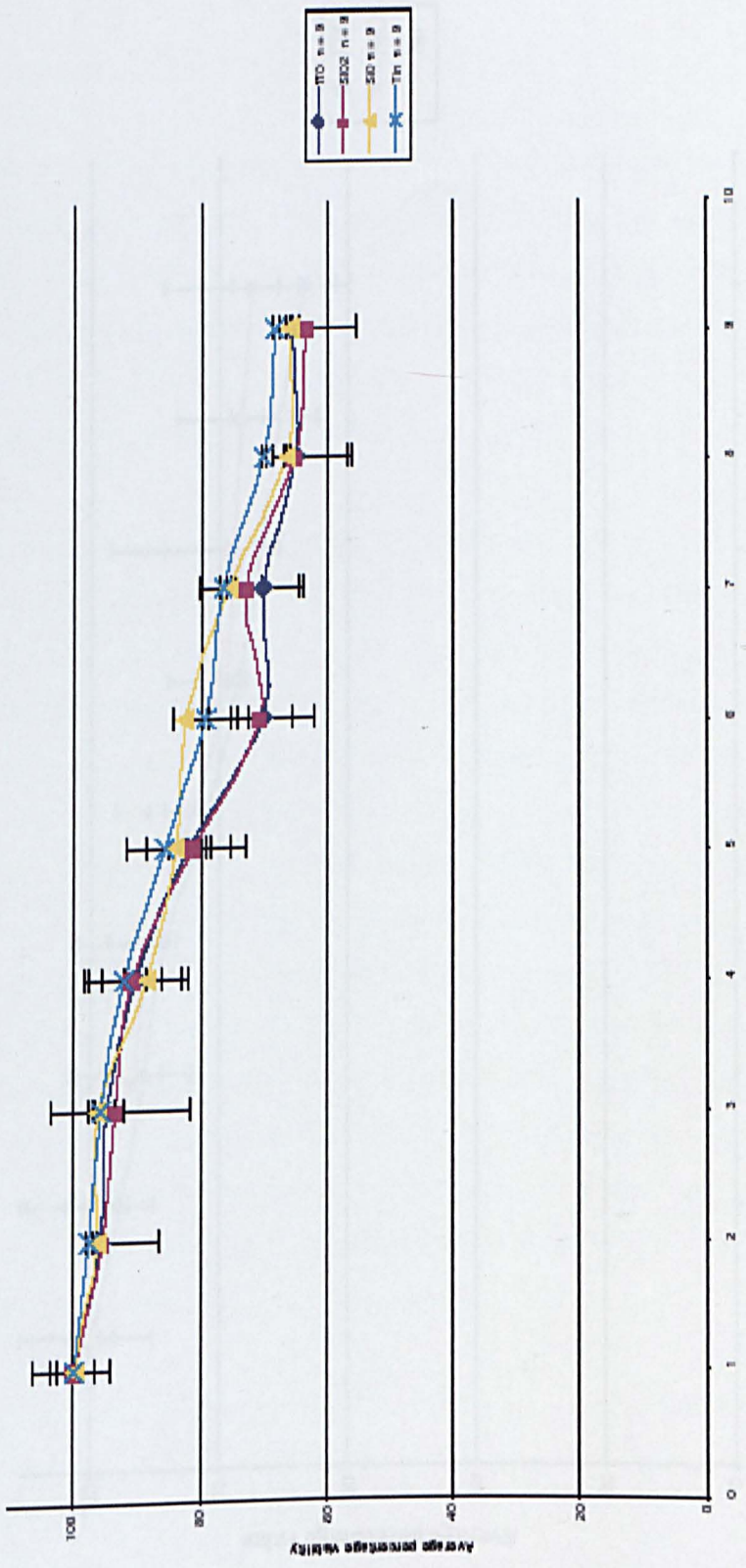

Graph 3.10 MTT assay for results ITO; SiO; SiO_2 and Sn. (n = 9 in all cases)

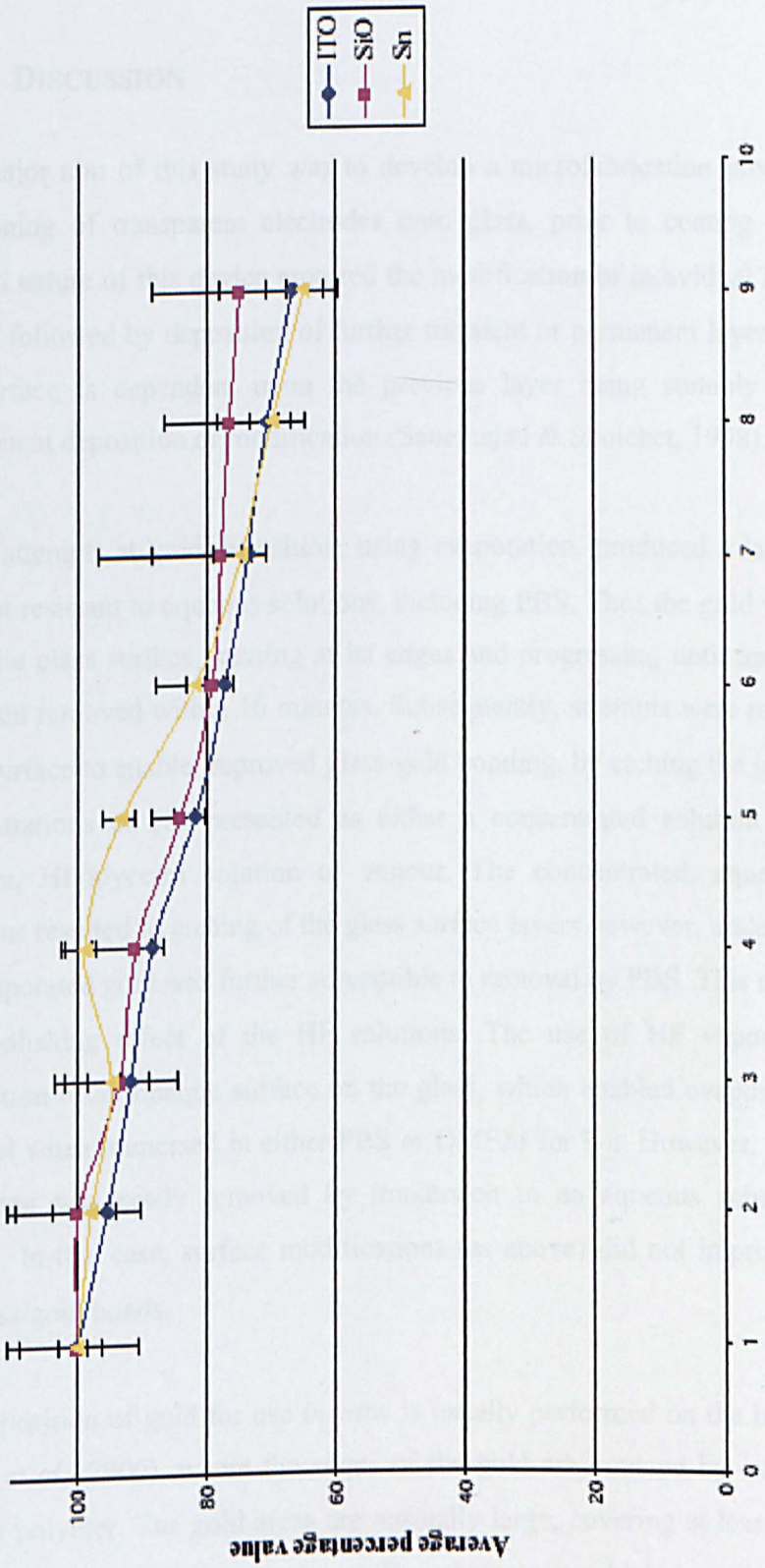

Graph 3.11 NRU assay results for ITO; SiO; SiO_2 and Sn. (n = 10 in all cases)

3.4 DISCUSSION

The major aim of this study was to develop a microfabrication process to enable the positioning of transparent electrodes onto glass, prior to coating with silicon. The layered nature of this device required the modification of individual layers on differing scales, followed by deposition of further transient or permanent layers. Modification of the surface is dependent upon the previous layer being suitably modified for the subsequent deposition or modification (Saneinejad & Shoichet, 1998).

Initial attempts at gold deposition, using evaporation, produced a layer of gold which was not resistant to aqueous solutions, including PBS. Thus the gold was seen to detach from the glass surface, starting at its edges and progressing until approximately 80 % had been removed within 10 minutes. Subsequently, attempts were made to modify the glass surface to enable improved glass-gold bonding, by etching the glass with differing concentrations of HF presented as either a concentrated solution (48 %), aqueous solution, HF/glycerol solution or vapour. The concentrated, aqueous and glycerol solutions resulted in etching of the glass surface layers however, under these conditions, the evaporated gold was further susceptible to removal by PBS. This may have been due to a polishing effect of the HF solutions. The use of HF vapour resulted in the production of an opaque surface on the glass, which enabled evaporated gold to resist removal when immersed in either PBS or DMEM for 2 h. However, gold deposited via sputtering was easily removed by immersion in an aqueous solution (PBS) or by wiping. In this case, surface modifications (as above) did not improve the stability of the glass/gold bonds.

The deposition of gold for use *in vitro* is usually performed on the base of a Petri dish (Yoon *et al.*, 2000), where the edges of the gold are covered by either photoresist or another polymer. The gold areas are normally large, covering at least 30 % of the base of the dish for each contact point. The photoresist which is added acts both as an electrical insulator and as a protective barrier to the aqueous solutions. However, in the current device, high precision etching (20 μm) of the deposited gold is required in order to produce electrodes, thus the protection offered by photoresist, as reported previously (Yoon *et al.*, 2000), would not be of benefit in this case.

Gold electrodes are routinely deposited upon silicon substrates in the microelectronics industry, thus an intermediate layer of silicon deposited onto the glass was expected to provide a suitable layer for gold to adhere to. The formation and properties of thin films deposited upon a substrate depend upon the physical and chemical natures of the substrate surface (Lewis & Anderson, 1978). In the current study, defects, such as blisters, occurring on the silicon surface were attributed to the presence of debris (see Figure 3.6). Furthermore, when the silicon/glass sample was sonicated (15 s), the silicon layer was disrupted causing pinholes to appear (Figure 3.7). Surface pre-treatments are an effective way to modify the properties of both the donor surface and the deposited film. Previously, the effectiveness of such treatments has been shown for tin oxide films prepared by chemical vapour deposition on glass substrates (Arai *et al.*, 1992), and platinum and nickel particles prepared by vacuum deposition on carbon and refractory oxide substrates (Arai *et al.*, 1985). In the current study, cleaning of the substrates with a 1:1 solution of sulphuric acid and hydrogen peroxide, and drying under nitrogen, enabled the production of even layers of sputtered silicon, which resisted sonication (30 min; Figure 3.8).

Once silicon had been sputtered onto glass, a layer of gold was evaporated on to the silicon surface, as a film approximately 1.1 μm in thickness (Figure 3.9). The gold layer was resistant to immersion in both PBS and DMEM (3 h). Under these conditions, there was no feathering of the edges and no creeping of the liquid under either of the deposited layers. Subsequently, a mask (PT1; Figure 3.10) was applied to the gold layer and etched with Aqua Regia (HCl: HNO_3; 3:1) for 12 h. In this case, the contact points appeared rounded and feathered when examined under the SEM (Figure 3.11), an effect which was probably caused by the prolonged etching process. This may also have contributed to resistances of greater than 20 $M\Omega cm^{-1}$. The gap (25 μm) on the original mask was therefore not resolved using this technique. Subsequent re-etching, or prolonging the etch time to 18 h, resulted in complete removal of the gold layer. Thus the use of Aqua Regia for etching was determined to be unsuitable for this application. Subsequently, potassium iodide was employed for gold etching, having a rapid reaction time (6 min) and resulting in significantly improved resolution of the edges of the contact strips, together with lower resistances ($2\Omega cm^{-1}$).

The second device to be developed required sputtered indium tin oxide (ITO) to be deposited onto a glass substrate. The main problems encountered here were with reproducibility of deposition and the inherent high resistances. This was due to the position of the substrate with respect to the target. The target emits plasma from the centre of the disc and, unless the substrate is positioned directly over the centre, the coating will be uneven. It can be seen in the sputter pattern diagram (Figure 3.2) that the position of the glass substrate is critical to the deposition profile of the final ITO film. By controlling the positioning of the substrate to the centre of the beam area, ITO deposition on the glass was controlled, although this limited the production of slides to one per sputter cycle. The result of centre positioning was an even coating of film (Figure 3.16) with consistent levels of resistance across the surface of the slide and reproducible results.

The target film resistance was 25 – 100 Ωcm^{-1}, similar to that of the Gross device. The resistance of the sheet, as indicated above, is dependent upon the position in the sputter plant (Figure 3.12), but can also be affected by pre- and post-deposition modification. Prior studies indicate that the effectiveness of pre-treatments to modify the properties of thin solid films is of key importance (Arai *et al.*, 1992; Chen *et al.*, 1987; Koch & Poppa, 1987a; 1987b; Laine *et al.*, 1963; McBreen *et al.*, 1981; McVicker *et al.*, 1978). For example, Koch & Poppa (1987a; 1987b) deposited palladium film on a mica substrate by vapour deposition, and demonstrated that there was a change in the number and structure of palladium particles by thermal pretreatment of the substrate. Surface hydroxyl groups present on the substrate were proposed as the cause for the changes observed. In the current study cleaning of the glass substrates in a solution of H_2SO_4 :H_2O_2, transferring to the sputter plant under nitrogen, and double evacuation of the sputter plant prior to deposition, improved the adherence of the ITO to the glass. Pre-, during, and post-deposition techniques as reported by Higuchi *et al.*, (1993; 1994) reduced the resistances of ITO films. Higuchi *et al.* utilised a two-tier approach for lowering film resistance, firstly heating the substrate to 250°C prior to and during the sputtering, followed by heating to 200 - 300°C under vacuum for up to 12 h. The cryopumped CVC plant used in the current study only enabled post-depositional modification. While annealing is ideally done in a vacuum environment (Higuchi *et al.*,

1993), use was made of two ovens, a Belling, giving controlled temperatures up to 275°C, and a furnace for controlled temperatures > 450°C.

The shapes of small particles from which the film is composed were more visible in the non-pretreated than pretreated glass substrate, an extreme example of this is shown in Figures 3.13, where projections of 10 – 15 μm can clearly be seen. Untreated glass, washed only in Decon 90 with mild sonication, produced these island structures on the surface. Samples further treated with H_2SO_4 and H_2O_2 and dried under nitrogen produced a different topography, as seen in Figure 3.14. Pretreatments of a glass substrate affect the electroconductivity of ITO film deposited on it by sputtering. The pretreatments probably influence the nucleation of the metals during the sputtering and the structure of ITO film formed by the following oxidation, the result of this is a modification of electroconductivity.

Post-depositional changes observed in the ITO films may be analogous to amorphous and polycrystalline silicon. ITO films that are deposited at moderate substrate temperatures (below 500 °C) have a polycrystalline structure. Hence these films contain a high density of structural defects, such as grain boundaries, interstitial atoms, and vacancies, in addition to some impurity atoms which may be either residual effects of pretreatment or emanating from the substrate as a leached product. Electrically active 'dangling bonds' might be expected in these films (McBreen *et al.*, 1981). Passivation of dangling bonds by hydrogen, as these ions can readily diffuse into the bulk of the film, has also been proposed by Keshmiri *et al.* (2001). Keshmiri suggests it is this that accounts for a considerable increase in carrier mobility, and hence electrical conductivity of zinc oxide films. This may account for some of the observed reduction in film resistances, however there is no indication as to the longevity of the effect. Keshmiri *et al.* (2002) suggested that the same is true for ITO, deposited at 200°C in a dry hydrogen atmosphere.

In the current study, the atmosphere was 'wet', the samples being annealed in a water-saturated atmosphere for 2 h at 200°C followed by 2 h in a dry atmosphere. As Figure 3.15 demonstrates, this technique resulted in surface modification suggesting

redefinition of grain boundaries during annealing, causing a restacking of the polycrystalline ITO. The use of the furnace (550°C) compromised the integrity of the substrate, causing the edges of the glass to buckle, thus it was decided that wet annealing followed by dry annealing would provide the most reproducible method for producing a transparent sheet of ITO with suitably low resistance (Figure 3.16).

The deposition of both positive and negative photoresist on to the surface of the ITO was investigated; a number of low resistance plates were produced, and either positive or negative photoresist was applied. During the masking procedure changes occur, altering the surface chemistry of the deposited films and thus their electrical properties. The mask used for this and all subsequent investigations, DMU-3d, is depicted in Figure 3.17.

The etch used in this series of investigations was 0.1 M HCl which worked well with both photoresists, however a finer definition of edges was observed when using the positive photoresist, thus this was employed for all subsequent masking requirements. Once the ITO had been etched and cleaned, a layer of silicon was sputtered onto the surface. This layer, due to the pre-treatments following ITO etching, was uniform. The depth of this layer was dependent upon both time and chamber conditions, however the average sputter rate was approximately 30 nm min^{-1}. Figure 3.18 depicts a cross section of the assembled device; the etched ITO layer is about 300 nm in thickness, the sharp edges being achieved using a positive photoresist and an HCl etch. The layer of silicon above the ITO is also about 300 nm in depth and therefore translucent.

The MTT and NRU assays (Doyle *et al.*, 1998) are routinely used to assess the cytotoxicity of composite materials (Fubini *et al.*, 2001; Risbud *et al.*, 2001), and thus provided the basis of the investigation into various concentrations of substrate compounds. Different cell concentrations were used to establish the growth curve (Graph 3.8) and to ascertain an optimal seeding density (Graph 3.9). The cells were cultured for 24 hrs until 70% confluent in the maximum concentration series, then incubated for a further 4 hours in the presence of MTT. Preparation of the samples included standing time (1 week), to enable any leaching to occur (Risbud *et al.*, 2001).

The growth curve results (n = 9 – 15) suggest that the optimal growth time for a seeding density of 4 x 10^6 was 30 hrs. The growth periods were modified to account for the post-inoculation incubation periods (MTT: 4 h, NRU: 3h). This ensured that the resultant cell growth did not then exceed the maximal cell density for the 96 well plate; in this scenario the plaque becomes non- viable (Graph 3.9), apoptosis is initiated and cell death occurs, which would result in inaccurate data. Seeding densities and time frames were similar to those reported by Fubini *et al.*, (2001), who investigated the toxicity of silica species on fibroblasts, and Risbud *et al.*, (2001), who investigated the biocompatibility of PTFE / wollastonite composites using endothelial cells and macrophages.

The results achieved with both the MTT and the neutral red assays indicate that the components of the device show low toxicity. In the concentrations investigated the LD50 (amount of chemical or toxin required to achieve a 50 % mortality) was not achieved. To achieve an LD50 with this method would present further problems, as the cell density should be optimised so as to minimise the effect of stressors on the cells which may induce apoptosis. As this cell line adheres to the bottom of the 96 well plate, then the addition of further metal particles affects the area of plastic that is available for cell contact. With the higher concentrations of metal in both the MTT and the neutral red assays it would be reasonable to assume that it was this that was beginning to affect the results.

Thus the results obtained from the current study demonstrate that an optimal device would be constructed from a glass substrate, with an ITO electrode layer deposited by sputtering. Once etched, a further layer of sputtered silicon is deposited to insulate the electrodes, and selective etching of this layer is performed to expose the electrode contact points to enable cellular interfacing. Finally, the components of this device were identified to be non-toxic, in the concentrations employed, thus demonstrating their usefulness for the intended purpose.

PAGE NUMBERING AS ORIGINAL

4 DEVICE VALIDATION

4.1 INTRODUCTION

This chapter describes the testing of two devices, the development and manufacture of which are detailed in Chapters 2 and 3. As stated previously the development of silicon-based substrate devices, such as DMU3, should enable the manufacture of new types of devices employing novel technologies for the generation of a three dimensional growth area. It was hoped that post-production validation of the current devices would provide information as to the overall resistance of the contact positions, the signal propagation and signal generation within the system, together with identifying any construction limitations which might compromise the signal to noise ratios.

This investigation involved analysis of signals generated by B50 cells grown on the DMU3 devices, which were tested in the Department of Neuroscience, University of Nottingham. The equipment consists of an inverted microscope connected to: (1) amplification circuitry, installed on the microscope stage area, (2) an analogue to digital converter which enables the analysis of any signal produced, using (3) the sophisticated signal separation techniques encoded into the Digital Signal Processor (DSP). Once a discriminated signal has been produced, it can then be analysed using the respective software packages installed on the system. This equipment is currently used for investigations into the stochastic firing patterns of rat neurones under specific stressors, e.g. Sokal *et al.,* (2000).

Prior to installation, the DMU3 device was compared with a Gross-manufactured device with respect to electrode impedance, according to the protocol described by Robinson (1968). Following installation on the microscope stage, the ITO edge connects from the DMU3 device created a circuit with the main processing rig via zebra contact strips. As previously stated in Chapter 1, sophisticated signal separation techniques are needed to overcome the effects of indirect or extraneous signals collected when recording data from the device. The function of the *Rasputin* (Realtime Acquisition System Programs

for Unit Timing In Neuroscience) equipment (Plexon, Texas, USA), is to isolate specific signals from the data produced and present them for further statistical analysis. The aim of this study was to record spontaneously produced electrical activity from B50 cells cultured on the DMU3 device. It was hoped that the signals recorded would have properties comparable to the baseline events reported by Sokal *et al.* (2000), using the same recording equipment and a Gross-manufactured device.

4.2 METHODS

4.2.1 Microelectrode arrays

The microelectrode arrays (MEAs) were manufactured as described in Chapter 3.

4.2.2 MEA preparation

MEAs were cleaned with diluted tissue grade glassware detergent and rinsed with double distilled water (15 min). A media chamber was attached to the MEA using silicone adhesive. The adhesive was allowed to cure for 48 hours in a sterile environment and rinsed in double distilled water (15 min) followed by PBS (5 and 3 min) immediately prior to culturing of B50 cells within the media chamber.

4.2.3 Cell culture

B50 cells were grown seeded (density of 4×10^6 ml^{-1}) in DMEM supplemented with 10% FCS, 1% L-glutamine, and 1% penicillin–streptomycin. Cultures were grown at 37°C in an atmosphere of 100% humidity and 5% CO_2 for 48 h prior to device testing.

4.2.4 Cell stimulation

To induce electrical activity within the cell culture, KCl (60 mMol; final concentration in 1 ml bath) was added to the DMEM 187 s after the initiation of recording.

4.2.5 Electrophysiological recording

The MEA was mounted on a microincubation/recording chamber (Gross and Schwalm, 1994) using a modified Zeiss Axiovert-10 inverted microscope stage, prior to initiation of electrophysiological recording. The microincubator temperature was maintained at 37°C using a TC-344 Dual Heater Controller (Warner Instruments Corp, USA). A modified 35 mm plastic Petri dish with a heated ITO glass window covered the chamber, preventing heat loss and condensation which would have resulted in media osmolarity fluctuations. An inlet in the Petri dish allowed the media to be gassed with moist 5% CO2: 95% air to maintain constant pH.

Simultaneous recording of both spike waveforms and spike event timestamps from the MEA was achieved using a multichannel acquisition processor (Plexon Inc. USA; http://www.plexoninc.com; Mason et al., 1998; Sameshima and Baccala, 1999). The processor provided programmable amplification, filtering (500 Hz–5 kHz), electrode-site switching, and digital signal processing of microelectrode signals, and was controlled by a host Pentium II 350 MHz PC running the Windows NT v.4 operating system.

4.2.6 ADC and DSP

Analogue to digital conversion (ADC) was performed by 4x16 simultaneously sampling 12-bit converters (40 kHz). Digital signal processing (DSP) was performed using Motorola DSP56002 microprocessors (40 MHz) for spike waveform capture and sorting. DSP programmes were downloaded from the host Pentium PC using custom designed software (*Rasputin*; Plexon Inc, USA). Spikes were sorted in real-time by the DSP microprocessors, using one pair of experimenter-defined graphical time/voltage windows per single-unit (neurone) or by template matching, with the capability to isolate up to four single units per microelectrode. Action potentials were monitored on a five-channel Tektronix 5110 series oscilloscope, multiple audio speakers and an eight-channel thermal chart recorder (Thermal Array Recorder WR 3600, Graphtec).

4.2.7 Data analysis

The time of spike events for all active channels were sent to the host PC through a 16-bit parallel bus at a rate of 2 MB data per second to an MXI-Bus interface board (National Instruments) mounted in the host PC. The data were initially recorded to the PC hard disk and subsequently transferred to an optical disk for archiving. Data were recorded in a Plexon file (.plx) format that consisted of the timestamps for the spike events, waveforms and file information. Data were analysed off-line using specialised multiple spike train analysis software designed to handle multiple large neuronal data sets; *SpikeWorks* (Plexon Inc, USA), followed by *NeuroEXplorer* (Nex Technologies, USA; http://www.neuroexplorer.com/).

4.3 RESULTS

The device, the production of which has been described in Chapter 3, was tested on the rig in the Department of Neuroscience, University of Nottingham. As described previously the device was validated as a running system, undergoing the same protocols as the established Gross device (Sokal *et al.*, 2000). The device was tested for electrode impedance measured with a 50 mV rms, 1 kHz sinusoidal signal, according to the method of Robinson (1968) (Table 4.1).

Cells were incubated 48 h prior to positioning of the device on the rig (Figure 4.1) and recording commenced after a 3 h stabilisation period. The device was unable to detect spontaneous activity from the neuronal cell culture, thus KCl (60 mMol) was added to the system to induce activity, which resulted in the recording of an evoked spike across several of the electrodes. The activity spikes thus recorded and processed via *SpikeWorks* (Figure 4.2) represent the additive sum of signals received per channel over the recording period (248 s). The recorded spikes, isolated in Figure 4.3, occurred at the 187 s time stamp; the time at which KCl (60 mMol) was added to the DMEM.

Device	Impedance range
DMU 1000 nm silicon	2.5 – 3.5 MΩ
DMU 650 nm silicon	1 – 2 MΩ
Gross Device (polysiloxane)	0.5 – 2 MΩ
Gross Device (Sokal *et al.*, 2000)	0.5 – 4 MΩ

Table 4.1 **Electrode impedance measured with a 50 mV rms, 1 kHz sinusoidal signal (Robinson, 1968)**

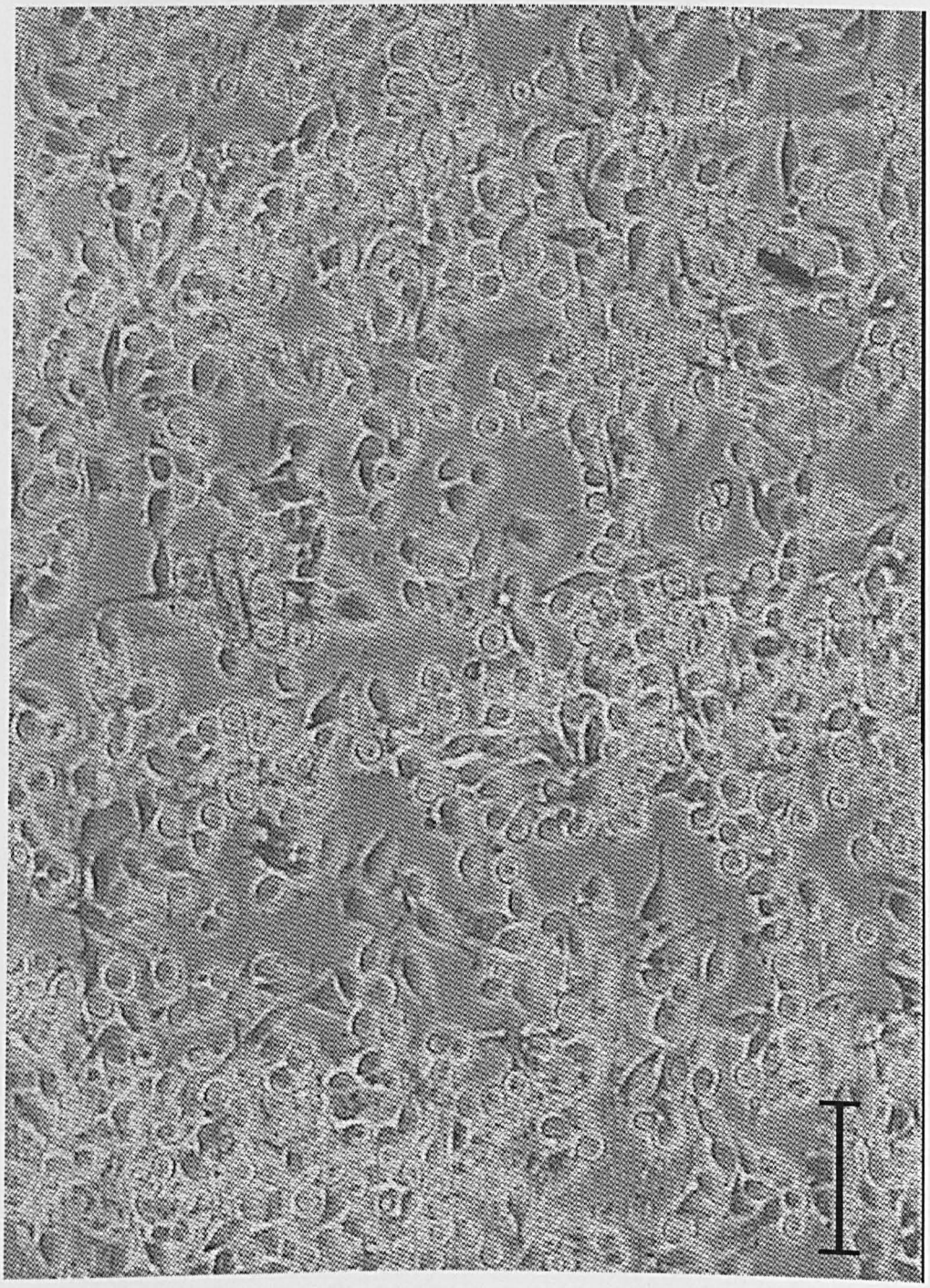

Figure 4.1 **B50 cells cultured (4 divisions) on DMU3a device (silicon depth 1 µm)**
Scale bar = approximately 25 µm

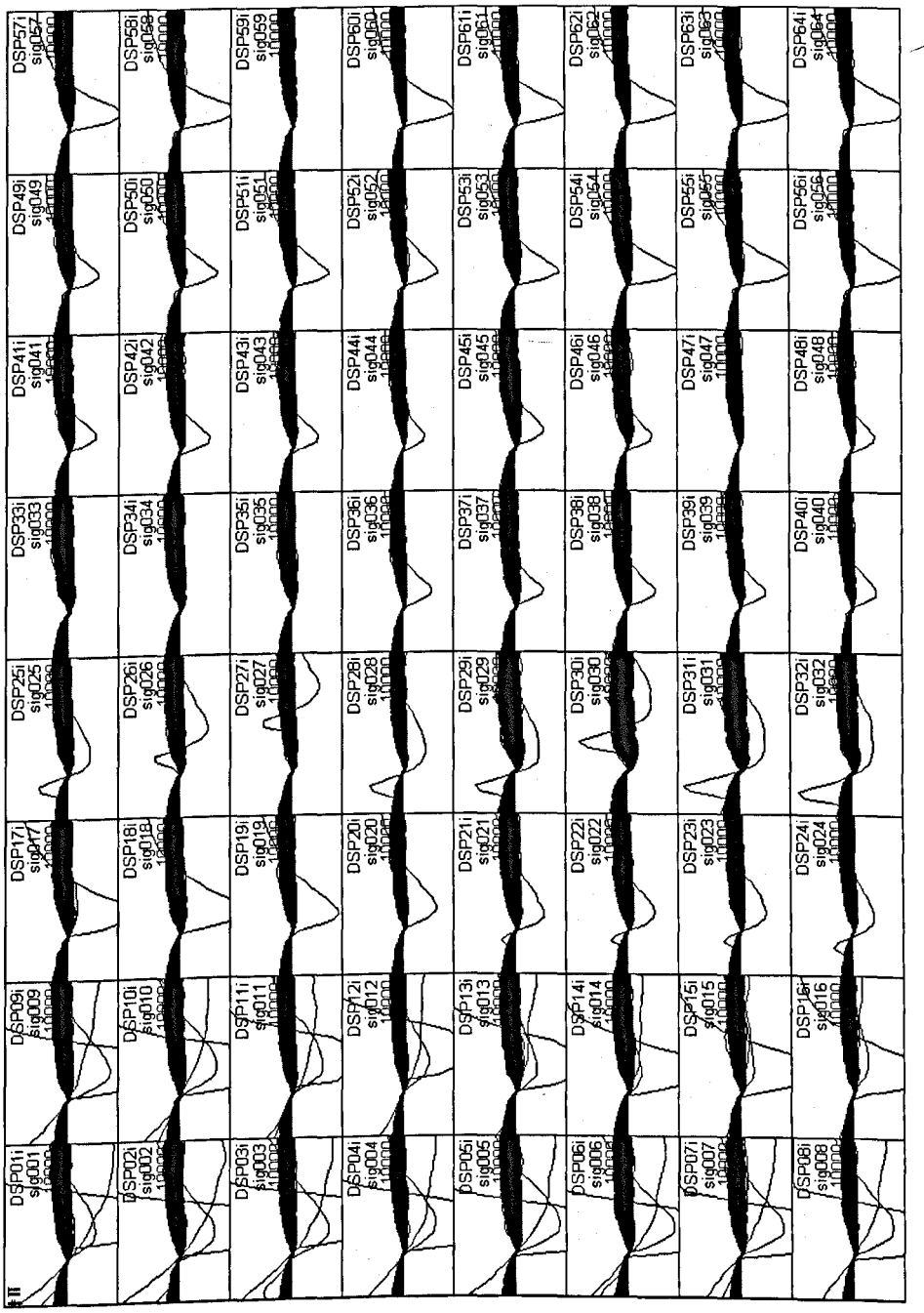

Figure 4.2 Spontaneous and evoked activity spikes recorded and processed via *SpikeWorks*.

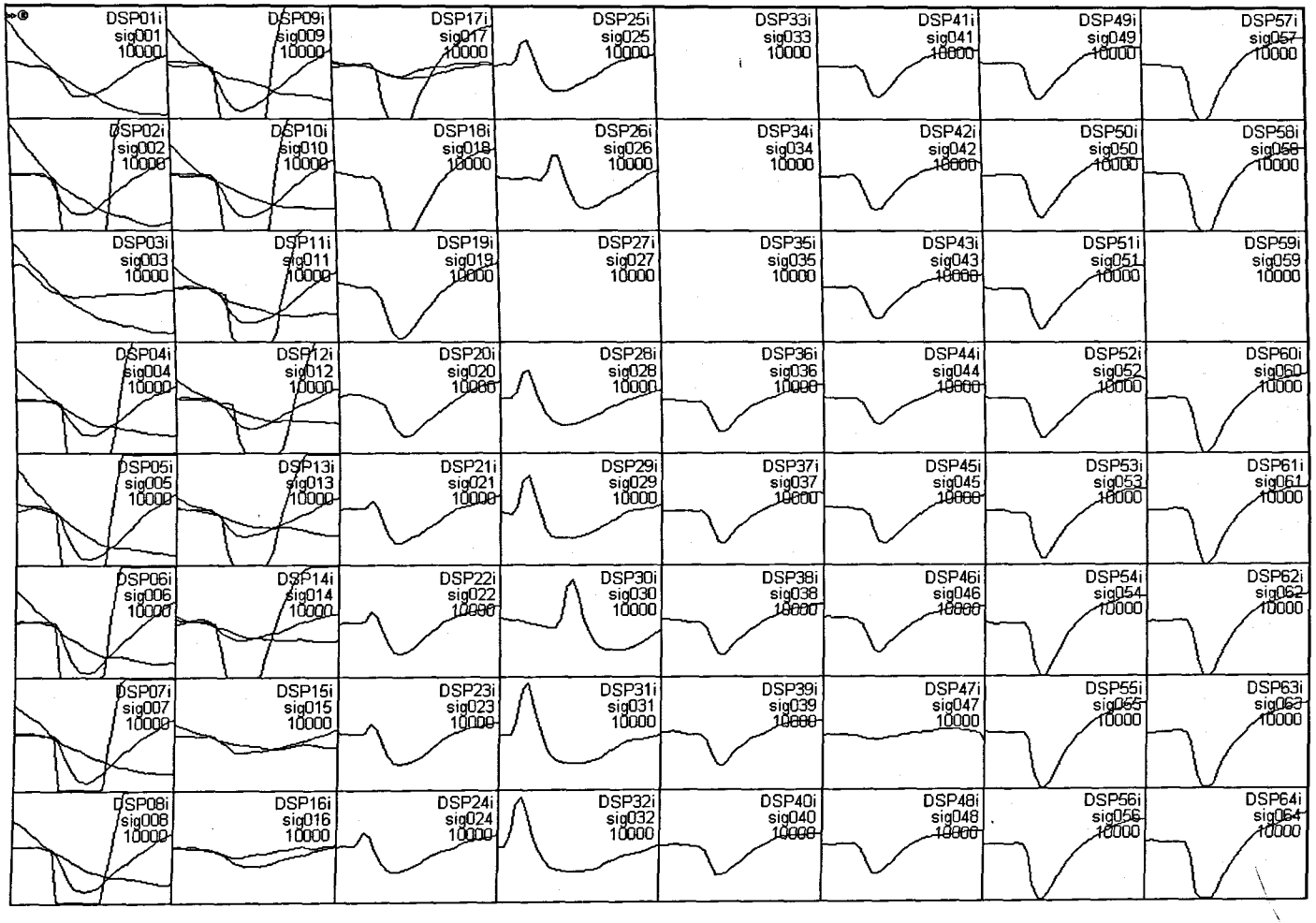

Figure 4.3 **Isolated activity spikes recorded and processed via *SpikeWorks*, following stimulation by the addition of KCl.**

4.4 DISCUSSION

The electrode impedance measurements recorded (Table 4.1) indicate that the De Montfort University devices (DMU3) were comparable, with respect to impedance, to the Gross devices in both published work (Sokal *et al.*, 2000) and to the Gross device tested concurrently with the two DMU devices.

Spontaneous activity within the neuronal culture was not recorded. In cell lines such as the B50, successive passage cycles can result in modification of the cell profile. Several studies have highlighted a tendency for cells to modify their characteristics. This retrograde development is not specific to cell lines, although the level of juvenile development does seem to be greater in cell lines than either organotypic cultures or primal cell cultures (Chung 1999; Ghahary 1994; MacKenzie 2000). Conversely, maturity of a specific cell culture also has an influence on the presence of spontaneous activity. For example, in the NTERA2 cell line (NT2) the formation of functional synapses is a late indication of neuronal differentiation. The establishment of functional synapses aids assessment of the neuronal characteristics between different cell lines. Retanoic acid-differentiated NT2 cell lines produce neuronal like processes (Leypoldt *et al.*, 2002) however, although the morphology is similar to primary neurones, they fail to exhibit spontaneous activity when cultured in DMEM for less than 5 division cycles (personal communication; Sokal, 2002). The lack of activity found in low division, primary, rat NT2 cultures parallels the lack of activity found in the B50 cultures (personal communication; Sokal, 2002). The original choice of the B50 cell line was due, in part, to its reported spontaneous activity (Schubert *et al.*, 1974), so this result was disappointing.

The introduction of a high dose of KCl caused the rapid depolarisation of the cells in the culture and it would appear that it was this that was recorded by the equipment. Thus the device successfully performed its intended function, the recording of cellular electrical activity.

In conclusion, the DMU3 series device was shown to successfully interface with the recording equipment with respect to electrical connectivity. The device functioned as a microelectrode array with impedance properties similar to that of the Gross-manufactured product, thus enabling the recording of signals from a neuronal culture incubated on the device.

CHAPTER 5
CONCLUSIONS AND FUTURE WORK

5 CONCLUSIONS AND FUTURE WORK

The work presented in this volume reports the development of an MEA, from identification of the cell type used during the development through to an assembled and working device.

Bayliss *et al.* (1999) had previously demonstrated the growth of B50 cells on silicon. In the current study, the B50 cellular morphology and distribution on *n*-type- and porous-silicon and on a glass substrate was examined, and the required surface modifications to assist cellular adhesion were identified. Curtis (1996; 2000) previously reported the use of adhesion molecules, such as poly-L-lysine, as a prerequisite for the growth and attachment of cell lines onto silicon and its derivatives. However, the current study has demonstrated that a rat hippocampal cell line will attach to both silicon wafers and silicon-based devices. The nature of these attachments is sufficient for the intended purpose of recording neuronal signals.

Planar MEAs, with or without patterning, have established a position in neuroscience as a tool for research. The cell types used on these devices differ from primary cultures to cell lines and from single cells to organotypic slices, each imposing different constraints, including longevity, morphological changes and response to chemical and electrical cues (Canepari *et al.*, 1997; Gross *et al.*, 1993; Jimbo *et al.*, 2000; Keefer, 2001; Rutten *et al.*, 1999; Van Pelt *et al.*, 1996).

Regehr *et al.* (1989) reported that increased levels of recording occurred when tight seals were achieved between the recording and stimulating electrode and the cells under investigation (from microvolts to tens of millivolts). In these situations, the threshold level required for stimulation is significantly reduced (Fromherz, 1999). Pancrazio (1998) described and demonstrated a complementary metal-oxide semiconductor (CMOS) amplifier-based-system for the recording of electrical stimuli from chick heart tissue. This device was of an embedded construction, whereby components were integrated into the silicon layer during the manufacturing process. The DMU3 device was constructed using sputtered silicon technology. This silicon was, as intended,

opaque to aid visualisation. The initial deposition of silicon could be increased to several μm in depth, thus enabling selective doping, masking and etching to produce onboard amplification, as described by Pancrazio *et al.* (1998). The growth area could then be etched to the required depth to aid visualisation. This embedded circuitry would, theoretically, improve the signal to noise rations by positioning an amplifier on the device and thus closer to the source of the signal.

Additional circuitry, as described above, would require further investigation of its cytotoxic potential, due to the introduction of elements such as boron and, to a lesser degree, arsenic. However, as the current study indicates, cytotoxicity was not induced in the B50 cell type by the components of the DMU3 devices. The use of different culture types may lead to cell growth and development being compromised. Stewart (2000) proposed methods of functionalising the surface of porous silicon to further reduce any negative effects on cell growth and development.

The final devices were constructed from a glass substrate, ITO electrodes and a silicon/porous silicon cellular growth area, these components being demonstrated to be non-cytotoxic to the B50 cell line employed. The DMU3 device differed from any previously developed device, as cellular attachment occurred following topographical modification of the silicon surface; the use of applied adhesion molecules, such as poly-L-lysine, was not required.

It is clear that the success of this technology will depend on whether the electronic hard-ware can be adapted to the requirements of living cells. Over the next few years, workers in the field may well move towards bridging the silicon:cell interface with signals of a different type which make use of the current moves forward in the sister technology of bio-sensors (chemical sensors using biological molecules). Furthermore, research into extending the life of the interfaced cells by adapting techniques used in pharmaceutical bioreactors will lengthen the device life. A solution to the problems of signal transduction may lie in the luminescent properties of nanostructured silicon, which could allow it to be linked to the data logger by optical fibres, removing the need to perforate a cell to determine a response. This could, in turn, enable the development

of new devices to replace damaged tissues in the eye, for example. There are also new semiconducting biomaterials on the horizon, such as superhard carbons, gallium and indium nitrides, and porous silicon/germanium, which may offer advantages for this application.

There are a number of aspects which would further elucidate the problems addressed in this project:

(1) Further understanding of the silicon:mammalian cell interface via:

i. Analysis of the chemical nature of the interface between living cells and semiconductor materials, using more specific receptor-sensitive ligand indicators.

ii. Profiling of multiple cell types, for example organotypic cultures on assembled arrays.

iii. Use of a three-dimensional structure to enable reading in different planes.

iv. Investigation as to the effects of surface topology on the biochemistry of the interfaced cells.

(2) Development of improved devices by:

i. The construction of an amplification circuit on board the device to reduce signal to noise ratio.

ii. Protection of unused electrodes by anchored lipid domes filled with either an isotonic solution, drug, gene sequence, or fluorescent marker. These would not only interface with a cell on contact, binding it to the electrode and internalising the contents of the lipid dome, but would also act as insulators for non-attached contact points thus improving the signal to noise ratio.

CHAPTER 6
REFERENCES

References

ALBERTS, B., BRAY, D., LEWIS, J., RAFF, M., ROBERTS, K. & WATSON, J.D. (1994) *Molecular Biology of the cell.* ISBN 0-8153-1619-4

AL-KINDI, M.J. & DUNLOP, J. (1989) Improved adaptive noise cancellation in the presence of signal leakage on the noise reference channel. *Signal Processing*, **17** (3): 241-250

ANDREW, R.D., ADAMS, J.R. & POLISCHUK, T.M. (1996) Imaging NMDA- and kainate- induced intrinsic optical signals from the hippocampal slice. *Journal of Neurophysiology*, **76**(4): 2707-2712

ARAI, M., HAMADA, S. & NISHIYAMA, Y. (1992) Effects of surface pretreatments of a glass substrate on the properties of tin oxide film prepared by plasma-assisted chemical vapor-deposition. *Bulletin Of The Chemical Society Of Japan.* **65** (4): 1141-1143.

ARAI, M., & NISHIYAMA, Y. (1985) Effects of surface pretreatments of a glass substrate on the properties of tin oxide film prepared by vacuum deposition, *Journal of Colloid and Interface Science* **104,** 175

ATTALLA, M.M., TANNENBAUM, E. & SCHEIBNER, E.J. (1959) Stabilization of silicon surfaces by thermally grown oxides, *Bell System Technical Jurnal.* **38**(3): 749 - 783

AUERBACH, H., SOLLER, B.R. & PEURA, R. A. (1994) *Proceedings of the 20th Annual Northeast Bioengineering Conference*, 108–109.

AZHDERIAN, E.M., HEFNER, D., LIN, C.H., KACZMAREK, L.K. & FORSCHER, P. (1994) Cyclic AMP modulates fast axonal transport in Aplysia bag cell neurons by increasing the probability of single organelle movement. *Neuron,* **12**(6): 1223-1233.

BAINES, D., MALLON, B.S. & LOVE, S. (1992) Effects of sodium butyrate on the expression of sodium channels by neuronal cell lines derived from the rat CNS. *Brain Research. Molecular Brain Research*, **16**(3-4): 330-338.

BANKER, G., & GOSLIN, K. (1998) *Culturing Nerve Cells.* ISBN: 0262024381

BANKS, D. (2002) Introduction to MEMS http://www.dbanks.demon.co.uk/ueng/

BARD, J. & FAULKNER, L.R. (1980) *Electrochemical Methods*; New York: Wiley.

BASARSKY, T.A, PARPURA, V. & HAYDON, P.G. (1994) Hippocampal synaptogenesis in cell culture: developmental time course of synapse formation, calcium influx, and synaptic protein distribution. *Journal of Neuroscience*, **14**(11 Pt 1): 6402-11.

BASMAJI, P. B. & GUIMARÃES, F. E.G. (1995) Evidence of localized luminescence centers in porous silicon. *Superlattices and Microstructures*, **17**(2): 155-155

BAYLISS, S.C. BUCKBERRY, L. HARRIS P.J. & ROUSSEAU, C. (1997a) Nanostructured Semiconductors: compatability with biomaterials. *Thin Solid Films*, **297**: 308 - 310

BAYLISS, S.C. BUCKBERRY, L. HARRIS P.J. & ROUSSEAU, C. (1997b) Phosphate and cell growth on nanostructured semiconductors. *Journal of Materials Science Letters*, **16**, 737 - 740

BAYLISS, S. C. HARRIS, P. J. & BUCKBERRY, L.D. (2000) Nature of the silicon-animal cell interface. *Journal of Porous Materials*, **7:** 191- 195

BEAN, R.C., SHEPHERD, W.C., CHAN, H., EICHNER, J. (1969) Discrete conductance fluctuations in lipid bilayer protein membranes. *Journal of General Physiology*. **53**: 741-757

BELL, A.J., & SEJNOWSKI, T.J. (1995) An information maximization approach to blind separation and blind deconvolution. *Neural Computation*, **7** (6): 1129-1159

Biggs, S., and Mulvaney, P., *J. Chem. Phys.* **100,** 8501 (1994).

BILLAT, S. (1996) Electroluminescence of heavily doped p-type porous silicon under electrochemical oxidation in galvanostatic regime. *Journal of the Electrochemical Society*, **143** (3): 1055-1061.

BOGUE, R.W. (1997) Novel porous silicon biosensor. *Biosensors and Bioelectronics*, **12** (1): R27-R29

BOPPART, S.A., WHEELER, B.C. & WALLACE, C.S. (1992) A flexible perforated microelectrode array for extended neural recordings. *IEEE Transactions on Biomedical Engineering*, **39** (1): 37-42

Bos, M. A., Shervani, Z., Anusiem, A. C. I., Giesbers, M., Norde, W., and Kleijn, J. M., *Colloids Surf. B* **3,** 91 (1994).

BRAUN, D. & FROMHERZ, P. (1998) Fluorescence interferometry of neuronal cell adhesion on microstructured silicon *Physical Review Letters*, **81** (23): 5241-5244

BRESSERS, P.M.M.C., KNAPEN, J.W.J., MEULENKAMP, E.A. & KELLY, J.J. (1992) Visible-light emission from a porous silicon solution diode. *Applied Physics Letters*, **61** (1): 108-110

BRETSCHER, M.S. (1992) Cells can use their transferrin receptors for locomotion. *EMBO Journal*, **11**(2):383-9.

BRITLAND, S. & MCCAIG, C. (1996) Embryonic Xenopus neurites integrate and respond to simultaneous electrical and adhesive guidance cues. *Experimental Cell Research*, **226** (1): 31-38

BRITLAND, S., MORGAN, H., WOJIAKSTODART, B., RIEHLE, M., CURTIS, A. & WILKINSON, C. (1996) Synergistic and hierarchical adhesive and topographic guidance of BHK cells. *Experimental Cell Research*, **228** (2): 313-325

BROWN, K.T. & FLAMING, D. G. (1977), *Neuroscience* **2**: 813–827

BRUNETTE, D. M. (1986a). Fibroblasts on micromachined substrata orient hierarchically to grooves of different dimensions. *Experimental Cell Research*, **164**: 11-26.

BRUNETTE, D. M. (1986b). Spreading and orientation of epithelial cells on grooved substrata. *Experimental Cell Research*, **167**: 203-217.

BSIESY, A., MULLER, F., LIGEON, M., GASPARD, F., HERINO, R., ROMESTAIN, R. & VIAL, J.C. (1993) Voltage-controlled spectral shift of porous silicon electroluminescence. *Physical Review Letters*, **71** (4): 637-640

BSIESY, A., MULLER, F., LIGEON, M., GASPARD, F., HERINO, R., ROMESTAIN, R. & VIAL, J.C. (1994) Relation between porous silicon photoluminescence and its voltage-tunable electroluminescence. *Applied Physics Letters*, **65** (26): 3371-3373

BUITENWEG, J. R., RUTTEN, W. L. C. & MARANI, E. (2000) Geometry based dynamic modeling of the neuron-electrode interface. *Proceedings of the 22nd Annual International Conference of the IEEE Engineering in Medicine and Biology Society*, (3): 2004–2007.

BURIAK, J.M., STEWART, M.P., CANHAM, L.T., REEVES, C.L., NEWEY, J.P., HOULTON, M.R. & COX, T. I. (1998) Functionalized porous silicon surfaces with dramatically improved stability in simulated blood plasma. *Abstracts of Papers of the American Chemical Society*, **218** (1): 54

BUSTEMANTE, J., DOCK., L., VAHTER, M., FOWLER, B. & ORRENIUS, S. (1997) The semiconductor elements arsenic and indium induce apoptosis in rat thymocytes. *Toxicology* **118**: 129,

BUZSAKI, G., & KANDEL, A. (1998) Somadendritic backpropagation of action potentials in cortical pyramidal cells of the awake rat. *Journal of Neurophysiology*, **79:** 1587–1591.

CAMPBELL, P.K., JONES, K.E., HUBER, R.J., HORCH, K.W. & NORMAN, R. A. (1991) A silicon-based, three-dimensional neural interface: manufacturing processes for an intracortical electrode array. *IEEE Transactions on Biomedical Engineering*, **38**: 758–768.

CANHAM, L.T. (1990) Silicon quantum wire array fabrication by electrochemical and chemical dissolution of wafers. *Applied Physics Letters*, **56** (10): 1046-1050

CANHAM, L. (1992) Silicon optoelectronics at the end of the rainbow. *Physics World*, **5** (3): 41-44

CANHAM, L.T. (1995) Bioactive silicon structure fabrication through nanoetching techniques. *Advanced Materials*, 7(10): 1033

CANHAM, L. T., REEVES, C. L., NEWEY, J. P. HOULTON, M. R., COX, T. I., BURIAK, J. M. & STEWART, M. P. (1999) Derivatized Mesoporous Silicon with Dramatically Improved Stability in Simulated Human Blood Plasma. *Advanced Materials*, **11**: 1505 - 1507

CARTS-POWELL, Y. (1998) Optical sensing - Porous silicon biosensor provides high sensitivity. *Laser Focus World*, **34** (1): 45

CEROFOLINI, G.F. (1998) A study of the ionic route for hydrogen terminations resulting after SiO2 etching by concentrated aqueous solutions of HF. *Applied Surface Science*, **133** (1-2): 108-114.

CHEN, J.K. & WISE, K.D. (1997) A silicon probe with integrated microheaters for thermal marking and monitoring of neural tissue. *IEEE Transactions on Biomedical Engineering.* **44**(8): 770-774

CHEN, R., LIN, D.L. & MENDOZA, B. (1993) Enhancement of the 3rd-order nonlinear-optical susceptibility in Si quantum wires. *Physical Review B*, **48** (16): 11879-11882.

CHIN, V., COLLINS, B.E. & SAILOR, M.J. (2001) Compatibility of primary hepatocytes with oxidized nanoporous silicon. *Advanced Materials*, **13** (24): 1877

CHO, C.H., SEO, Y.S., PARK, J.D., KIM, Y.Y. & LEE, K.W. (2000) Raman scattering of a porous silicon superlattice. *Journal of the Korean Physical Society*, **37** (5) :770-773.

CHOI, E.T. & CALLOW, A.D., (1994) Implantation biology: the host response and biomedical devices, Greco, R. S. (ed.); *Boca Raton, FL: CRC Press*, Chapter 3.

CHUNG G. H., ISHIDA K., YAMAGUCHI D. T., MILLER T. A. (1999) Serial Passage of MC3T3-E1 Cells Alters Osteoblastic Function and Responsiveness to Transforming Growth Factor ß-1 and Bone Morphogenetic Protein-2 *Biochemical and Biophysical Research Communications*, **265** (1): 246-251

CICHOCKI, A. & UNBEHAUEN, R. (1996) Robust neural networks with on-line learning for blind identification and blind separation of sources. *IEEE Transactions on Circuits and Systems I - Fundamental Theory and Applications*, **43** (11): 894-906

CLARK, P., CONNOLLY, P., CURTIS, A. S. G., DOW, J. A. T. & WILKINSON, C. D.W. (1990). Topographical control of cell behavior: II. Multiple grooved substrata. *Development*, **108**: 635-644.

CLARK, P., CONNOLLY, P., CURTIS, A. S. G., DOW, J. A. T. & WILKINSON, C. D. W. (1991). Cell guidance by ultrafine topography in vitro. *Journal Cell Science*, **99**: 73-77.

COLLINS, S.D., GONZALEZ, C. & SMITH, R.L. (1997) Microfabrication creates mesoscopic optical systems. *Laser Focus World*, **33** (5): 187

CONDEELIS, J., BRESNICK, A., DEMMA, M., DHARMAWARDHANE, S., EDDY, R., HALL, A.L., SAUTERER, R. & WARREN, V. (1990) Mechanisms of amoeboid chemotaxis: an evaluation of the cortical expansion model. *Developmental Genetics*, **11**(5-6): 333-340.

CORNER, M.A. (1994) Reciprocity of structure-function relations in developing neural networks: the Odyssey of a self-organizing brain through research fads, fallacies and prospects. *Progress in Brain Research*, **102**:3-31

COSTERTON, J.W. & STEWART, P. S. (2001) Battling Biofilm. *Scientific American*, **285**: 75–81.

CULLIS, A.G., CANHAM, L.T., & CALCOTT, P.D.J. (1997) The structural and

luminescence properties of porous silicon. *Journal of Applied Physics*, **82** (3): 909-965.

CURTIS, A. S. G. (2000) Personal communication. 3rd. EPSRC Meeting, Stirling April 6th 2000.

CURTIS, A. S. G. & CLARK, P. (1990). The effects of topographic and mechanical properties of materials on cell behavior. *Critical Reviews in Biocompatability*, **5**, 343-362.

CURTIS, A. S. G. & WILKINSON, C. D. W. (1998) Topographical control of cells. *Biomaterials*, **18**: 1573.

CURTIS, A. QUINN, R. & MCGRATH, M. (1996) Activation of neuron adhesion and neurite extension by tethered neurotrophins and adhesion molecules. *Experimental Biology Online*, **1**(1).

DALE, H.H., FELDBERG, W., & VOGT, M. (1936) Release of acetylcholine at voluntary nerve endings. *Journal of Physiology*. **88**: 353-380

DELLASANTINA, C.C., KOVACS, G.T.A., & LEWIS E.R. (1997) Multi-unit recording from regenerated bullfrog eighth nerve using implantable silicon-substrate microelectrodes. *Journal of Neuroscience Methods*, **72** (1): 71-86

DESILVA, M.S., ZHANG, Y., HESKETH, P.J., MACLAY, G.J., GENDEL, S.M. & STETTER, J.R. (1995) Impedance based sensing of the specific binding reaction between *staphylococcus enterotoxin-b* and its antibody on an ultra-thin platinum film. *Biosensors and Electronics*, **10**: 675 – 682

DIMILLA, P.A., BARBEE, K. & LAUFFENBURGER, D.A. (1991) Mathematical model for the effects of adhesion and mechanics on cell migration speed. *Biophysical Journal*, **60**(1): 15-37.

DOYLE, A., GRIFFITHS, J. B., & NEWELL, D. (Eds), (1998) *Cell and Tissue Culture: Laboratory Procedures*. John Wiley & Sons, New York

DUCKER, W.A., SENDEN, T.J. & PASHLEY, R.M. (1992) Forces between mica surfaces in the presence of rod-shaped divalent counterions. *Langmuir*, **8**: 1831

DUNN, G. A. & BROWN, A. F. (1986). Alignment of fibroblasts on grooved surfaces described by a simple geometric transformation. *Journal of Cell Science*, **83**: 313-340.

DUONG, D.H. & CHANG, T. (1998) The influence of electric fields on the epileptiform bursts induced by high potassium in CA3 region of rat hippocampal slices. *Neurological Research*, **20**(6): 542-548.

EDDOWES, M. J. (1990) Anodic-dissolution of p-type and n-type silicon - kinetic-study of the chemical mechanism *Journal of Electroanalytical Chemistry*, **280**: 297 - 310

EDERTH, T. (2000) Substrate and Solution Effects on the Long-Range "Hydrophobic" Interactions between Hydrophobized Gold Surfaces *The Journal of Physical Chemistry B*. **104**, 9704 - 9712.

EGERT, U., SCHLOSSHAUER, B., FENNRICH, S., NISCH, W., FEJTL, M., KNOTT, T., MULLER, T. & HAMMERLE, H. (1998) A novel organotypic long-term culture of the rat hippocampus on substrate-integrated multielectrode arrays. *Brain Research Protocols*, **2** (4): 229-242

EKEROTH, J., KONRADSSON, P., BJOREFORS, F., LUNDSTROM, I. & LIEDBERG, B. (2002) Monitoring the interfacial capacitance at self-assembled phosphate monolayers on gold electrodes upon interaction with calcium and magnesium. *Analytical Chemistry*, **74**(9): 1979-1985

EKINS, R.P. (1998). Ligand assays: from electrophoresis to miniaturized microarrays. *Clinical Chemistry*, **44** (9): 2015-2030

ELHOUICHET, H. & OUESLATI, M. (2001) Photoluminescence properties of porous silicon nanocomposites. *Materials Science and Engineering B - Solid State Materials for Advanced Technology*, **79** (1): 27-30

FAßBENDER, F., SCHMITT, G., SCHÖNING, M. J., LÜTH, H., BUß, G. & SCHULTZE, J. -W. (2000) Optimization of passivation layers for corrosion protection of silicon-based microelectrode arrays. *Sensors and. Actuators B*, **68**: 128–133.

FAUCHET, P.M. (1997) Coherent phenomena in semiconductor quantum wells *Summaries of Papers Presented at the Quantum Electronics and Laser Science Conference, (QELS '97)*: 148 -149

FAUCHET, P.M. (1998) Progress toward nanoscale silicon light-emitters. *Selected Topics in IEEE Journal on Quantum Electronics*, **4** (6): 1020 -1028

FORSCHER, P., LIN, C.H. & THOMPSON, C. (1992) Novel form of growth cone motility involving site-directed actin filament assembly. *Nature*, **357**(6378): 515-518

FROMHERZ, P. (1996) Interfacing neurons and silicon by electrical induction. *Physics*, **100** (7):1093-1102

FROMHERZ, P. (1999) Extracellular recording with transistors and the distribution of ionic conductances in a cell membrane. *European Biophysics Journal*, **28** (3): 254-258

FROMHERZ, P. & LAMBACHER, A. (1991) Spectra of voltage-sensitive fluorescence of styryl-dye in neuron membrane. *Biochimica et Biophysica Acta*, **1068**: 149-156

FROMHERZ, P., OFFENHAUSSER, A., VETTER, T. & WEIS, J. (1991) A neuron-silicon junction - a retzius cell of the leech on an insulated-gate field-effect transistor *Science*, **252** (5010): 1290-1293

FROMHERZ, P. & STETT, A. (1995). Silicon-neuron junction - capacitive stimulation of an individual neuron on a silicon chip. *Physical Review Letters*, **75** (8): 1670-1673

FROSCH, C & DERICK, I. (1957) Surface protection and selective masking during diffusion in silicon, *Journal of the Electrochemical Society*. **104**: 547-552

FUBINI, B., FENOGLIO, I., ELIAS, Z. & POIROT, O. (2001) Variability of biological responses to silicas: effect of origin, crystallinity, and state of surface on generation of reactive oxygen species and morphological transformation of mammalian cells. *Journal of Environmental Pathology, Toxicology, and Oncology.* **20** Suppl 1:95-108

FUTAGI, T., MATSUMOTO, T., KATSUNO, M., OHTA, Y., MIMURA, H. & KITAMURA, K. (1992) Visible electroluminescence from p-type crystalline silicon porous silicon n-type microcrystalline silicon carbon pn junction diodes. *Japanese Journal Of Applied Physics Part 2 - Letters*, **31** (5b): L616-L618.

GABURRO, Z., FAGLIA, G., BARATTO, C., SBERVEGLIERI, G. & PAVESI, L. (2001) Multiparametric gas sensors with porous silicon optical microcavities. *International Semiconductor Conference, 2001. CAS 2001 Proceedings*, **1**(1): 19 -22

GEDDES, L. A. (1972) Electrodes and the Measurement of Bioelectric Events. *New York: Wiley.*

GERSTEIN, G.L. (2000) Cross-correlation measures of unresolved multi-neuron recordings. *Journal of Neuroscience Methods*, **100**: 41–51.

GESTELAND, R. C., HOWLAND, B., LETTVIN, J.Y., & PITTS, W. H. (1959) *Proceedings IRE* 1856–1862.

GHAHARY, A; SHEN, Y J; SCOTT, P G; TREDGET, E E (1994) Expression of mRNA for transforming growth factor-beta 1 is reduced in hypertrophic scar and normal dermal fibroblasts following serial passage in vitro, *The Journal of Investigative Dermatology,* **103***(5): 684-686*

GLUCKMAN, B.J., NEEL, E.J., NETOFF, T.I., DITTO, W.L., SPANO, M.L. & SCHIFF, S.J. (1996) Electric field suppression of epileptiform activity in hippocampal slices. *Journal of Neurophysiology*, **76**(6): 4202-4205.

GÖPEL, W., ZIEGLER, C., BREER, H., SCHILD, D., APFELBACH, R., JOERGES, J. & MALAKA, R. (1998) Bioelectronic noses: a status report - Part 1. *Biosensors and Bioelectronics*, **13** (3-4): 479-493

GRATTAROLA, M. & MARTINOIA, S. (1993) Modeling the neuron-microtransducer junction: from extracellular to patch recording. *IEEE Transactions on Biomedical Engieering*, **40:** 35–41.

GRATTAROLA, M., BOVE, M., VERRESCHI, G., MARTINOIA, S. & TEDESCO, M. (1996) The neuro-electronic interface: Measurements and model predictions. *Journal Of Materials Science - Materials In Medicine*, **7** (6): 363-366

GRAY, C.M. & SINGER, W. (1989) Stimulus-specific neuronal oscillations in orientation columns of cat visual cortex. *Proceedings of the National Academy of Sciences USA*, **86**: 1698- 702.

GRAY, C.M., MALDONADO, P.E., WILSON, M. & MCNAUGHTON, B. (1995) Tetrodes markedly improve the reliability and yield of multiple single-unit isolation from multi-unit recordings in cat striate cortex. *Journal of Neuroscience Methods*, **63**(1–2): 43–54.

GROSS, G., RHOADES, B., REUST, D. & SCHWALM, F. (1993) Stimulation of monolayer networks in culture through thin-film indium-tin oxide recording electrodes *Journal of Neuroscience Methods*, **50** (2): 131-143

GUENTER G.W., HARSCH, A., RHOADES B.K., & GÖPEL, W. (1997), Odor, drug and toxin analysis with neuronal networks in vitro: extracellular array recording of network responses, *Biosensors and Bioelectronics* **12**(5): 373-393

GUNDERSEN, R.W. (1987) Response of sensory neurites and growth cones to patterned substrate of laminin and fibronectin in vitro *Developmental Biology*, **121:** 423–431

GUPTA, P., DILLON, A.C. & BRACKER, A.S. (1991) FTIR studies of H_2O and H_2O decomposition on porous silicon surfaces. *Surface Science*, **245** (3): 360-372

HALIMAOUI, A., OULES, C., BOMCHIL, G., BSIESY, A., GASPARD, F., HERINO, R., LIGEON, M. & MULLER, F. (1991) Electroluminescence in the visible range during anodic-oxidation of porous silicon films. *Applied Physics Letters*, **59** (3): 304-306.

HAMMARBACK, J. A., MCCARTHY, J. B., PALM, S. L., FURCHT, L. T. & LETOURNEAU, P. C. (1988) Growth cone guidance by substrate-bound laminin pathways is correlated with neuron-to-pathway adhesivity. *Developmental Biology*, **126**: 29–39

HANEIN, Y., PAN, Y.V., RATNER, B.D., DENTON, D.D. & BOHRINGER, K.F. (2001) Micromachining of non-fouling coatings for bio-MEMS applications. *Sensors and Actuators B - Chemical*, **81** (1): 49-54

HARRISON, R.G. (1912) The cultivation of tissues in extraneous media as a method of morphogenetic study. *Anatomical Record*, **6**:181-193

HEIDUSCHKA, P., ROMANN, I., ECKEN, H., SCHONING, M., SCHUHMANN, W. & THANOS, S. (2001) Defined adhesion and growth of neurones on artificial structured substrates. *Electrochimica Acta*, **47** (1-2): 299-307

HERINO, R. (1997) In: *Pore size distribution in PS*, Canham, L. (Ed.); Short Run Press Ltd., Exeter: London. EMIS Datareviews Series **18**: 89-96.

HIGUCHI. M., UEKUSA, S., NAKANO, R. & YOKOGAWA, K. (1993) Micrograin structure influence on electrical characteristics of sputtered indium tin oxide-films. *Journal Of Applied Physics.* 74 (11): 6710-6713

HIGUCHI, M., UEKUSA, S., NAKANO, R. & YOKOGAWA, K. (1994) Postdeposition annealing influence on sputtered indium tin oxide film characteristics. *Japanese Journal of Applied Physics* **33** (1A): 302-306

HINES, M.A., CHABAL, Y.J. & HARRIS, T.D. (1994) Measuring the structure of etched silicon surfaces with raman-spectroscopy. *Journal of Chemical Physics*, **101** (9): 8055-8072.

HIRSCHMAN, K.D., TSYBESKOV, L., DUTTAGUPTA, S.P. & FAUCHET, P.M. (1996) Silicon-based visible light-emitting devices integrated into microelectronic circuits. *Nature*, **384** (6607): 338-341.

HLADKY, S.B. & HAYDON, D.A. (1970) Discreteness of conductance change in bimolecular lipid membranes in the presence of certain antibiotics. *Nature*. **225**: 451-453.

HODGKIN, A.L. & HUXLEY, A.F. (1952) A quantitative description of membrane current and its application to conduction and excitation in nerve. *Journal of Physiology*, **117**: 500.

HODGKIN, A.L., HUXLEY, A.F., KATZ, B. (1949) Ionic currents underlying activity in the giant axon of the squid. *Arch Sci Physiol* **3**: 129–140.

HORBETT, T. A. (1982) In: *Biomaterials: Interfacial Phenomena and Applications*, Cooper, S. L. & Peppas, N.L. (Eds.); Washington DC: American Chemical Society, 1982, p.233.

HU, K. & BARD, A.J. (1997) Use Of Atomic Force Microscopy For The Study Of Surface Acid-Base Properties Of Carboxylic Acid-Terminated Self-Assembled Monolayers. *Langmuir* (19): 5114-5119.

HURLEY, P.K., ARNOLD, G., HALL, S., ECCLESTON, W. & KEEN, J. (1991) Electrical properties of thermally oxidised porous silicon. *Proceedings IEEE International SOI Conference*: 178 –179.

IMAI, K. (1981) A new dielectric isolation method using porous silicon. *Solid-State Electronics*, **24** (2): 159

JANSHOFF, A., DANCIL, K.P.S, STEINEM, C., GREINER, D.P., LIN, V.S.Y, GURTNER, C., MOTESHAREI, K., SAILOR, M.J. & GHADIRI, M.R. (1998) Macroporous p-type silicon Fabry-Perot layers. Fabrication, characterization, and applications in biosensing. *Journal of the American Chemical Society*,. **120**: 12108-12116.

JENKNER, M., FROMHERZ, P. (1997) Biostability of membrane conductance in cell adhesion observed in a neuron transistor. *Physical Review Letters*, **79** (23): 4705-4708

JIMBO, Y. & KAWANA, A. (1992) Electrical stimulation and recording from cultured neurons using a planar electrode array. *Bioelectrochemistry and Bioenergetics*, **29**: 193-204

JOHN, G.C. & SINGH, V.A. (1995) Diffusion-induced nucleation model for the formation of porous silicon. *Physical Review B*, **52** (15): 11125-11131.

JOHNSON, L.J., D.F. HANLEY, & THAKOR, N.V. (2000) Optical light scattering imaging of cellular and sub-cellular morphology changes in stressed rat hippocampal slices. *Journal of Neuroscience Methods*, **98**(1): 21-31.

JOSHI, D.D., DANG, A., YADAV, P., QIAN, J., BANDARI, P.S., CHEN, K., DONNELLY, R., CASTRO, T., GASCON, P., HAIDER, A., RAMESHWAR, P. (2001) Negative feedback on the effects of stem cell factor on hematopoiesis is partly mediated through neutral endopeptidase activity on substance P: a combined functional and proteomic study. *Blood* **1**;98(9): 2697-706

JUNG, D.R., KAPUR, R., ADAMS, T., GIULIANO, K.A., MRKSICH, M., CRAIGHEAD, H.G. & TAYLOR, D.L. (2001) Topographical And Physicochemical Modification Of Material Surface To Enable Patterning Of Living Cells. *Critical Reviews In Biotechnology.* **21** (2): 111-154 2001

JUNG, K.H., SHIH, S. & KWONG, D.L. (1993) Developments in luminescent porous silicon. *Journal of the Electrochemical Society*, **140** (10): 3046-3064

KAMALESH, S., TAN, P., WANG, J., LEE, T., KANG, E-T. & WANG, C-H. (2000) Biocompatibility of electroactive polymers in tissues. *Journal of Biomedical Materials Research*, **52** (3): 467-478

KANDEL, E. R., SCHWARTZ, J. H. & JESSELL, T. M. (1991) *Principles of Neural Science.* Norwalk, CT: Appleton & Lange.

KANEMITSU, Y. & UTO, H. (1994) Slow decay dynamics of visible photoluminescence from nanometer-size silicon crystallites. *Superlattices and Microstructures*, **15** (1): 29-29

KANEMITSU, Y., OKAMOTO, S. & MITO, A. (1995) 3rd-order nonlinear-optical susceptibility and photoluminescence in porous silicon. *Physical Review B*, **52** (15): 10752-10755.

KATO, K., ITO, T. & HIRAKI, A. (1988) Initial oxidation process of anodized porous silicon with hydrogen-atoms chemisorbed on the inner surface. *Japanese Journal of Applied Physics Part 2 – Letters*, **27**(8): L1406 - 1409

KEEFER, E.W., GRAMOWSKI A., STENGER, D.A., PANCRAZIO, J.J. & GROSS, G.W. (2001) Characterization of acute neurotoxic effects of trimethylolpropane phosphate via neuronal network biosensors. *Biosensors & Bioelectronics,* **16**: 513–525

KELLY, M.T., CHUN, J.K.M. & BOCARSLY, A.B. (1994) High efficiency chemical etchant for the formation of luminescent porous silicon. *Applied Physics Letters*, **64**:1693

KELLY, M.J., GUILINGER, T.R. & TSAO, S.S. (1988) Silicon electrochemistry related to the formation of porous silicon. *Proceedings IEEE SOS/SOI Technology Workshop*: 17

KESHMIRI S.H. & ROKN-ABADI R.M. (2001) Enhancement of drift mobility of zinc oxide transparent-conducting films by a hydrogenation process, *Thin Solid Films* **382**(1): 230-234

KHOUW, I.M.S.L., VAN WACHEM, P.B., MOLEMA, G., PLANTINGA, J.A., DE LEIJ, L.F.M.H. & VAN LUYN, M.J.A., (2000) The foreign body reaction to a biodegradable biomaterial differs between rats and mice. *Journal of Biomedical Materials Research*, **52** (3):439-446

KIDD, K.R., DAL PONTE, D.B., KELLAR, R.S. & WILLIAMS, S.K. (2002) A comparative evaluation of the tissue responses associated with polymeric implants in the rat and mouse. *Journal of Biomedical Materials Research*, **59** (4):682-9

KILBY, J.S. (1976) Invention of the intergrated circuit. *IEEE Transactions on Electonic Devices*. 648 - 654.

KOCH, R., & POPPA, H., (1987) The effect of mica surface dehydroxylation on particulate palladium vapor deposits *Thin Solid Films* **151:** 365

KOCH, R. & POPPA, H., (1987) the influence of the mica surface-composition on the growth-morphology of discontinuous epitaxial palladium vapor deposits. *Journal of Vacuum Science & Technology A-Vacuum Surfaces and Films* **5**: 1485

KONAKA, S., TABE, M. & SAKAI, T. (1982) A new silicon-on-insulator structure using a silicon molecular-beam epitaxial-growth on porous silicon. *Applied Physics Letters*, **41** (1): 86-88

KOPP, J. BANNASCH, H. ANDREE, C. & STARK, G.B. (1996) Cultured keratinocytes seeded on a silicon-collagen-matrix-sheet to cover full thickness wounds. *Langenbecks Archiv Fur Chirurgie*, **S1**: 229-301.

KOSHIDA, N. & KOYAMA, H. (1992) Visible electroluminescence from porous silicon. *Applied Physics Letters*, **60** (3): 347-349.

KOSHIDA, N., KOYAMA, H., YAMAMOTO, Y. & COLLINS, G.J. (1993) Visible electroluminescence from porous silicon diodes with an electropolymerized contact. *Applied Physics Letters*, **63** (19): 2655-2657.

KOVACS, G.T.A., (1994) In: *Enabling Technologies for Cultured Neural Networks*. Stenger, D.A., McKenna, T.M. (Eds.); San Diego: Academic Press, Chapter 7

KOVACS, G.T.A., STORMENT, C.W., & ROSEN, J.M. (1992) Regeneration microelectrode array for peripheral-nerve recording and stimulation. *IEEE Transactions on Biomedical Engineering*, **39**(9), 893-902.

KOZLOWSKI, F. & LANG, W. (1992) Spatially resolved Raman measurements at electroluminescent porous n-silicon. *Journal Of Applied Physics*, **72** (11): 5401-5408.

KRISTENSEN, B.W., NORABERG, J., THIÉBAUD, P., KOUDELKA-HEP, M., ZIMMER, J. (2001) Biocompatibility of silicon-based arrays of electrodes coupled to organotypic hippocampal brain slice cultures *Brain Research*. **896**: 1–17.

KUFFLER, S.W & NICHOLLS, J.G. (1966) The physiology of neuroglial cells. *Ergebnisse der Physiologie*, **57**:1-90. Review.

LAMBACHER, A. & FROMHERZ, P. (2002) Luminescence of dye molecules on oxidized silicon and fluorescence interference contrast microscopy of biomembranes *Journal of the Optical Society of America B* **19**: 1435-1453

LARRSON, P., THOMSON, B.O., ARONSSON, M., RODAHL, J. & LAUSMAA, G (1996) Bone response to surface-modified titanium implants: studies on the early tissue response to machined and electropolished implants with different oxide thicknesses. *Biomaterials*, **17**, 605

LAUFFENBURGER, D.A. & HORWITZ, A.F. (1996) Cell migration: a physically integrated molecular process. *Cell*, **84**(3): 359-369.

LAWSON, M.A., & MAXFIELD, F.R. (1995) Ca(2+)- and calcineurin-dependent recycling of an integrin to the front of migrating neutrophils. *Nature*, **377**(6544): 75-79.

LEYPOLDTA, F. FLAJOLETB, M. & METHNERA, A (2002) Neuronal differentiation of cultured human NTERA-2cl.D1 cells leads to increased expression of synapsins, *Neuroscience Letters* **324** 37–40

LEHMANN, V. (1993) The physics of macropore formation in low-doped n-type silicon. *Journal of the Electrochemical Society. Electrochemical Society Letters*, **140** (10): 2836-2844

LEHMANN, V. & FÖLL, H. (1990) Formation mechanism and properties of electrochemically etched trenches in n-type silicon. *Journal of the Electrochemical Society*, **137** (2): 653-659

LEHMANN, V. & GOSELE, U. (1991). Porous silicon formation - a quantum wire effect. *Applied Physics Letters*, **58** (8): 856-858

LEHMANN, V. & GRUNING, U. (1997) The limits of macropore array fabrication. *Thin Solid Films*, **297** (1-2): 13-17

LEHMANN, V., JOBST, B., MUSCHIK, T., KUX, A. & PETROVAKOCH, V. (1993) Correlation between optical-properties and crystallite size in porous silicon. *Japanese Journal Of Applied Physics part 1 - regular papers, short notes & review papers*, **32** (5a): 2095-2099

LEWICKI, M.S. (1998) A review of methods for spike sorting: the detection and classification of neural action potentials. *Computational Neural Systems*, **9**: R53–78.

LEWIS, B. & ANDERSON, J.C. (1978). Nucleation and Growth of Thin Films. *Academic Press*, New York.

LI, K.H., DIAZ, D.C., HE, Y.S., CAMPBELL, J.C. & TSAI, C.C. (1994) Electroluminescence from porous silicon with conducting polymer film contacts. *Applied Physics Letters*, **64** (18): 2394-2396.

LIN, C.H. & FORSCHER, P. (1993) Cytoskeletal remodeling during growth cone-target interactions. *Journal of Cell Biology*, **121**(6): 1369-1383.

LIN, C.H. & FORSCHER, P. (1995) Growth cone advance is inversely proportional to retrograde F-actin flow. *Neuron*, **14**(4): 763-771.

LIN, C.H., ESPREAFICO, E.M., MOOSEKER, M.S. & FORSCHER, P. (1997) Myosin drives retrograde F-actin flow in neuronal growth cones. *Biological Bulletin*, **192**(1): 183-185.

LIN, C.H., THOMPSON, C.A. & FORSCHER, P. (1994) Cytoskeletal reorganization underlying growth cone motility. *Current Opinion in Neurobiology*, 4(5): 640-647.

LING, G. (1975) The mechanism of cellular resting potential according to the association-induction hypothesis and the perfused squid axon: correcting a misrepresentation. *Physiological Chemistry Physica.* 7(1):91-93

LOCKHART, D.J., DONG, H., BYRNE, M.C., FOLLETTIE, M.T., GALLO, M.V., CHEE, M.S., MITTMANN, M., WANG, C., KOBAYASHI, M., HORTON, H. & BROWN, E.L. (1996) Expression monitoring by hybridization to high-density oligonucleotide arrays. *Nature Biotechnology*, **14** (13):1675-1680

LOEB, L. & FLEISHER, M. S. (1917). On the factors which determine the movements of tissues in culture media. *Journal of Medical Research.* 37, 75-99

LÖSTER, K. & HORTSTKORTE, R. (2000) Enzymatic quantification of cell-matrix and cell-cell adhesion. *Micron,* **31** (1): 41-53.

MACKENZIE K. L., FRANCO S., MAY C., SADELAIN M., MOORE M.A. S. (2000) Mass Cultured Human Fibroblasts Overexpressing hTERT Encounter a Growth Crisis Following an Extended Period of Proliferation. *Experimental Cell Research.***259**, (2): 336-350

MACVICAR, B.A. & HOCHMAN, D. (1991) Imaging of synaptically evoked intrinsic signals in hippocampal slices. *Journal of Neuroscience*, **11**:1458-1469.

MAEDA, E., ROBINSON, H.P.C. & KAWANA, A. (1995) The mechanisms of generation and propagation of synchronized bursting in developing networks of cortical-neurons *Journal of Neuroscience*, **15** (10): 6834-6845

MAHER, M.P., DVORAK-CARBONE, H., PINE, J., WRIGHT, J.A. & TAI, Y.C. (1999a) Microstructures for studies of cultured neural networks. *Medical and Biological Engineering and Computing*, **37** (1): 110-118

MAHER M.P. PINE J. WRIGHT J. & TAI Y.C. (1999b) The neurochip: a new multielectrode device for stimulating and recording from cultured neurons. *Journal of Neuroscience Methods*, **87** (1): 45-56

MARTINOIA, S., BOVE, M., TEDESCO, M., MARGESIN, B. & GRATTAROLA, M. (1999) A simple microfluidic system for patterning populations of neurons on silicon micromachined substrates. *Journal of Neuroscience Methods*, **87**(1): 35-44.

MCNAUGHTON, B.L., O'KEEFE, J.O. & BARNES, C.A. (1983) The stereotrode: a new technique for simultaneous isolation of several single units in the central nervous system from multiple unit records. *Journal of Neuroscience Methods*, **8**:391–7.

MEISTER, M., PINE, J. & BAYLOR, D.A. (1994) multi-neuronal signals from the retina - acquisition and analysis. *Journal Of Neuroscience Methods*, **51** (1): 95-106

MEISTER, M., WONG, R. O., BAYLOR, D. A. & SHATZ, C. J. (1991) Synchronous bursts of action potentials in ganglion cells of the developing mammalian retina. *Science*, **252**: 939-943.

MEMMING, R. & SCHWANDT, G. (1966) Anodic Dissolution Of Silicon In Hydrofluoric Acid Solutions. *Surface Science.* **4** (2): 109

MEMMING, R. & SCHWANDT, G. (1966) Potential Distribution And Formation Of Surface States At Silicon-Electrolyte Interface *Surface Science.* **5**(1): 97

MEULENKAMP, E.A., CLEIJ, T.J. & KELLY, J.J. (1994) Electroluminescence and chemiluminescence of porous silicon in nonaqueous solution. *Journal of the Electrochemical Society*, **141** (5): 1157-1161.

MEULENKAMP, E.A., PETER, L.M., RILEY, D.J. & WIELGOSZ, R.I. (1995) On the mechanism of the voltage tuning of photoluminescence and electroluminescence in porous silicon. *Journal of Electroanalytical Chemistry*, **392** (1-2): 97-100.

MEYER, E., MÜLLER, P. & FROMHERZ, P. (1997) Cable properties of dendrites in hippocampal neurons of the rat mapped by a voltage-sensitive dye. *European Journal of Neuroscience*, **9**, 778-785

MEYER-FRANKE, A., TROPAK, M.B., RODER, J.C., FISCHER, P., BEYREUTHER, K., PROBSTMEIER, R. & SCHACHNER, M. (1995) Functional topography of myelin-associated glycoprotein. II. Mapping of domains on molecular fragments. *Journal of Neuroscience Research,* **41** (3):311-23.

MIKULEC, F.V., KIRTLAND, J.D. & SAILOR, M.J. (2002) Explosive nanocrystalline porous silicon and its use in atomic emission spectroscopy. *Advanced Materials*, **14** (1): 38-41.

MIYAKE, T., SOEKI, S. & KATO, H. (1990) Molecular-beam study of sticking of oxygen on Si(100) *Physical Review Bi,* **42** (18): 11801-11807

MOGILNER, A. & OSTER, G. (1996) Cell motility driven by actin polymerization. *Biophysical Journal*, **71**(6): 3030-3045.

MOORE, G.E. (1965) Cramming more components onto integrated circuits. *Electronics*, **38**: 8.

MRKSICH, M., DIKE, L.E., TIEN, T.Y., INGBER, D.E. & WHITESIDES, G.M. (1997). Using microcontact printing to pattern the attachment of mammalian cells to self-assembled monolayers of alkanethiolates on transparent films of gold and silver. *Experimental Cell Research*, **235**, 305-313

MULLER, M. & SOMJEN, G. (1999) Intrinsic optical signals in rat hippocampal slices during hypoxia-induced spreading depression-like depolarization. *Journal of Neurophysiology*, **82**(4): 1818-1831

NAFTEL, S.J., COULTHARD, I., JIANG, D.T., SHAM, T.K., YATES, B.W. & TAN, K.H. (2000) The role of oxygen in the photoluminescence of porous silicon: some recent advances. *Physica status solidi (a)*, **182:** 373-379

NAMAVAR, F., MARUSKA, H.P. & KALKHORAN, N.M. (1992) Visible electroluminescence from porous silicon np heterojunction diodes. *Applied Physics Letters*, **60** (20): 2514-2516.

NAVARRO, X., CALVET, S., BUTI, M., GOMEZ, N., CABRUJA, E., GARRIDO, P., VILLA, R. & VALDERRAMA, E. (1996) Peripheral nerve regeneration through microelectrode arrays based on silicon technology. *Restorative Neurology and Neuroscience*, **9** (3): 151-160

NEHER, E. & SAKMANN, B. (1976) Single-channel currents recorded from membrane of denervated frog muscle fibres. *Nature*. **260**: 799-802.

NORDSLETTEN, L., HOGASEN, A.K.M., KONTTINEN, Y.T., SANTAVIRTA, S., ASPENBERG, P. & AASEN, A.O. (1996) Human monocytes stimulation by particles of hydroxyapatite, silicon carbide and diamond: in vitro studies of new prosthesis coatings. *Biomaterials*, **17**, 1521.

OGDEN, D. (1994) *Microelectrode Techniques, The Plymouth Workshop Handbook*; Cambridge: Company of Biologists.

PANCRAZIO, J.J., BEY, P.P. JR., LOLOEE, A., MANNE, S., CHAO, H.C., HOWARD, L.L., GOSNEY, W.M., BORKHOLDER, D.A., KOVACS, G.T., MANOS, P., CUTTINO, D.S. & STENGER, D.A. (1998) Description and demonstration of a CMOS amplifier-based-system with measurement and stimulation capability for bioelectrical signal transduction. *Biosensors & Bioelectronics* **13**(9): 971-919.

PALECEK, S.P., SCHMIDT, C.E., LAUFFENBURGER, D.A. & HORWITZ, A.F. (1996) Integrin dynamics on the tail region of migrating fibroblasts. *Journal of Cell Science*, **109** (5): 941-52.

PAPAGEORGIOU, D., BLEDSOE, S. C., GULARI, M., HETKE, J.F., ANDERSON, D.J. & WISE, K.D., (2001). Presented at the 14th IEEE International Conference on Micro Electro Mechanical Systems.

PARCE, J.W., OWICKI, J.C. & KERCSO, K.M. (1989) Detection of cell-affecting agents with a silicon biosensor. *Science*, **246** (4927): 243-247

PESKIN, C.S., ODELL, G.M. & OSTER, G.F. (1993) Cellular motions and thermal fluctuations: the Brownian ratchet. *Biophysical Journal*, **65**(1): 316-24.

PETER, L.M. & WIELGOSZ, R.I. (1996) Light-induced electroluminescence of porous silicon layers on p-si in persulfate solution. *Applied Physics Letters*, **69** (6): 806-808

PETER, L.M., BLACKWOOD, D.J. & PONS, S. (1989) In situ characterization of the illuminated silicon-electrolyte interface by FTIR-spectroscopy. *Physics Review Letters*, **62** (3): 308-311.

PFRIEGER, F.W. & BARRES, B.A. (1997) Synaptic efficacy enhanced by glial cells in vitro. *Science,* **277**(5332): 1684-7.

PICKERING, H.W. (1984) Role of gas-bubbles and cavity dimensions on the e-ph-anion concentrations inside cavities. *Journal of the Electrochemical Society*, **131** (8): C299

POLISCHUK, T.N. & ANDREW, R.D. (1996) Real-time imaging of intrinsic optical signals during early excitotoxicity evoked by domoic acid in the rat hippocampal slice. *Canadian Journal of Physiological Pharmacology*, **74**(6): 712-722

POTTER, S.M. & DEMARSE, T.B. (2001) A new approach to neural cell culture for long-term studies. *Journal of Neuroscience Methods*, **110** (1 -2): 17-24

QIN, G. G., HUANG, Y. M., ZONG, B. Q., ZHANG, L. Z. & ZHANG B. R. (1994) A comparison study of electroluminescence from Au/native oxide/p-Si and Au/porous Si diodes. *Superlattices and Microstructures*, **16** (4): 387-387

RAMAKERS, G., OESTREICHER, A., WOLTERS, P., VANLEEUWEN, F., DEGRAAN, P. & GISPEN, W. (1991) Developmental changes in B-50 (GAP-43) in primary cultures of cerebral cortex: B-50 immunolocalization, axonal elongation rate and growth cone morphology. *International Journal of Developmental Neuroscience*, **9**(3): 215

REGEHR, W.G., PINE, J. & RUTLEDGE, D.B. (1988) A long-term in vitro silicon-based microelectrode-neuron connection. *IEEE Transactions on Biomedical Engineering*, **35**(12):1023 –1032.

REGEHR, W.G., PINE, J., COHAN, C.S., MISCHKE, M.D. & TANK D.W (1989) Sealing cultured invertebrate neurons to embedded dish electrodes facilitates long-term stimulation and recording. *Journal Of Neuroscience Methods*, **30** (2): 91-106

RISBUD M.V. HAMBIR, S., JOG, J. & BHONDE, R. (2001) Biocompatibility assessment of PTFE / wollastonite composites using endothelial cells and macrophages, *Journal of Biomaterial Science - Polymer Edition*, **12** (11): 1177–1189

ROBINSON, D.A. (1968) Electrical Properties Of Metal Microelectrodes *Proceedings IEEE* **56**: 1065–1071

ROBINSON, H. P. C., KAWAHARA, M., JIMBO, Y., TORIMITSU, K., KURODA, Y. & KAWANA, A. (1993) Periodic synchronized bursting and intracellular calcium transients elicited by low magnesium in cultured cortical-neurons. *Journal of Neurophysiology*, **70**: 1606-1616.

ROVENSKY, Y. A. & SAMOILOV, V. I. (1974). Morphogenetic response of cultured normal and transformed fibroblasts, and epitheliocytes to cylindrical substratum surface. *Journal of Cell Science*, **107**, 1255-1263.

ROVENSKY, Y. A., SLAVNAYA, I. L. & VASILIEV, J. M. (1971). Behavior of fibroblast-like cells on grooved surfaces. *Experimental Cell Research*, **65**, 193-201.

SAILOR, M.J., TROGLER, W.C. & LETANT, S. (2001) Using quantum dots and molecular wires for chemical sensing. *Abstract Papers American Chemical Society*, **221**: 421-Coll Part 1.

SAMESHIMA, K. & BACCALA, L.A. (1999) Using partial directed coherence to describe neuronal ensemble interactions. *Journal of Neuroscience Methods*. **94**(1): 93-103.

SANEINEJAD, S. & SHOICHET M.S. (1998) Patterned glass surfaces direct cell adhesion and process outgrowth of primary neurons of the central nervous system *Journal of Biomedical Materials Research* **42** (1): 13-19

SCHMITT, G., SCHULTZE, J. -W., FAßBENDER, F., BUß, G., LÜTH, H. & SCHÖNING, M. J. (1999) Passivation and corrosion of microelectrode arrays. *Electrochimica Acta*, **44** 3865–3883.

SCHUBERT, D., HEINEMANN, S., CARLISLE, W., TARIKAS, H., KIMES, B., PATRICK, J., STEINBACK, J.H., CULP, W. & BRANDT, B.L. (1974) Clonal cell lines from the rat central nervous system. *Nature*, **249**: 224-227

SEMICONDUCTOR INDUSTRY ASSOCIATION 1999.
http://notes.sematech.org/1999_SIA)Roadmap/Home.htm

SMITH, R.A. (1979). *Semiconductors*. Cambridge University Press.

SMITH, R.L. & COLLINS, S.D. (1989) Generalized-model for the diffusion-limited aggregation and eden models of cluster growth. *Physics Review A*, **39** (10): 5409-5413

SMITH, R. L. & COLLINS, S. D. (1992) Porous silicon formation mechanisms. *Journal of Applied Physics*, **71**: R1

SNOW, R.W., TAYLOR, C.P. & DUDEK, F.E. (1983) Electrical and optical changes in slices of rat hippocampus during spreading depression. *Journal of Neurophysiology*, **50**: 561-572.

SOKAL, M., MASON, R. & PARKER, T.L. (2000) Multi-neuronal recordings reveal a differential effect of thapsigarin and bicuculline- or gabazine-induced epileptiform excitability in rat hippocampal neuronal networks. *Neuropharmacology*, **39**: 2408 – 2417

SORRIBAS, H., BRAUN, D., LEDER, L., SONDEREGGER, P. & TIEFENAUER, L. (2001) Adhesion proteins for a tight neuron-electrode contact. *Journal of Neuroscience Methods*, **104** (2): 133-141

SREENIVAS, K., MANSINGH, A. (1985) The growth and structure of rf sputtered indium tin oxide thin-films. *Applied Surface Science*, **22** (3): 670-680

SREENIVAS, K., RAOM T.S., MANSINGH, A., CHANDRA, S. (1985) Preparation and characterization of rf sputtered indium tin oxide-films. *Journal of Applied Physics*, **57** (2): 384-392

STALLCUP, W.B. (1977) Specificity of adhesion between cloned neural cell lines. *Brain Research* **126**(3): 475- 486

STAROVOITOV, A. & BAYLISS, S. (1998) Structured luminescent porous silicon layers produced with laser assisted chemical etching. *Applied Physics Letters*, **73**(9): 1284-1286

STAROVOITOV, A. & BAYLISS, S. (2000) Laser structuring of luminescent porous silicon during etching. *Journal of Porous Materials*, **7** (1-3): 367-371

STECKL, A.J., XU, J. & MOGUL, H.C. (1993) Photoluminescence of Chemically Etched Polycrystalline and Amorphous Si Thin Films. *MRS Proceedings of Symposium on Silicon-Based Optoelectronics Materials*, **298**: 211-216.

STEINER, P., KOZLOWSKI, F. & LANG, W. (1993) Light-emitting porous silicon diode with an increased electroluminescence quantum efficiency. *Applied Physics Letters*, **62** (21): 2700-2702.

STELZLE, M., WAGNER, R., JAGERMANN, W. & FRÖHLICH, R. (1997) *Proceedings of the 18th Annual International Conference of the IEEE*; **1**: 114.

SUGIYAMA, K., IGARASHI, T. & MORIKI, K. (1990) Silicon-hydrogen bonds in silicon native oxides formed during wet chemical treatments. *Japanese Journal of Applied Physics 2*, **29** (12): L2401-L2404

SUNADA, T., YASAKA, T., & TAKAKURA, M. (1990) The role of fluorine termination in the chemical-stability of HF-treated Si surfaces. *Japanese Journal of Applied Physics 2*, **29** (12): L2408-L2410

SVESSON, I., ATRURSSON, E., LEANDERSON, P., BERGLIND R. & LINDGREN, F. (1997) Toxicity in vitro of some silicon carbides and silicon nitrides: Whiskers and powders. *American Journal of Industrial Medicine*, **31**: 335.

TANAKA, T., TANIGAWA, T., NOSE, T., IMAI S. & HAYASHI, Y. J. (1994) In-vitro cytotoxicity of silicic-acid in comparison with that of selenious acid. *Trace Elements in Experimental Medicine*, 7(3): 101-111

TENGVALL, P., LESTELIUS, M., LIEDBERG, M. & LUNDSTROEM, I. (1992). Plasma protein and antisera interactions with L-cysteine and 3-mercaptopropionic acid monolayers on gold surfaces. *Langmuir,* **8;** 1236–1238.

TESCHKE, O., GALEMBECK, F., GONCALVES, M.C. & DAVANZO, C.U. (1994) Photoluminescence spectrum redshifting of porous silicon by a polymeric carbon layer. *Applied Physics Letters.* **64** (26): 3590 - 3592.

THEUINISSEN, M.J.J. (1972) Etch channel formation during anodic dissolution of *n-type* silicon in aqueous hydrofluoric acid. *Journal of the Electrochemical Society*, **119**(3): 351 – 360

THI, H.L.N. & JUTTEN, C. (1995) Blind source separation for convolutive mixtures. *Signal Processing*, **45** (2): 209-229

THIÉBAUD, P., BEURET, C., KOUDELKA-HEP, M., BOVE, M., MARTINOIA, S., GRATTAROLA, M., JAHNSEN, H., REBAUDO, R., BALESTRINO, M., ZIMMER, J. & DUPONT, Y., (1999) An array of Pt-tip microelectrodes for extracellular monitoring of activity of brain slices. *Biosensors and Bioelectronics*, **14**: 61–65

THOMAS, C.A. JR, SPRINGER, P.A., LOEB, G.E., BERWALD-NETTER, Y. & OKUN, L.M. (1972) A miniature microelectrode array to monitor the bioelectric activity of cultured cells. *Experimental Cell Research,* **74**(1): 61-66

THUST, M., SCHONING, M.J. & FROHNHOFF, S. (1996) Porous silicon as a substrate material for potentiometric biosensors. *Measurement Science and Technology*, **7** (1): 26-29

TRUCKS, G.W., RAGHAVACHARI, K., HIGASHI, G.S. & CHABAL, Y.J. (1990) Mechanism of HF etching of silicon surfaces - a theoretical understanding of hydrogen passivation. *Physical Review Letters*, **65** (4): 504-507

TRUCKS, G.W., RAGHAVACHARI, K., HIGASHI, G.S. & CHABAL, Y.J. (1991) Mechanism of HF etching of silicon surfaces - a theoretical understanding of hydrogen passivation – reply. *Physical Review Letters*, **66** (12): 1648-1648.

TURNER, D., AITKEN, P. & SOMJEN, G. (1995) Optical mapping of translucence changes in rat hippocampal slices during hypoxia. *Neuroscience Letters*, 195: p. 209-213

TURNER, D. R. (1958a) Electropolishing Silicon In Hydrofluoric Acid Solutions. *Journal Of The Electrochemical Society.* **105** (7): 402-408

TURNER, D. R. (1958) Electropolishing Silicon In Hydrofluoric Acid Solutions. *Journal Of The Electrochemical Society.* **105**(3): C55-C56

TURNER, D. R. (1962) In: *The Electrochemistry of Semiconductors*, Holmes P. J. (Ed.), Academic, London: 179

UHLIR, A. (1956) Electrolytic Shaping Of Germanium And Silicon. *Bell System Technical Journal.* **35**(2): 333-347

UOSAKI, K., KONDO, T. & NOGUCHI, H. (1996) Visible electroluminescence from p-type porous silicon in electrolyte solution. *Journal of Physical Chemistry*, **100** (11): 4564-4570

VAN COMPERNOLLE, D. & VAN GERVEN, S. (1992) Signal separation in a symmetric adaptive noise canceler by output decorrelation. *IEEE ICASSP*, **4**: 221-224

VASSANELLI, S. & FROMHERZ, P. (1999) Transistor probes local potassium conductances in the adhesion region of cultured rat hippocampal neurons. *Journal of Neuroscience*, **19** (16): 6767-6773

VENKATESWARA RAO, A. OZANAM, F. &. CHAZALVIEL, J.-N (1991) In situ Fourier-transform electromodulated infrared study of porous silicon formation – evidence for solvent effects on the vibrational linewidths. *Journal of the Electrochemical Society*, **138**: 153

WALLMAN, L., ZHANG, Y.Z., LAURELL, T. & DANIELSEN, N. (2001) The geometric design of micromachined silicon sieve electrodes influences functional nerve regeneration. *Biomaterials*, **22** (10): 1187-1193

WEBB, A., CLARK, P., SKEPPER, J., COMPSTON, A., & WOOD, A. (1995) Guidance of oligodendrocytes and their progenitors by substratum topography *Journal of Cell Science* **108**, 2747-2760

WEGENER, J., KEESE, C.R., & GIAEVER, I. (2000) Electric cell-substrate impedance sensing (ECIS) as a noninvasive means to monitor the kinetics of cell spreading to artificial surfaces. *Experimental Cell Research.* **259**(1):158-66.

WEILAND, J.D. & ANDERSON, D.J. (2000) Chronic Neural Stimulation With Thin-Film, Iridium Oxide Electrodes. *IEEE Transactions On Biomedical Engineering.* **47** (7): 911-918

WEISS, P. (1934). In vitro experiments on the factors determining the course of the outgrowing nerve fiber. *Journal of Experimental Zoology*, **68**, 393-448.

WEISS, P. (1941). Nerve patterns: The mechanics of nerve growth. *Growth, third growth symposium,* **5**: 163-203

WEISS P. (1963) The cell as unit. *Journal of Theoretical Biology.* **5** (3): 389-397.

WEIS, R. & FROMHERZ, P. (1997) Frequency dependent signal transfer in neuron transistors. *Physical Review E*, **55** (1): 877-889 Part B

WEIS, R., MULLER, B., FROMHERZ, P. (1996) Neuron adhesion on a silicon chip probed by an array of field-effect transistors. *Physical Review Letters*, **76** (2): 327-330

WELDON, M.K., QUEENEY, K.T., ENG, J. JR., RAGHAVACHARI, K. & CHABAL, Y.J. (2002) The surface science of semiconductor processing: gate oxides in the ever-shrinking transistor. *Surface Science*, **500**: 859–878

WILSON, R.J.A., BRECKENRIDGE, L., BLACKSHAW, S.E., CONNOLLY, P., DOW, J.A.T., CURTIS, A.S.G. & WILKINSON, C.D.W. (1994) Simultaneous multisite recordings and stimulation of single isolated leech neurons using planar extracellular electrode arrays. *Journal of Neuroscience Methods*, **53** (1): 101-110

WOOD, A. T. (1988). Contact guidance on microfabricated substrata: the response of teleost fin mesenchyme cells to repeating topographical patterns. *Journal of Cell Science.* **90**, 667-681.

YANG, Y., ZHANG, S.F., KINGSTON, M.A., JONES, G., WRIGHT, G. & SPENCER, S.A. (2000) Glucose sensor with improved haemocompatibilty. *Biosensors and Bioelectronics*, **15**: 221–227.

ZANGOOIE, S., BJORKLUND, R. & ARWIN, H. (1998) Protein adsorption in thermally oxidized porous silicon layers. *Thin Solid Films*, **313**: 825-830

ZHANG, M., DESAI, T. & FERRARI, M. (1998) Proteins and cells on PEG immobilized silicon surfaces. *Biomaterials*, **19**: 953–960.

ZIEGLER, C., GÖPEL, W., HAMMERLE, H., HATT, H., JUNG, G., LAXHUBER, L., SCHMIDT, H.L., SCHUTZ, S., VOGTLE, F. & ZELL, A. (1998) Bioelectronic noses: A status report. Part II *Biosensors and Bioelectronics*, **13** (5): 539-571

ZURER, P. (1997) Porous silicon biosensor. *Chemical Engineering*, **75** (37): 7